Department of Precision and Microsystems Engineering

Design of a hip orthosis that uses a compliant mechanism to correct Trendelenburg gait

Stijn Bosselaar

Report no : 2025.033
Coach : Prof. dr. ir. J.L. Herder
Professor : Prof. dr. ir. J.L. Herder
Specialisation : Mechatronic System Design
Type of report : MSc Thesis
Date : 10 July 2025

Delft University of Technology

Master thesis

Design of a hip orthosis that uses a compliant mechanism to correct Trendelenburg gait

Author
Stijn Bosselaar 4484789

July 10, 2025

Preface

This thesis marks the final step in completing my Master's degree in Mechanical Engineering at the Delft University of Technology.

I chose this project because I was looking for something with societal relevance, and because of my longstanding interest in human biomechanics. With both of my parents working as physiotherapists, this field has always appealed to me.

The project builds upon previous research initiated in collaboration with Rijndam Revalidatie. I would like to thank Rutger Osterthun, rehabilitation physician, as well as the several staff members for the insightful conversations that helped me gain a better understanding of the clinical context of this work.

I would like to express special thanks to my daily supervisor, Just Herder, for his support and guidance throughout this project, particularly in light of the personal challenges I faced during this period. I am also grateful to Bram Sterke for his supervision during the initial phase of the thesis, and to Dave Sonneveld and Ron van Ostayen for their help with COMSOL. I would also like to thank Simone Schoon, orthopedic instrument maker, for her expert advice, and the 3mE workshop staff for their assistance in building my scale model.

Finally, I wish to thank my family and friends for their encouragement and support throughout this process.

Stijn Bosselaar
Delft, June 2025

Abstract

Trendelenburg gait is an abnormal gait pattern caused by failure of the hip abduction mechanism. Under the external adduction moment caused by the body weight, this results in excessive adduction characterized by a drop of the pelvis on the contralateral side. Existing assistive devices are inadequate for this condition. Therefore, this thesis aimed to develop a hip orthosis that uses a compliant mechanism to correct Trendelenburg gait. Compared to traditional mechanisms, compliant mechanisms offer several advantages in orthotic applications, including compactness, low mass, adaptability to misalignment, and adjustable levels of support. However, despite these benefits being recognized, research on practical implementation remains limited.

The design process distinguished between the attachment parts and the mechanism of the orthosis. For the attachment parts, the goal was to evaluate whether the established orthotic methods and materials are suitable for this application. A preliminary design confirmed their suitability. For the mechanism, the goal was to develop an innovative compliant solution by either advancing previous work or introducing a new concept. The latter showed more potential for flexion stiffness minimization, as well as a lightweight and compact design and was therefore selected for further development.

Two mechanism design variations were developed: one using a conventional leaf flexure and one using a leaf flexure incorporating warping constraints. As anticipated, warping constraints enabled further reduction of the flexion stiffness. The hip flexion moment required to achieve a 30° flexion angle was 7.9 Nm in the design using a conventional leaf flexure, and 0.55 Nm in the design using a leaf flexure incorporating warping constraints. This result indicates the potential of warping constraints for broader implementation in compliant mechanisms to improve the ratio between lateral and bending stiffness in leaf flexures at large deflections. The main tradeoff for this improvement was increased mass, from 0.36 kg to 0.98 kg. Both designs provided sufficient adduction stiffness to constrain adduction under the adduction moment applied by the body weight, and are therefore effective in correcting Trendelenburg gait.

The resulting overall orthosis design is a promising solution, providing the foundation for future research to validate its technical and clinical performance and development into a usable product.

Contents

Preface **i**

Abstract **ii**

1 Introduction **1**
1.1 Trendelenburg gait . . . 1
1.2 Problem statement . . . 1
1.3 Objective . . . 1
1.4 Thesis outline . . . 2

2 Background **3**
2.1 Introduction . . . 3
2.2 Trendelenburg gait . . . 3
2.3 Assessment of state-of-the-art solutions . . . 8
2.4 Previous research . . . 12
2.5 Potential of compliant mechanisms in orthoses . . . 13
2.6 Summary of key findings . . . 15

3 Design foundation **16**
3.1 Introduction . . . 16
3.2 The hypothetical patient . . . 16
3.3 Analysis of functional needs . . . 16
3.4 Requirements list . . . 17

4 Preliminary attachment parts design **20**
4.1 Introduction . . . 20
4.2 Design process . . . 20
4.3 Design evaluation . . . 25
4.4 Artist impression . . . 26

5 Orthosis mechanism concept phase **27**
5.1 Introduction . . . 27
5.2 Concept generation . . . 27
5.3 Qualitative concept evaluation . . . 33
5.4 Quantitative evaluation of Concepts 4 and 8 . . . 33
5.5 Concept selection . . . 41
5.6 Scale model for concept validation . . . 42

6 Orthosis mechanism design phase **44**
6.1 Introduction . . . 44
6.2 FEM software selection . . . 44
6.3 Mechanism design using a conventional leaf flexure . . . 48
6.4 Mechanism design using a leaf flexure incorporating warping constraints . . . 63

7 Discussion **75**
7.1 Interpretation of design performance . . . 75
7.2 Reflection on using a compliant mechanism . . . 79
7.3 Comparison with existing designs . . . 80
7.4 Future research . . . 81
7.5 Broader implications . . . 84

8 Conclusion **86**

Bibliography **88**

A State-of-the-art hip orthoses **93**
A.1 Introduction . . . 93
A.2 Newport Hip Orthosis by Orthomerica . . . 93
A.3 S-form hip brace, WISH type by Gunma University . . . 94
A.4 California Hip Orthosis by Orthomerica . . . 94
A.5 Hiploc Evo by Thuasne . . . 95
A.6 DonJoy X-Act ROM Hip Brace by DJO Global . . . 95
A.7 TLC Abduction Brace by Optec . . . 96
A.8 SofTec Coxa by Bauerfeind . . . 96
A.9 Rebound Hip by Össur . . . 97
A.10 Hip One by Medi . . . 97
A.11 Dynacox Evolution by Teufel . . . 98
A.12 Lerman Hip Abduction Rotation Orthosis 2000 by Becker Orthopedic . . . 98
A.13 Unloader Hip by Össur . . . 99
A.14 Cosa Active by Ottobock . . . 99

B Finite Element Method (FEM) models **100**
B.1 Introduction . . . 100
B.2 COMSOL model for approximating the load distribution shape between the patient's body and the attachment parts of the orthosis . . . 101
B.3 COMSOL model for stiffness analysis of the orthosis attachment parts . . . 108
B.4 SolidWorks model for the preliminary design of Concept 4 . . . 112
B.5 SolidWorks model for the preliminary design of Concept 8 . . . 116
B.6 Beam Code model for FEM software selection . . . 121
B.7 COMSOL model for FEM software selection . . . 125
B.8 COMSOL model for the mechanism design using a conventional leaf flexure . . . 131
B.9 COMSOL model for the mechanism design using a leaf flexure incorporating warping constraints . . . 143

1 Introduction

1.1 Trendelenburg gait

Trendelenburg gait is an abnormal gait pattern caused by failure of the hip abduction mechanism. In the stance phase of the gait cycle, during single-limb support, the body weight applies an external adduction moment about the hip joint of the limb in stance. In healthy individuals, this is counteracted by an abduction moment generated by the hip abductor muscles. In case of Trendelenburg gait this mechanism fails, resulting in excessive adduction characterized by a drop of the pelvis on the contralateral side. Trendelenburg gait accelerates joint wear in the hip, knee, and ankle, and often leads to inactivity.

1.2 Problem statement

The devices currently used to assist patients with Trendelenburg gait are limited to wheelchairs and crutches, both of which have major drawbacks. Wheelchairs facilitate mobility but limit overall physical activity, while crutches require significant upper body strength and occupy the hands.

A hip orthosis that supports the hip abduction mechanism by constraining adduction would offer a more suitable solution. However, state-of-the-art hip orthoses typically only serve as a reminder about harmful positions in patients who retain muscle strength. As a result, they are not designed to correct movement by force, and thus lack the load-bearing capacity to constrain adduction under the adduction moment generated by the body weight. Moreover, their attachment parts are not designed for effective and comfortable force transfer to the patient's body.

Previous research introduced the conceptual design of a hip orthosis specifically aimed at correcting Trendelenburg gait [1]. While the concept showed promise, it was not developed into a functional design. Its feasibility and effectiveness therefore remain unproven, and it cannot yet be considered a viable solution.

This concept used a compliant mechanism, where motion is achieved through elastic deformation rather than the joints and linkages used in traditional mechanisms. Compliant mechanisms offer several potential benefits in orthotic application, including compactness, low mass, adaptability to misalignment, and adjustable levels of support. Although these benefits are recognized, research on their practical implementation in orthoses remains limited.

1.3 Objective

Given the lack of an orthotic solution for Trendelenburg gait, and the recognized yet underexplored benefits of compliant mechanisms in orthoses, the objective of this thesis is to develop a hip orthosis that uses a compliant mechanism to correct Trendelenburg gait.

The design process distinguishes between the attachment parts and the mechanism of the orthosis. For the attachment parts, the goal is to evaluate whether the established methods and materials for orthotic design are suitable for this specific application. For the mechanism, the goal is to develop an innovative compliant solution. This may involve further developing the previously researched design or introducing a new concept, depending on which proves more promising.

1.4 Thesis outline

The thesis is structured as follows:

Chapter 2 provides background information detailing the topics introduced above. It analyzes human gait and the failure mechanism behind Trendelenburg gait, assesses state-of-the-art solutions, introduces the previously researched design, and outlines the potential benefits and challenges of compliant mechanisms in orthotic applications.

Chapter 3 lays the foundation for the orthosis design. It introduces the representative patient, identifies the functional needs of the orthosis, and translates these into quantified design requirements.

Chapter 4 presents a preliminary design for the attachment parts of the orthosis. In addition to evaluating suitability of the established orthotic methods and materials, this design helps define the design margins available for the orthosis mechanism.

Chapter 5 describes the concept phase of the orthosis mechanism. Various concepts, including the one from previous research, are evaluated to identify the most promising solution.

Chapter 6 describes the design phase of the orthosis mechanism. The concept selected in the previous phase is developed into a detailed design.

Chapter 7 discusses the performance of the resulting orthosis design, reflects on the use of a compliant mechanism, compares the design to state-of-the-art orthoses as well as the previously researched design, outlines the directions for future research, and highlights broader implications.

Finally, Chapter 8 summarizes the conclusions of this thesis.

2 Background

2.1 Introduction

This chapter begins with an analysis of Trendelenburg gait in Section 2.2. Subsequently, state-of-the-art solutions are explored and assessed in Section 2.3. Section 2.4 introduces a previously developed conceptual design for a compliant hip orthosis aimed at correcting Trendelenburg gait. Building on this, the potential of compliant mechanisms in orthotic applications is explored in Section 2.5. The chapter concludes with a summary of its key findings in Section 2.6, which provides the rationale for this thesis project.

2.2 Trendelenburg gait

This section provides a thorough understanding of Trendelenburg gait by analyzing the human gait cycle, with a focus on the role of the hip abduction mechanism.

2.2.1 Anatomical views

During gait analysis, the human body can be viewed from various orientations. For the purposes of this thesis, three specific orientations are used: the anterior view, posterior view, and lateral view. These views are illustrated in Figure 2.1

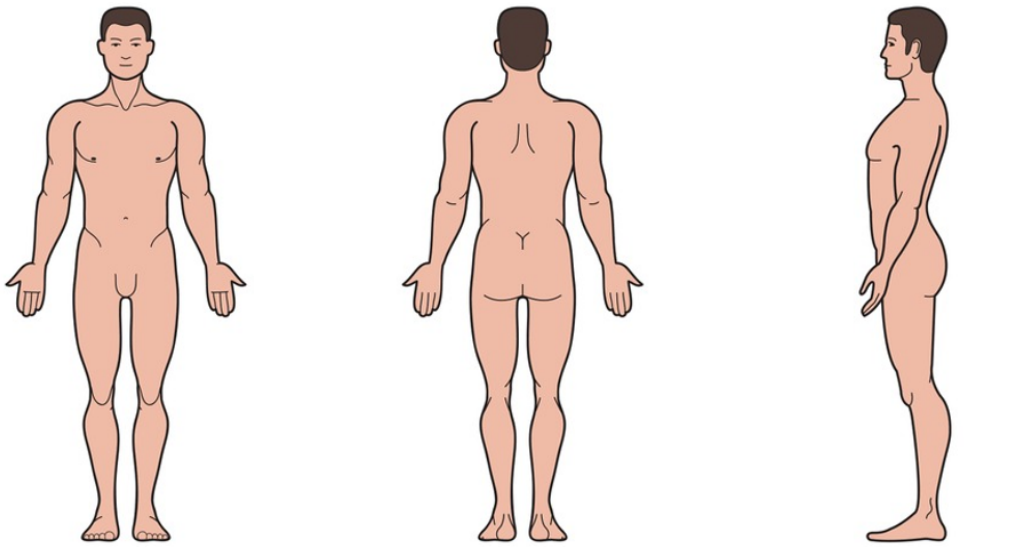

(a) Anterior view. (b) Posterior view. (c) Lateral view.

Figure 2.1: Overview of the three relevant views for the thesis [2].

2.2.2 The human gait cycle

One cycle of human gait is defined as the period between two consecutive ground contacts of the same leg. During the cycle, this leg goes through two phases: the stance phase and the swing phase. The stance phase lasts approximately 60% of the gait cycle, while the swing phase takes up the remaining 40%. The stance phase is split up into double-limb support and single-limb support. The human gait cycle and its phases are illustrated in Figure 2.2 [3].

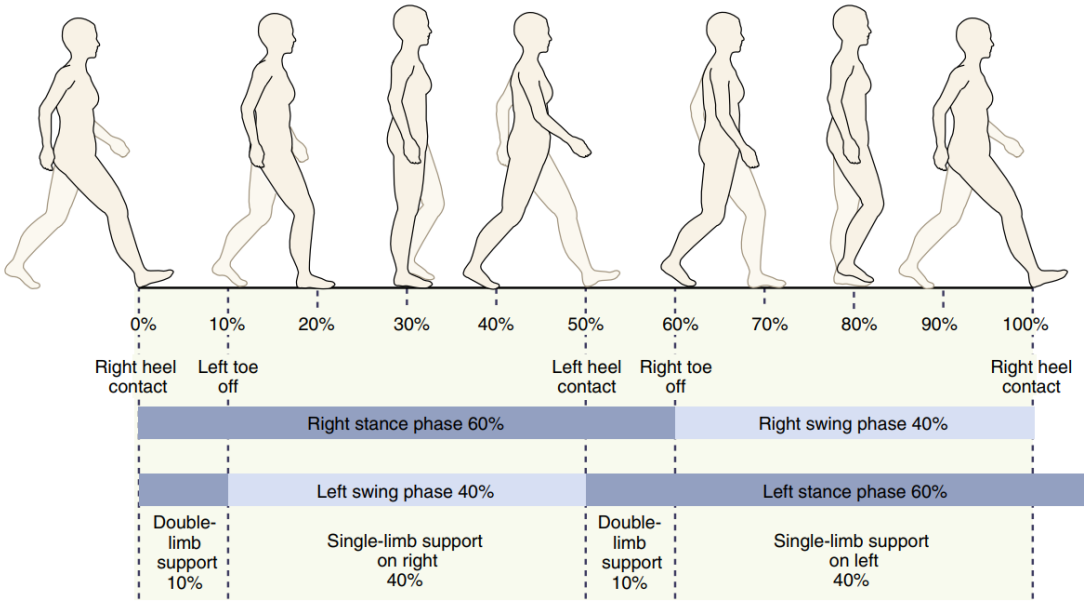

Figure 2.2: The human gait cycle in the lateral view. [3]

2.2.3 Movements of the hip

The hip joint is a connection point between the pelvis and the upper leg bone. It is a spherical joint, meaning that it allows three rotational degrees of freedom. Medical literature defines two opposite joint movements for each degree of freedom, resulting in six hip movements: flexion/extension, abduction/adduction, and internal/external rotation. Figure 2.3 illustrates these movements by upper leg movement while the pelvis remains stationary.

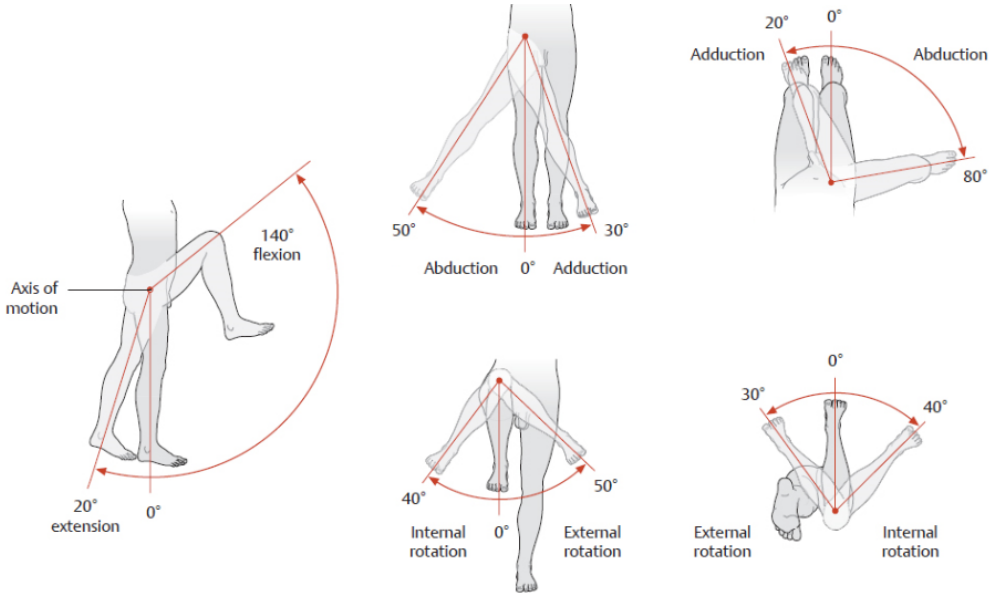

Figure 2.3: The six movements of the hip visualized by upper leg movement [4].

2.2.4 Mechanism of hip abduction

Figure 2.4 illustrates the three main hip abductor muscles: the gluteus medius, the gluteus minimus, and the tensor fasciae latae. Their orientation explains their role in facilitating abduction. They are located on the lateral side of the body, connecting the pelvis to the (upper) leg. When considering the pelvis a fixed structure, one can imagine that contraction of the abductor muscles pulls the leg outward, aligning exactly with how hip abduction was visualized in Figure 2.3.

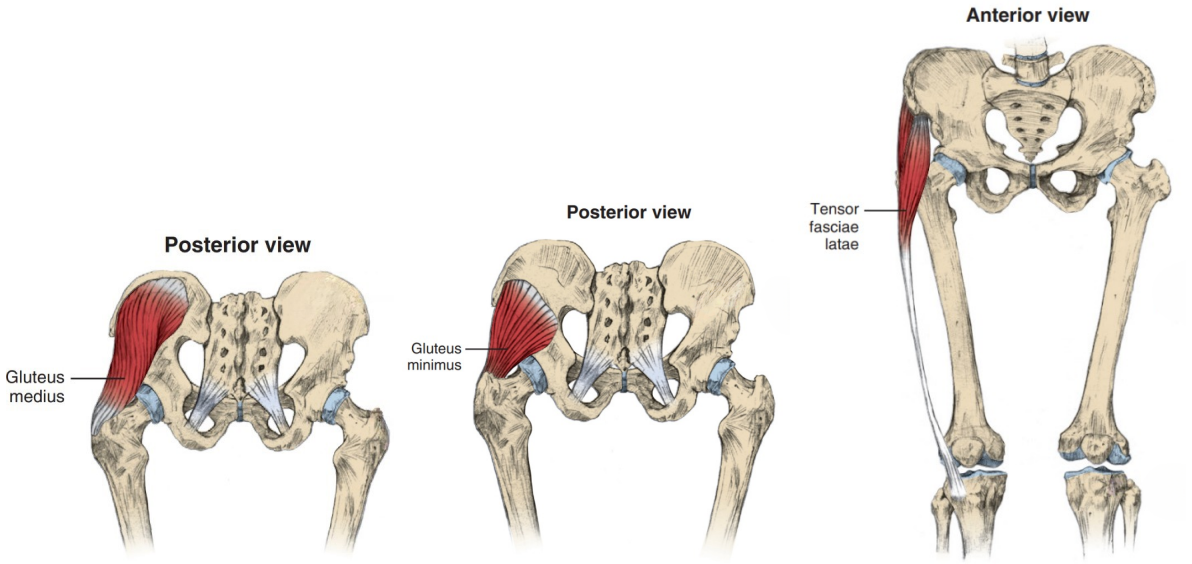

(a) Gluteus medius. (b) Gluteus minimus. (c) Tensor fasciae latae.

Figure 2.4: The three main hip abductor muscles. [3]

2.2.5 Hip abduction during gait

Figures 2.5 and 2.6 show the hip joint angles and moments during gait in healthy individuals at different walking paces [5]. Between 10% and 50% of the gait cycle (the single-limb support phase), the hip abductor muscles generate a substantial hip abduction moment of up to 0.8 Nm/kg. Interestingly, this is not accompanied by a large abduction angle. In fact, a slight adduction angle of up to 7° is observed during this part of the gait cycle. This indicates that rather than generating abduction, the role of the hip abductor muscles during this part of the gait cycle is to limit adduction.

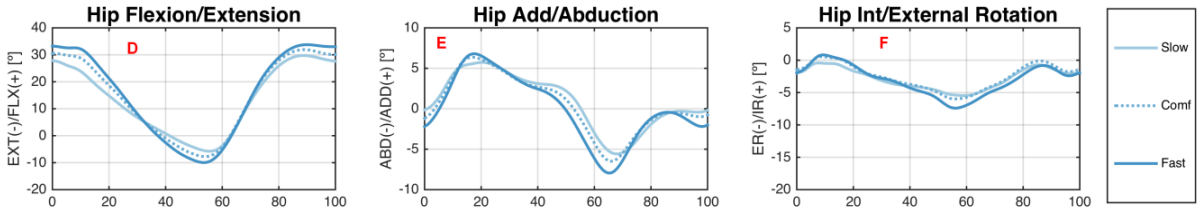

Figure 2.5: Hip joint angles during gait in healthy individuals at different walking paces [5].

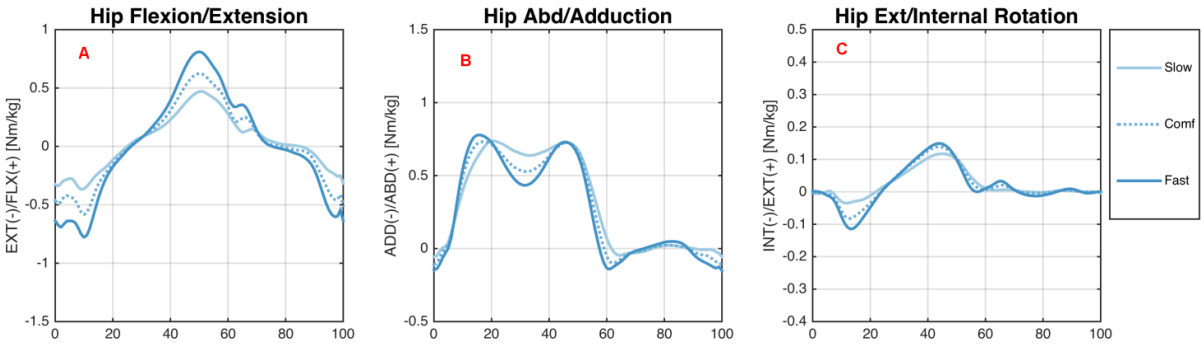

Figure 2.6: Hip joint moments during gait in healthy individuals at different walking paces [5].

This functionality is illustrated in Figure 2.7. During the single-limb support phase of the gait cycle, the body weight exerts an external adduction moment about the hip joint of the limb in stance. To counteract this, the hip abductor muscles generate an internal hip abduction moment of equal magnitude, maintaining equilibrium and preventing excessive adduction.

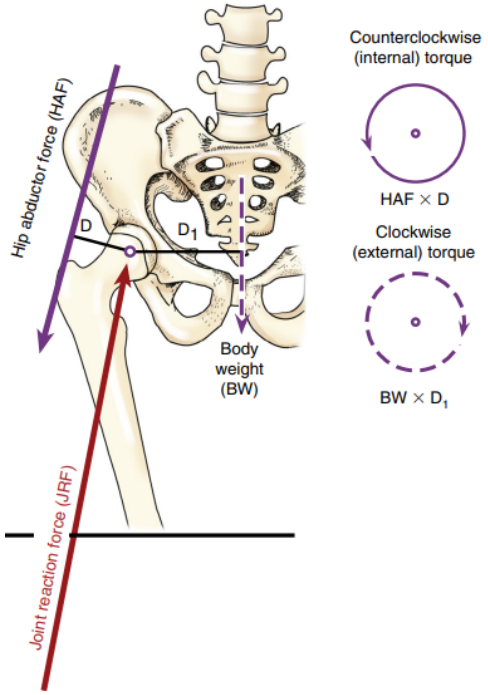

Figure 2.7: Moment equilibrium of the hip joint of the limb in stance during the single-limb support phase of the gait cycle, in anterior view [3].

The reason why hip adduction in this phase of the gait cycle is limited to 7° rather than eliminating adduction altogether is visualized in Figure 2.8. A small adduction angle is required to balance the center of gravity over the foot in stance.

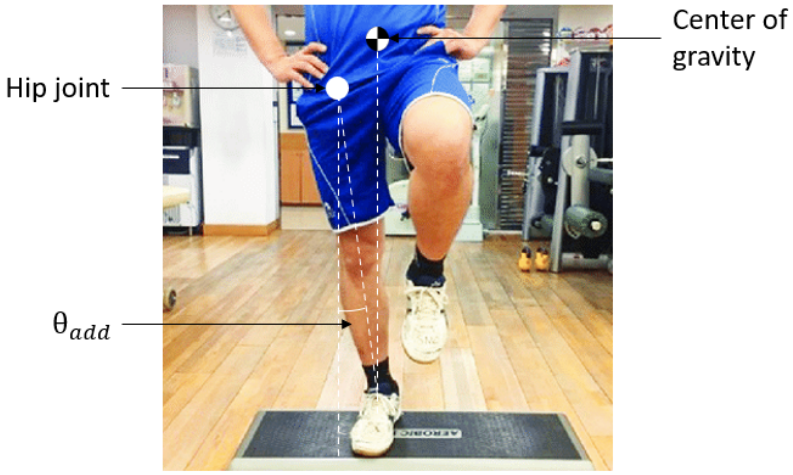

Figure 2.8: Balancing mechanism of the human body in the single-limb support phase of the gait cycle [6].

2.2.6 Hip abduction failure and Trendelenburg gait

Trendelenburg gait occurs when the hip abduction mechanism fails, resulting in excessive adduction in the single-limb support phase of the gait cycle. This is characterized by a drop of the pelvis on the contralateral side of the limb in stance. Patients may try to compensate this by leaning the upper body towards the leg in stance, in order to decrease the moment arm of the body weight. This way the external adduction moment by the body weight reduces and therefore less internal abduction moment needs to be generated by the hip abductor muscles. This is called compensated Trendelenburg gait. The different gait types are illustrated in Figure 2.9. [3, 4, 7–10]

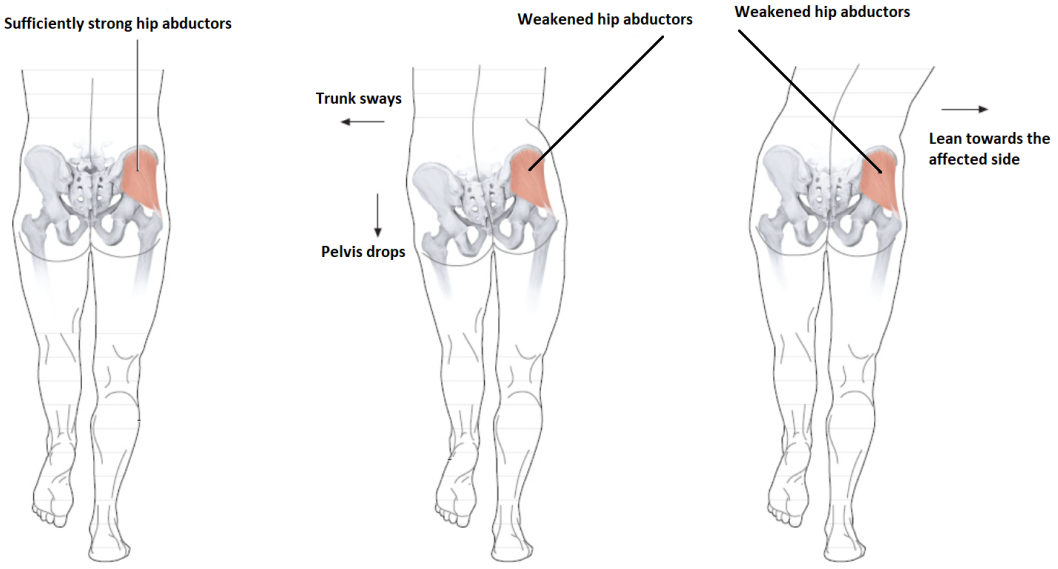

(a) Normal human gait. (b) Trendelenburg gait. (c) Compensated Trendelenburg gait.

Figure 2.9: Different gait types in posterior view [4].

2.2.7 Conditions that may cause Trendelenburg gait

Underlying conditions that may cause failure of the hip abduction mechanism, and thus Trendelenburg gait, can be categorized into two main categories: either the hip abductor muscles generate insufficient force, or they operate at a mechanical disadvantage. Depending on the condition and its severity, this can lead to partial or complete failure of the hip abduction mechanism, which can be reversible or irreversible. Typically, these conditions appear on one side, leading to unilateral cases of Trendelenburg gait.

Examples of an insufficiency in hip abductor muscle force are: [7, 11, 12]

- Muscle slack due to bone overgrowth that causes muscle insertions to approach each other. This can happen in e.g. Legg-Calvé-Perthes disease [13]. Muscles lose their strength in a slacked or stretched position [14].
- Post-operative failure of repair of abductor muscle and/or tendon tissue after a total hip replacement [15].
- Atrophy of the hip abductor muscles, for example due to osteoarthritis [16, 17].
- Damage to the Superior Gluteal Nerve that normally innervates the abductor muscles. This can happen due to a fracture or dislocation, or during a surgical procedure [18].

Examples of a mechanical disadvantage are: [7, 11, 12]

- Decreased moment arm due to bone overgrowth that causes muscle insertions to move closer to the joint. This can happen in e.g. Legg-Calvé-Perthes disease [13].
- An unstable fulcrum that causes dysfunction of the lever. This can happen in e.g. Developmental Dysplasia where the ball and socket configuration of the hip joint is compromised due to the socket not being deep enough [19].

2.3 Assessment of state-of-the-art solutions

This section reviews currently used assistive devices (wheelchairs and crutches), highlighting their drawbacks. Based on these limitations, a hip orthosis is proposed as a more effective solution. The section then explores currently available hip orthoses that are potentially suitable for correcting Trendelenburg gait, and assesses their effectiveness in practice.

2.3.1 Currently used assistive devices

Trendelenburg gait accelerates joint wear in the hip, knee, and ankle [7]. It also leads to discomfort and instability, which can reduce physical activity. An inactive lifestyle is associated with both physical and mental health issues [20], which is why the WHO recommends 30 minutes of daily active walking for adults [21]. For patients with Trendelenburg gait, achieving this level of activity is often not possible.

Despite these challenges, current assistive devices are limited to wheelchairs and crutches [22]. While wheelchairs facilitate mobility, they do not support walking or an active lifestyle. Crutches, though they enable walking, have major drawbacks: they require significant upper body strength, cause physical discomfort, and occupy the hands.

Given these limitations, alternative solutions should be considered. Hip orthoses are promising candidates, as they are designed to provide hip support during gait. They facilitate mobility, keep the hands free, and promote physical activity.

2.3.2 Exploration of potentially suitable hip orthoses

As described in Section 2.2, Trendelenburg gait characterizes by excessive adduction in the single-limb support phase of the gait cycle. This occurs due to failure of the hip abduction mechanism, being unable to compensate for the adduction moment caused by body weight. Therefore, an orthosis to correct Trendelenburg gait must provide an adduction constraint, while allowing flexion/extension to facilitate walking.

Appendix A presents a selection of currently available hip orthoses that offer this functionality. These orthoses can be categorized into two distinct groups, which are detailed below.

Category 1: Joint-and-bar mechanism

The vast majority of all currently available hip orthoses fall into this category. One or more revolute joints align with the hip joint on the lateral side of the patients body. From this joint, two bars reach to an upper body and leg attachment part. The joint-and-bar mechanism is usually made of steel or aluminum, or a combination of both. The attachment parts contain rigid shell elements that are made of the thermoplastic materials polyethylene or polypropylene. On the inside they are padded for which a variety of materials may be used, ranging from plastic and rubbery materials like acrylonitrile butadiene styrene (ABS) and ethylene vinyl acetate, to more garment-like materials such as polyamide, polyurethane, elastane, polyester, viscose and cotton. Buckles that can be fastened with hook and loop straps are used as the closure system. An example of one of these orthoses is the Newport Hip Orthosis by Orthomerica, which is shown in Figure 2.10.

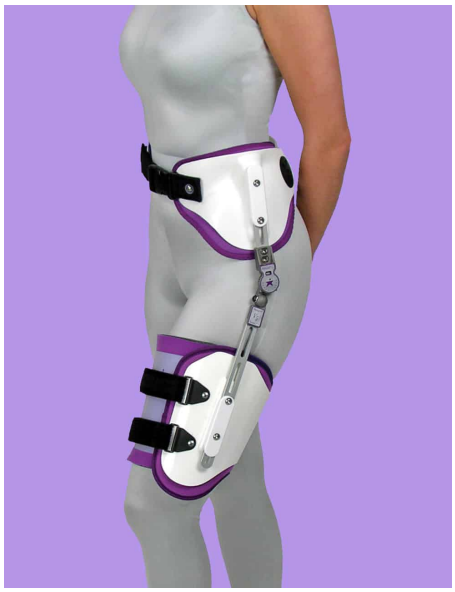

Figure 2.10: Newport Hip Orthosis by Orthomerica. [23]

These orthoses are used to guide and limit hip joint movement in the swing phase of the gait cycle. This is achieved with the mechanical joint(s) aligning with the hip joint on the lateral side of the patient's body. The joints can be adjusted to limit the range of flexion/extension and abduction/adduction and, in many cases, can also be set to a fixed angle of abduction/adduction. Rather than constraining hip movement by force, these orthoses serve as a sensory reminder to avoid harmful positions. The patient is expected to correct their movement path using their own muscle force. Consequently, these orthoses are prescribed for conditions in which muscle strength is preserved. [24–26]

Typical indications for prescribing these orthoses include:

- Surgical procedures near the hip joint. Preventing large hip movement angles and guiding hip motion supports recovery and relieves pain [25, 27].
- Luxation risk of the hip joint. This is often the case after a total hip arthroplasty [28], but it also applies to non-surgical scenarios such as hip dysplasia. The orthosis helps prevent movements that could increase the risk of dislocation [29, 30].
- Painful hip conditions like osteoarthritis or coxitis. Wearing the orthosis in combination with exercise therapy has shown to have positive effect on both pain and hip function [31].

Category 2: Garment-like

This is a small category of two hip orthoses made entirely out of garment-like materials to improve patient comfort. These orthoses were developed by Össur and Ottobock, two global leaders in orthotic and prosthetic innovation.

Össur developed the Unloader Hip orthosis, which is shown in Figure 2.11. It consists of Lycra shorts, to which a belt is attached that wraps around the pelvis. A strap crosses the upper leg, pulling it into external rotation and abduction. Unlike the hip orthoses in Category 1, which function during the swing phase of the gait cycle, the Unloader Hip orthosis provides assistance to the limb in stance, during the single-limb support phase. Its purpose is to unload the hip joint in patients with hip osteoarthritis. The main contribution to hip loading during gait is the activation of the hip abductor muscles, which are recruited on the stance side in the single-limb support phase of the gait cycle. The contraction of the hip abductor muscles leads to a compressive load on the hip joint, pushing the ball and socket into each other. The resulting reaction force contributes to the pain experienced by people with hip osteoarthritis. The unloading effect of the Unloader Hip orthosis is twofold: first, the leg is pulled into external rotation and abduction which changes the contact area of the internal reaction force in the hip joint; second, the hip abductor muscles are supported, meaning that less muscle force is required to constrain adduction, which results in a lower internal reaction force in the hip joint.
A study with fourteen participants showed immediate reduction of pain for nine of the participants, and a reduction of the internal abduction moment generated by the abductor muscles of 9.3%. [32, 33]

Ottobock developed the Cosa Active hip orthosis, which is shown in Figure 2.12. This hip orthosis is used to correct scissor gait in children who suffer from cerebral palsy. Scissor gait is a gait pattern caused by tension in the hip adductor muscles, resulting in the legs crossing each other in scissor-like fashion. The orthosis contains pads on the inner thighs to prevent adduction by pushing the legs away from each other. A study on the effectiveness is conducted where the sit-to-stand activities of children with cerebral palsy is timed. The results indicate that the anti-adduction pads effectively prevent the legs from crossing, which positively impacted the sit-to-stand activities. [34–36]

Figure 2.11: Unloader Hip by Össur. [33]

Figure 2.12: Cosa active by Ottobock. [35]

2.3.3 Assessment of explored hip orthoses

The explored hip orthoses with potential suitability to correct Trendelenburg gait are assessed for their effectiveness in practice. For this assessment, orthopedic instrument maker Simone Schoon, an expert in the field, was consulted [19].

Category 1: Joint-and-bar mechanism

Category 1 currently available hip orthoses incorporate a joint-and-bar mechanism that can be used to constrain adduction while providing flexion/extension freedom. Although this might suggest suitability for correcting Trendelenburg gait, these orthoses are not effective in practice.

First, they lack the structural strength and stiffness to handle the adduction moment applied by the body weight. The orthoses in this category are typically prescribed for patients who retain muscle function and primarily serve as a sensory reminder to avoid harmful positions. Upon this feedback, the patient is expected to correct their movement path themselves. Consequently, they are not designed to bear significant load.

Second, the attachment parts of these orthoses are not able to effectively and comfortably transfer the mechanism's adduction constraint to the patient's body. The attachment parts of these orthoses are confection rather than custom-made, meaning that they do not provide a secure and precise fit. This results in relative motion between the attachment parts and the patient's body, which prevents proper transfer of the mechanism's adduction constraint. Furthermore, the lack of a tailored fit can lead to pressure points, causing discomfort for the patient.

Category 2: Garment-like
Category 2 includes two fundamentally different hip orthoses. The Unloader Hip by Össur pulls the leg into external rotation and abduction, and supports the hip abductor muscles on the stance side in the single-limb support phase of the gait cycle. The required internal abduction moment to constrain adduction in this part of the gait cycle reduced by 9.3%. To effectively correct Trendelenburg gait, this percentage needs to be 100, as many patients suffer from complete failure of the hip abduction mechanism. The Cosa active by Ottobock corrects scissor gait in children who suffer from cerebral palsy, using pads on the inner thighs that prevent adduction. In case of cerebral palsy, the limb in swing shows excessive adduction, while in case of Trendelenburg gait this is the limb in stance. This orthosis prevents adduction by pushing the leg in swing away from the leg in stance, which is not applicable in case of Trendelenburg gait.

2.4 Previous research

Previous research presented the conceptual design of a hip orthosis specifically designed to correct Trendelenburg gait [1]. The design used a compliant mechanism, meaning that motion is achieved through elastic deformation rather than joints and linkages as in traditional mechanisms [37]. The mechanism consists of two parallel leaf flexures, both arranged in series with a wire flexure, as illustrated in Figure 2.13. One of the main goals of this study was to maximize the stiffness ratio between hip adduction and flexion/extension. The stiffness ratio, measured at a 0° flexion/extension angle, was $\frac{k_{add}}{k_{f/e}} = 1.7 \cdot 10^3$, which is a promising result. However, future research is required to evaluate the actual effectiveness of the design.

First, the research only considers the ratio between the adduction and flexion/extension stiffness. The actual required adduction stiffness to correct Trendelenburg gait, and required flexion/extension compliance to facilitate effortless walking are not examined. As a result, material and dimensional selection were not studied. Also, the stiffness ratio was only measured at a 0° flexion/extension angle. Trendelenburg gait occurs in the single-limb support phase of the gait cycle on the stance side. Figures 2.2 and 2.5 show that during this phase, the limb in stance moves from 8° extension to 30° flexion. Therefore, the adduction stiffness must be evaluated throughout this entire range of motion. Furthermore, the sole focus of this research was placed on the mechanism of the orthosis, leaving the attachment parts out of scope. Lastly, no testing on persons was done to investigate how the orthosis affects gait.

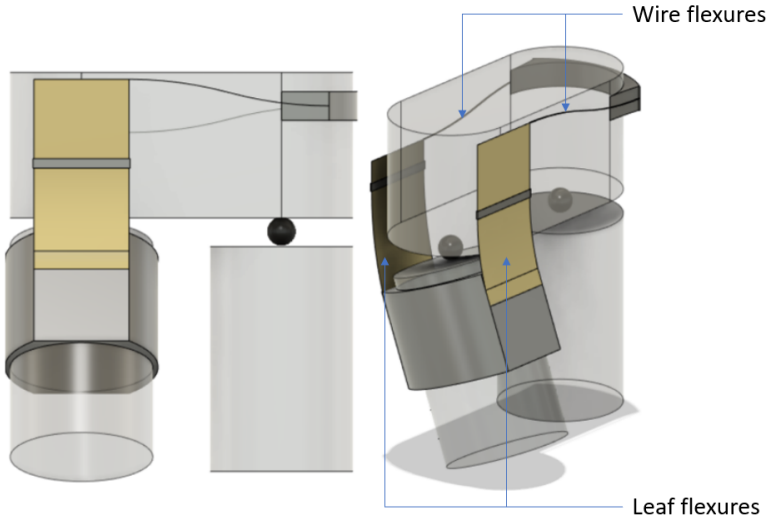

Figure 2.13: Conceptual hip orthosis design presented in [1].

2.5 Potential of compliant mechanisms in orthoses

Current research on compliant mechanisms has predominantly focused on precision engineering. The use of a compliant mechanism in the previously researched design sparked interest in exploring its potential for orthotic applications as well. Despite being a relatively underexplored field, various compliant orthosis designs have been studied, including hand orthoses, a scoliosis orthosis, a knee orthosis, and a neck orthosis [38–42]. This section outlines the benefits and challenges associated with compliant mechanisms in orthoses, as identified in these studies.

2.5.1 Benefits of compliant mechanisms

Compact and lightweight solutions

Compliant mechanisms typically require fewer and simpler components than traditional mechanisms. This may lead to a more compact and lightweight solution which improves patient comfort. Their space-efficiency is further enhanced by their compliant nature, allowing them to adapt to the curves of the human body.

Adaptation to misalignment

Unlike traditional mechanisms, compliant mechanisms do not have strict rotation axes, allowing them to adapt to misalignment. Alignment of mechanical joints in orthoses with anatomical joints in patients is a common challenge in orthotics due to the complex kinematics of the human body, the uniqueness of each patient, and even the variability within a patient over time [43]. Even minor misalignment, particularly in orthoses with custom-made attachment parts designed for a tailored fit that minimizes play, can lead to highly uncomfortable motion for the patient. This discomfort arises because the natural kinematic path cannot be followed. Additionally, considering that compliant mechanisms do not have strict rotation axes, they are less restrictive to adjacent joints, allowing these joints to utilize the same degrees of freedom provided by the mechanism.

Adjustable level of support

The level of support provided by a compliant mechanism can be customized by adjusting the stiffness of its components. This allows for a precise design that ensures sufficient support *in addition* to the remaining muscle strength the patient still has. This prevents the muscles from becoming overly reliant on the device, which stimulates muscle growth or slows down muscle decrease. Adjustments can be made over time to accommodate changes in the patient's strength, making compliant mechanisms very suitable for orthoses used in medical rehabilitation programs [44].

2.5.2 Challenges of compliant mechanisms

Design process

The design process of compliant mechanisms is typically much more complex than that of traditional mechanisms due to the complex kinematic paths that are difficult to analyze. Consequently, nonlinear FEM analysis is often required to accurately predict how geometries deform under load.

The Freedom And Constraint Topologies (FACT) method, introduced by Jonathan Hopkins, is a design method that aids in overcoming these complexities. It provides a systematic approach for selecting the compliant components needed to achieve a desired set of degrees of freedom. A practical tool for this design method is the FACT table, which is shown in Figure 2.14. This table shows the freedom and constraint systems for different (combinations of) compliant components.

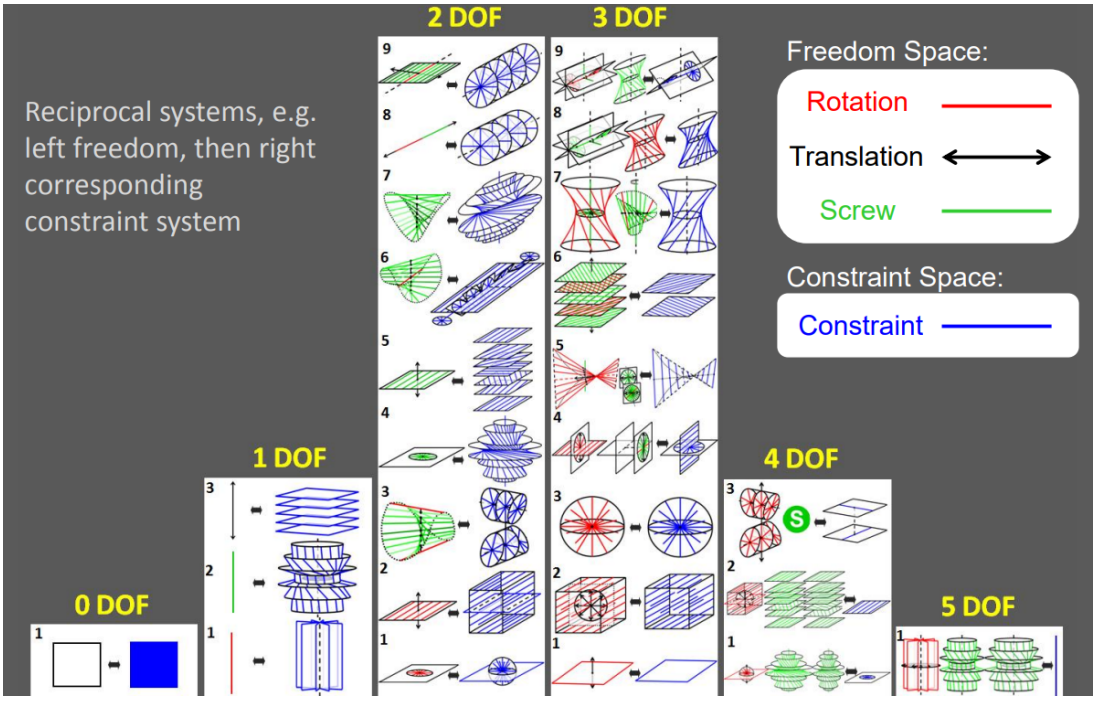

Figure 2.14: FACT table by Jonathan Hopkins [45].

Support stiffness

The support stiffness of compliant mechanisms often deteriorates with increasing deflection. A typical example is the reduction in lateral stiffness of leaf flexures during bending. In the undeformed configuration, lateral stiffness of a leaf flexure is primarily determined by its in-plane bending stiffness. However, as bending increases, torsional stiffness becomes a significant contributor. Since torsion is a mode of compliance, as illustrated in the FACT table in Figure 2.14, the overall lateral stiffness decreases with increasing bending deflection. [46]

Methods to maintain high lateral stiffness in leaf flexures at large deflections focus on enhancing torsional stiffness without significantly compromising bending stiffness. Two approaches found in literature are triangular torsion reinforcement structures [47] (see Figure 2.15) and warping constraints [48] (see Figure 2.16). Triangular torsion reinforcement structures have been extensively studied and demonstrated to be effective both theoretically and experimentally. Their main drawback is that they are very space consuming. Warping constraints on the other hand, have only been investigated in a single theoretical study but show promising effectiveness and are much more space-efficient than torsion reinforcement structures.

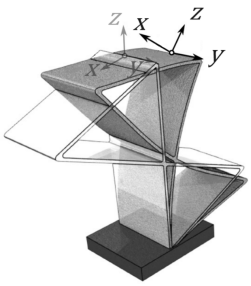

Figure 2.15: Leaf flexure with triangular torsion reinforcement structures [47].

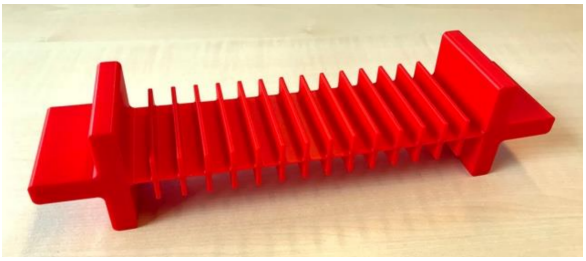

Figure 2.16: Leaf flexure incorporating warping constraints [48].

Other

General other challenges caused by the fact that compliant mechanisms obtain movement through elastic deformation are that some stiffness in the compliant direction always remains, and that the range of motion is limited by the maximum elastic deformation of the material. Additionally, fatigue is a known failure mode for compliant mechanisms subjected to repeated motion. In these cases, a fatigue analysis is essential, further complicating the design process. [45]

2.6 Summary of key findings

This chapter identified a clear gap in orthotic design: the absence of a hip orthosis suitable for correcting Trendelenburg gait. State-of-the-art hip orthoses are not designed to constrain movement by force. As a result, they lack the load-bearing capacity required to effectively constrain hip adduction under the adduction moment generated by body weight. Additionally, they incorporate confection attachment parts, rather than custom-made, resulting in ineffective and uncomfortable constraint transfer to the patient's body. The previous researched design introduced in Section 2.4 offers a promising solution, but additional research is needed to test its actual effectiveness and to enable its practical implementation.

Additionally, the potential of incorporating compliant mechanisms in orthoses was examined. Despite being an underexplored field, various benefits were identified, including the potential for a lightweight and compact solution, adaptability to misalignment, compliance to adjacent joints, and adjustable levels of support. Challenges lie in the design process being complex compared to traditional mechanisms, loss of support stiffness at large deflections, limited elasticity and fatigue. However, mitigation methods exist to address these challenges, such as the FACT method for compliant mechanism design and implementation of torsion reinforcement structures and warping constraints to maintain support stiffness at large deflections.

Given the identified gap in orthotic design, this thesis proposes the development of a new hip orthosis aimed at correcting Trendelenburg gait. In light of the recognized yet underexplored potential of compliant mechanisms in orthotic applications, the design will incorporate a compliant mechanism rather than a traditional mechanism. This approach ensures a contribution to both the fields of orthotic design and compliant mechanisms.

Chapter 3 proceeds by establishing the design foundation.

3 Design foundation

3.1 Introduction

This chapter lays the foundation for the orthosis design. The patient for whom the orthosis will be designed is introduced in Section 3.2. Next, Section 3.3 provides an analysis of functional needs based on the findings from Chapter 2. These needs are then translated into quantified requirements in Section 3.4.

3.2 The hypothetical patient

This thesis does not consider one or more specific patients. Rather, a hypothetical patient is introduced for which the orthosis will be designed. Figure 3.1 shows the measurements of this hypothetical patient, derived from anthropometric data. The patient is assumed to have unilateral Trendelenburg gait with 100% loss of hip abduction function.

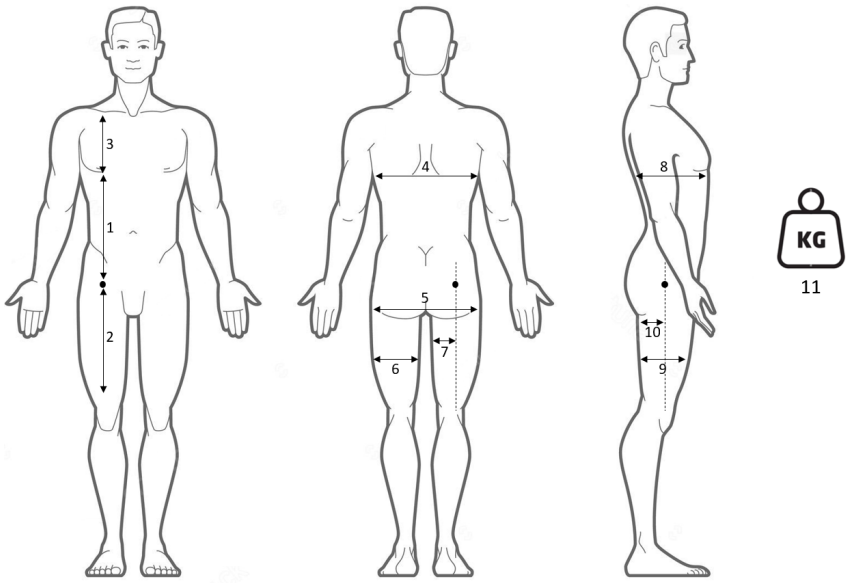

Figure 3.1: Measurements of the hypothetical patient derived from anthropometric data in adults of 20 years and older [49].

1: 0.35 m.
2: 0.35 m.
3: 0.10 m.
4: 0.40 m.
5: 0.40 m.
6: 0.15 m.
7: 0.075 m.
8: 0.30 m.
9: 0.15 m.
10: 0.075 m.
11: 71 kg.

3.3 Analysis of functional needs

Based on the findings of Chapter 2, the functional needs of a hip orthosis to correct Trendelenburg gait are formulated. The functional needs of the orthosis are split into three categories: the mechanism of the orthosis, the attachment parts of the orthosis, and the orthosis in general.

Mechanism
The mechanism of the orthosis defines the degrees of freedom and constraints of the hip joint. Given that the hypothetical patient used in this thesis has 100% loss of hip abduction function, effective correction of Trendelenburg gait requires full restriction of adduction under the adduction moment applied by the body weight. Meanwhile, a degree of freedom for flexion/extension is essential to facilitate walking. The remaining hip movements – abduction and internal/external rotation – do not require specific degrees of freedom or constraints, as the angular displacement for these movements remains below 8° during gait (see Figure 2.5). Given that the human body is not completely rigid, these small movements are assumed to be achieved by natural deformation of the body.

Since compliant mechanisms lose their support stiffness with displacement, it is crucial to ensure sufficient adduction stiffness in all positions. Additionally, adequate compliance for flexion/extension must be maintained, as compliant mechanisms inherently exhibit stiffness in the compliant directions. Finally, due to the repeated deformation and loading cycles during walking, a fatigue analysis of the mechanism is critical during its design.

Attachment parts
The function of the attachment parts of the orthosis is to transfer the mechanism's adduction constraint to the patient's body. The attachment parts design should be focused on transferring this constraint effectively and comfortably.

General
The general functional needs of the orthosis are aimed at improving patient comfort during walking by promoting a compact and lightweight design. Compatibility with general activities of daily life, such as sitting or toilet visits, are not considered.

3.4 Requirements list
This section translates the functional needs to quantified requirements using the same three categories. All non-referenced quantifications are derived from Chapter 2. The requirements include **must** and **should** statements to indicate their importance. The **must** statements represent critical pass or fail stages that are essential for a satisfactory design. The **should** statements describe traits or characteristics that are not absolutely necessary but can improve the orthosis' performance through optimization.

1. Mechanism:

   (a) *The mechanism of the orthosis **must** provide an adduction constraint with sufficient stiffness to ensure that if the body weight applies a 57 Nm adduction moment, the resulting adduction angle in the mechanism itself remains below 1.0°. This requirement must hold throughout the entire range of motion, from 8° extension to 30° flexion.*

   The maximum expected adduction moment by the body weight is 0.8 Nm/kg, which equals 57 Nm for the hypothetical patient introduced in Section 3.2. This load occurs during the single-limb support phase of the gait cycle, where the hip joint moves from 8° extension to 30° flexion. The same section explains that up to 7° of adduction is necessary to maintain balance by keeping the center of mass over the foot in stance. However, this small adduction angle is expected to occur naturally due to the deformability of the human body. Therefore, the mechanism itself must provide sufficient stiffness to ensure that its own contribution to adduction remains negligible, here defined as smaller than 1.0°.

(b) *The mechanism of the orthosis **must** provide a degree of freedom for flexion/extension with low enough flexion stiffness to ensure that the hip flexion moment required to achieve a 30° flexion angle is smaller than 43 Nm. Additionally, the flexion stiffness **should** be minimized.*

The maximum hip flexion angle that is seen during gait is 30°. The maximum allowed hip flexion moment required to achieve this angle is derived from muscle fatigue literature. A force of 15% of the maximum voluntary contraction (MVC) of a muscle is believed to induce minimal fatigue [50]. For the hip flexor muscles, the MVC is 4.0 Nm/kg [51], meaning that a 0.6 Nm/kg hip flexion moment results in minimal fatigue, which equals 43 Nm for the hypothetical patient introduced in Section 3.2. However, further minimization of flexion stiffness is important as it reduces walking effort and improves patient comfort. Hip extension during gait occurs due to the forward swing of body weight while the stance leg remains grounded, rather than active hip extensor muscle effort. Therefore, the extension stiffness of the mechanism is not a design concern.

(c) *The maximum von Mises stress in the mechanism of the orthosis if the body weight applies a 57 Nm adduction moment, **must** remain below the material's infinite life fatigue limit. This requirement must hold throughout the entire range of motion, from 8° extension to 30° flexion.*

These conditions represent the maximum expected adduction load and flexion/extension range of motion, and thus include the highest expected stress. This conservative design constraint prevents fatigue failure under repeated loading.

2. Attachment parts:

(a) *The attachment parts of the orthosis **must** be custom-made.*

This ensures a tailored fit that effectively transfers the mechanism's adduction constraint to the patient's body and prevents pressure points.

(b) *The loads on the patient's body, resulting from transfer of the mechanism's adduction constraint, **must** be perpendicular to the skin surface.*

This ensures optimal constraint transfer and comfort by avoiding skin movement and shear forces.

(c) *The pressure on the patient's body, resulting from transfer of the mechanism's adduction constraint, **should** be minimized.*

Pressure minimization in an application that requires significant force transfer enhances patient comfort.

(d) *The attachment parts of the orthosis **must** be sufficiently stiff to ensure that if the body weight applies a 57 Nm adduction moment, the resulting adduction deformation of the attachment parts themselves remains below 1.0°.*

Adduction deformation of the attachment parts of the orthosis must remain negligible to ensure effective transfer of the adduction constraint to the patient's body.

3. General:

   (a) *The combined mass of the mechanism and attachment parts of the orthosis **must** be smaller than 5.0 kg, and **should** be minimized.*

   There is no guideline available in literature specifying a maximum acceptable mass for orthoses. The hip orthoses outlined in Appendix A weigh up to 2.3 kg which is therefore known to be acceptable. Since a hip orthosis designed to correct Trendelenburg gait has higher mechanical demands, a greater mass is justifiable. However, a mass exceeding 5.0 kg is expected to significantly reduce wearability. Additionally, minimizing mass is encouraged to improve patient comfort.

   (b) *The combined thickness of the mechanism and attachment parts of the orthosis, including both the material thickness and the clearance between the patient's body and the orthosis, **must** be smaller than 5.0 cm, and **should** be minimized.*

   A maximum overall thickness of 5.0 cm is consistent with the hip orthoses outlined in Appendix A and is therefore considered acceptable. Further minimization is desirable for both aesthetic and practical reasons.

   (c) *The combined surface area of the patient's body that is covered by the mechanism and attachment parts of the orthosis **should** be minimized.*

   Reducing coverage is beneficial for both aesthetic and practical reasons.

4 Preliminary attachment parts design

4.1 Introduction

This chapter presents a preliminary design for the attachment parts, developed using established orthotic methods and materials. The goal is to evaluate the suitability of these methods and materials for this specific application, and to determine the design margins available for the orthosis mechanism.

The design process is described in Section 4.2, after which Section 4.3 evaluates the resulting design against the requirements outlined in Section 3.4. This evaluation confirms the suitability of the established orthotic methods and materials, and identifies the design margins available for the orthosis mechanism. The chapter concludes with an artist impression in Section 4.4.

4.2 Design process

The attachment parts design must satisfy all **must** statements in Requirements 2a through 3c. Additionally, optimization for the **should** statements is encouraged to improve its performance. Based on expert advice from Simone Schoon [19], pressure minimization is prioritized, as this application is expected to involve relatively high force transfer between the attachment parts and the patient's body.

The design process is mainly guided by the attachment-parts-specific requirements, 2a through 2d. First, a custom-made approach is enabled through material selection (Requirement 2a). Subsequently, the placement and size of the attachment parts, including all dimensions except its thickness, are determined to ensure that loads are perpendicular to the skin surface and that pressure is minimized (Requirements 2b and 2c). Finally, the thickness is determined to provide sufficient stiffness (Requirement 2d).

4.2.1 Material selection

Requirement 2a states that the attachment parts of the orthosis must be custom-made. In this preliminary design, this is ensured through material selection that supports a custom-made manufacturing process.

Custom-made attachment parts are typically made from thermoplastic materials through a thermoforming process. Material thickness ranges from 2.0 mm to 8.0 mm, depending on the requirements of the specific application. If greater strength, stiffness, or lower weight is needed than thermoplastics can provide, carbon fiber is used as an alternative [19].

Being the standard first choice in orthotic design, a thermoplastic part is first proposed. This can later be adjusted to carbon fiber if necessary.

Filled thermoplastics compatible with thermoforming can achieve a Young's modulus of up to 25 GPa. A typical density is $1.25 \cdot 10^3$ kg/m^3, and a typical Poisson's ratio is 0.33. Therefore, these values will be used in the analyses of this design process [52].

4.2.2 Placement

Requirement 2b states that loads on the patient's body, resulting from transfer of the mechanism's adduction constraint, must be perpendicular to the skin surface. Requirement 2c states that the pressure of these loads on the patient's body should be minimized.

Given that these loads constrain adduction, they generate an abduction moment about the hip joint. Therefore, an abduction force system with components perpendicular to the skin surface and great potential for pressure minimization is first determined.

Figure 4.1 illustrates three possible abduction forces acting perpendicular to the skin surface. Pressure minimization can be achieved by increasing the moment arms about the hip joint and distributing loads over a larger surface area. Among the three options, the second force offers the best potential for both properties and is therefore selected.

Since an abduction force alone does not create equilibrium, reaction forces must be introduced. These forces are applied to the stance leg as this in contact with the ground. Like the abduction force, they must also be perpendicular to the skin surface and minimized in pressure.

Figure 4.2 shows the resulting abduction force system, revealing the necessity of two attachment parts: one on the upper leg, and one on the upper body.

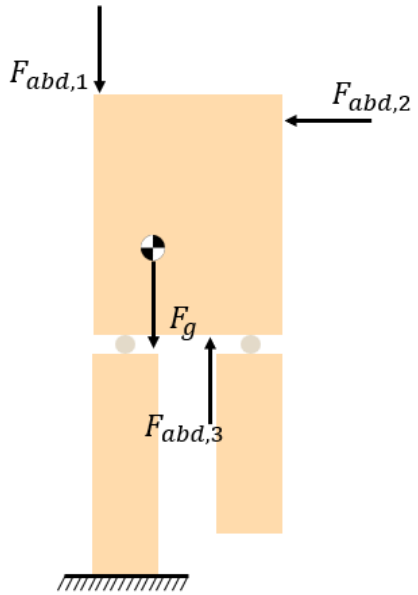

Figure 4.1: Three possible abduction forces.

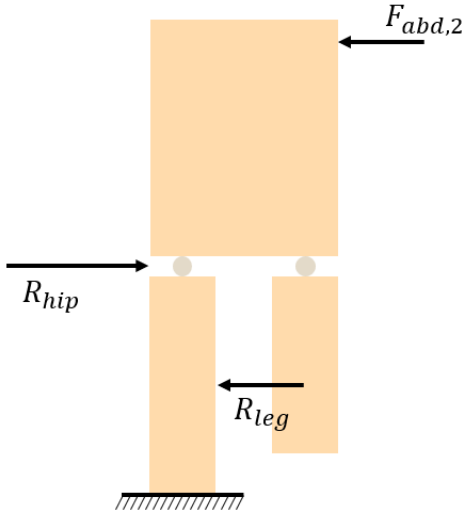

Figure 4.2: Selected abduction force system.

4.2.3 Size

Since pressure minimization is prioritized among the **should** statements in the requirements, the dimensions of the attachment parts should be maximized to achieve optimal load distribution. This must be done within the spatial constraints of the hypothetical patient introduced in section 3.2. Given the absence of a specific patient for this thesis, simplified shapes are used for the patient's body. Figure 4.3 shows the resulting dimensions selected for the attachment parts, excluding their thickness.

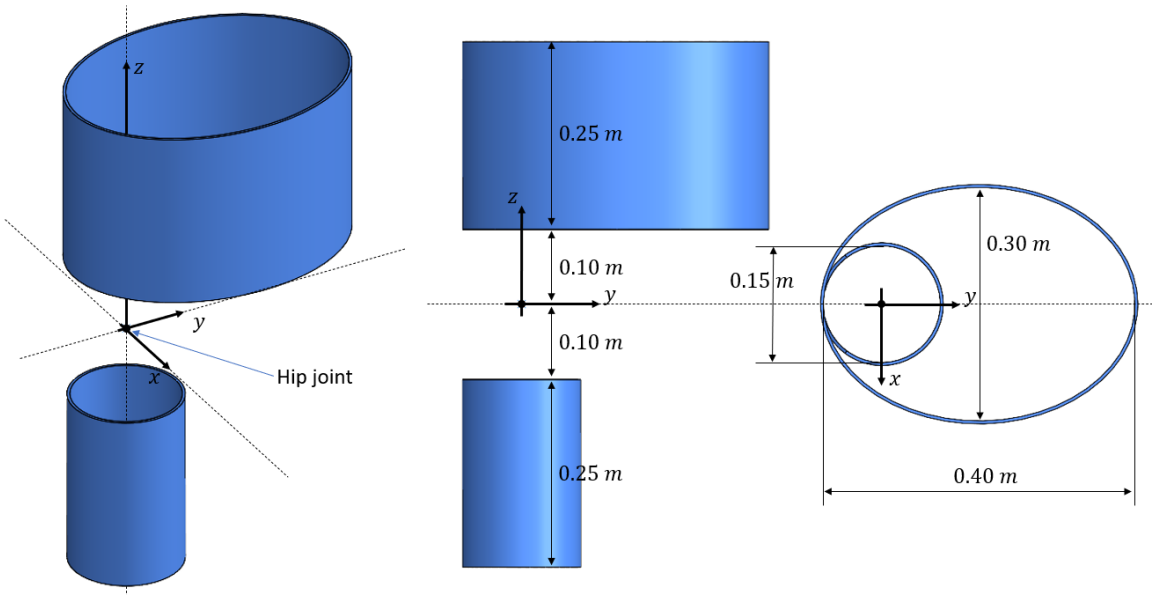

Figure 4.3: Dimensions of the attachment parts, excluding their thickness.

4.2.4 Thickness

Requirement 2d states that the attachment parts must be sufficiently stiff to ensure that if the body weight applies a 57 Nm adduction moment, the resulting adduction deformation of the attachment parts themselves remains below 1.0°.

Load distribution approximation

First, it needs to be approximated how the 57 Nm adduction moment distributes across the attachment parts.

The *shape* of this load distribution is assessed using the 2D COMSOL Finite Element Method (FEM) model illustrated in Figure 4.4. Two blocks of material are used to simulate the upper leg of the limb in stance, and the upper body of the patient. The attachment parts of the orthosis are modeled as a splint lateral to the patient's body that is fixed to the upper body and upper leg. For the human body, a linear elastic and isotropic material model is assumed. The exact stiffness of the material is irrelevant, since the sole focus of this model is to determine the *shape* of the load distribution, while the *magnitude* of the load distribution is computed in subsequent steps. In this case, common material properties for steel types are implemented. A rigid material model is applied to the attachment parts, considering that the attachment parts are supposed to be much stiffer than the human body. The leg and upper body material blocks are both hinged in the hip joint. Aside from this point, there is no contact between the two bodies, meaning that their boundaries are free to separate and intersect with each other. The bottom edge of the leg is fixed to the ground. A load is applied at the center of gravity, in the negative z-direction to generate an adduction moment about the hip joint. Again, since the sole focus of this analysis is to determine the *shape* of the load distribution, the magnitude of this load is irrelevant. In this case, a unit load is applied. The default physics-controlled mesh is used with the element size set to *Extremely fine*. Reaction forces are only evaluated at mesh nodes, meaning that a finer mesh gives a smoother reaction force curve. A stationary study step is added to perform a linear analysis.

For a detailed description of the input data of this model, see Appendix B.2.

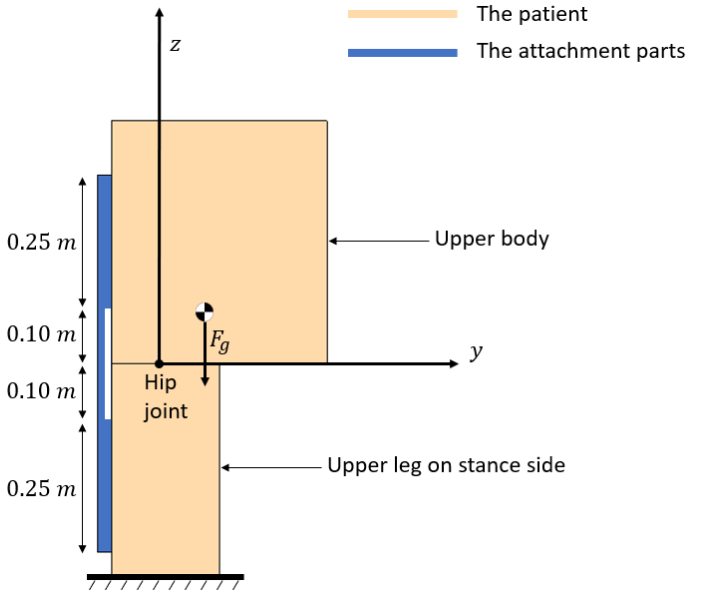

Figure 4.4: 2D COMSOL model in developed to determine the *shape* of the load distribution between the patient's body and the attachment parts of the orthosis, when an adduction moment is applied.

Figure 4.5 shows the reaction force on the patient's body along the line of contact attachment parts of the orthosis. The load distribution on the attachment parts is equal and in opposite direction. For practical purposes, this load distribution is approximated as plotted in Figure 4.6. Here, the load's magnitude is represented by the yet to be determined parameter A.

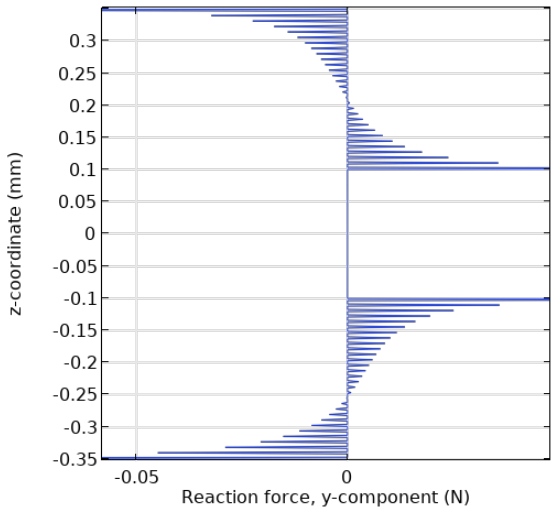

Figure 4.5: Reaction force on the patient's body along the line of contact with the attachment parts of the orthosis.

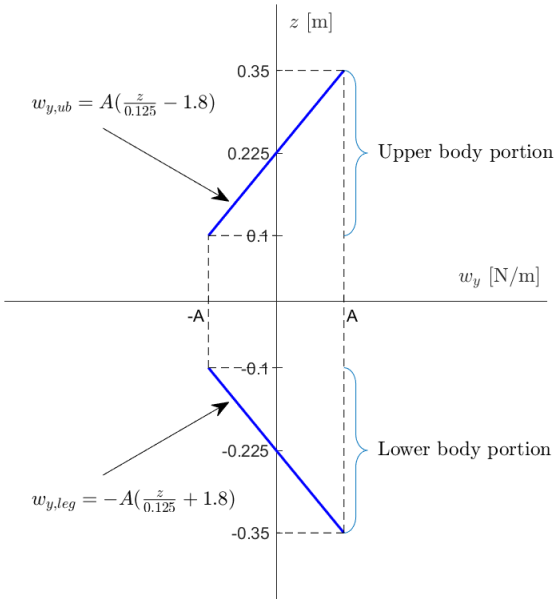

Figure 4.6: Approximated load distribution on the attachment parts of the orthosis along the line of contact with the patient's body.

The *magnitude* of the load distribution is determined by deriving the value of the parameter A. This is based on the knowledge that this load distribution is a consequence of the 57 Nm adduction moment applied by the body weight. Hence, the adduction moment of this load distribution also equals 57 Nm. This applies to both the upper body and leg portion. For the upper body portion, A is derived as follows:

$$
\begin{aligned}
M_{add,ub} &= 57 \text{ Nm} \\
\int_{0.10}^{0.35} w_{y,\text{ub}} \cdot z \, dz &= 57 \text{ Nm} \\
\int_{0.10}^{0.35} A \left(\frac{z}{0.125} - 1.8 \right) z \, dz &= 57 \text{ Nm} \\
\implies A &= 5.5 \cdot 10^3 \text{ N/m}
\end{aligned}
$$

Stiffness analysis

Now that the load distribution on the attachment parts is established, their thickness must be selected to ensure sufficient stiffness. A COMSOL FEM model is developed to conduct a stiffness analysis. This model uses the geometry provided in Figure 4.3, which is imported to COMSOL using the LiveLink for SolidWorks option.

The Solid Mechanics interface is selected to define the physics of the model. The previously determined load distribution is applied to the attachment parts along the edges that are highlighted red in Figure 4.7a. Figure 4.7b illustrates the resulting load in COMSOL. The faces highlighted red in Figure 4.7c are subjected to a fixed constraint.

The default physics-controlled mesh is selected, as it provides sufficient computational efficiency for this analysis. The analysis is performed using a stationary study, while enabling the *Include geometric nonlinearity* option.

A detailed description of the input data for this COMSOL FEM model can be found in Appendix B.3.

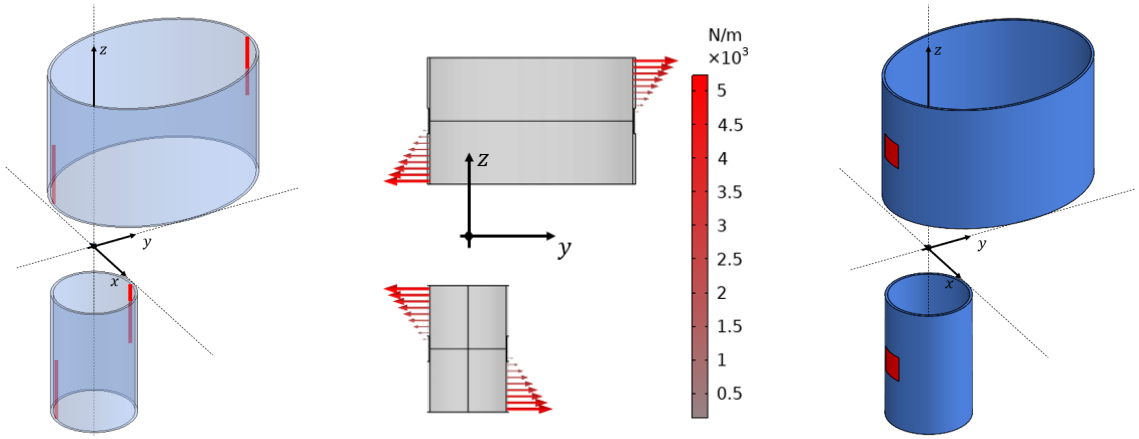

(a) Edges to which the load is applied.

(b) Load distribution result in COMSOL.

(c) Faces subjected to a fixed constraint.

Figure 4.7: Illustration of the boundary conditions applied to the attachment parts.

For varying values of the thickness, the resulting adduction deformation of the attachment parts was measured following the method illustrated in Figure 4.8. Table 4.9 shows that at a thickness of 5.0 mm, the adduction deformation is smaller than 1.0°, indicating sufficient stiffness to meet Requirement 2d. This thickness falls within the normal range of 2.0 mm to 8.0 mm, as specified in Section 4.2.1, indicating that adjustment to carbon fiber is not necessary.

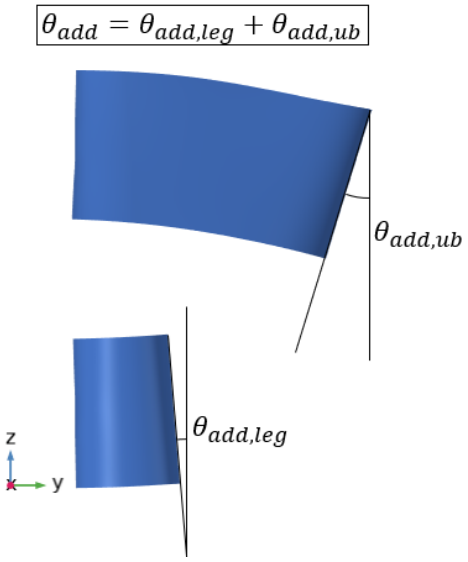

Figure 4.8: Measurement method for the adduction deformation.

Thickness (mm)	θ_{add} (°)
1.0	18.63
2.0	8.47
3.0	3.84
4.0	2.01
5.0	0.78

Figure 4.9: Adduction deformation for varying values of the thickness.

4.3 Design evaluation

Section 4.2 presented a preliminary attachment parts design, developed using the established methods and materials for orthotic design. In this section, the design is evaluated with respect to the requirements outlined in Section 3.4. Whether or not the **must** statements are satisfied will indicate the suitability of these established methods and materials for this application. The extent to which the design remains within the limits specified in the **must** statements determines the margins available for the mechanism design.

The requirements specific to the attachment parts have already been accounted for during the design process. Therefore, this evaluation focuses on the general orthosis requirements, 3a through 3c, concerning the orthosis' mass, thickness, and surface area.

The mass and thickness of the preliminary attachment parts design is 2.5 kg and 5.0 mm, respectively. The **must** statements in Requirements 3a and 3b specify that the mass and thickness of the orthosis as a whole must be smaller than 5.0 kg and 5.0 cm. Therefore, the mechanism design must have a mass smaller than 2.5 kg and a thickness smaller than 4.5 cm.

The internal surface area of the preliminary attachment parts design is 0.39 cm^2. Requirement 3c does not incorporate a **must** statement specifying a maximum allowable surface area, but promotes minimization. In this attachment parts design, maximization of surface area was chosen to minimize pressure on the patient's body. However, for the mechanism design, surface area minimization remains important.

The preliminary attachment parts design satisfies all **must** statements with sufficient margin left for the

mechanism design. These results confirm the suitability of the established orthotic methods and materials for this application.

4.4 Artist impression

This chapter presented a preliminary attachment parts design developed using the established techniques for custom-made orthoses. Given the absence of a specific patient for this thesis, measurements of the hypothetical patient introduced in Section 3.2 were used with simplified shapes for the human body. Figure 4.10 shows an artist impression of what the design would look like on an actual patient, when a thermoforming process is implemented to adapt to the curves of their body.

Chapter 5 proceeds with the concept phase for the orthosis mechanism.

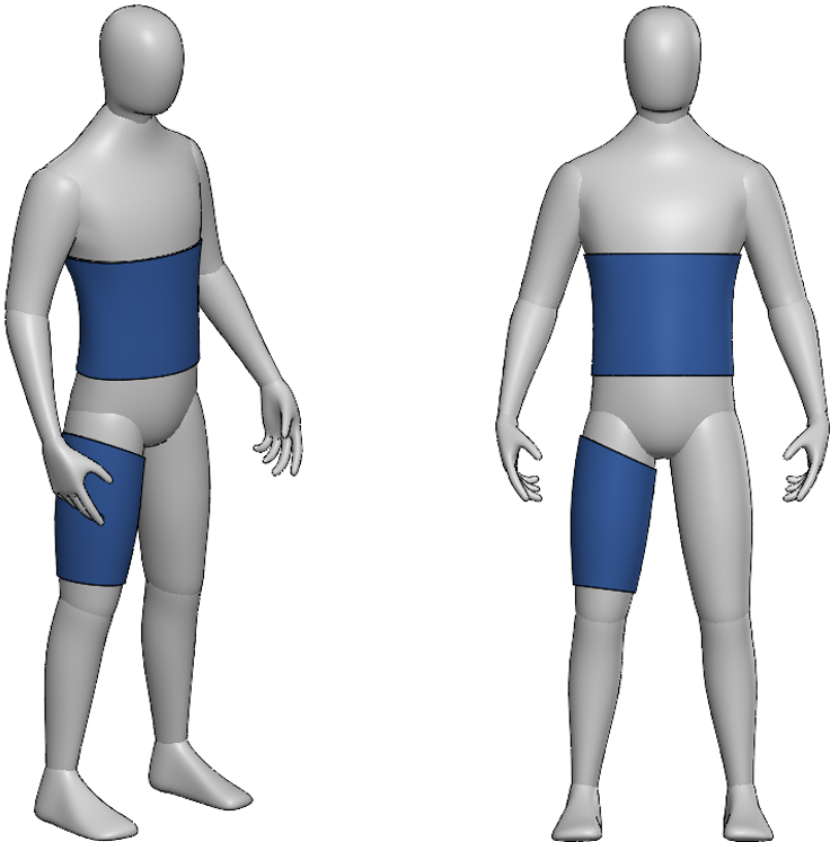

Figure 4.10: Artist impression of the attachment parts of the orthosis in isometric and anterior view.

5 Orthosis mechanism concept phase

5.1 Introduction

This chapter describes the concept phase for the orthosis mechanism. It begins with the generation of nine concepts in Section 5.2, one of which represents the concept of the previously researched design introduced in Section 2.4. Section 5.3 qualitatively evaluates these concepts, identifying the two most promising solutions. Section 5.4 follows with a quantitative evaluation of these two concepts, conducted by developing a preliminary design for each and evaluating its performance. Based on this evaluation, Section 5.5 selects the most promising concept to be taken forward into the design phase. The chapter concludes with a validation of the selected concept's working principle using a scale model in Section 5.6.

5.2 Concept generation

The FACT method for compliant mechanism design, introduced in Section 2.5, is used to generate concepts. This method offers a systematic approach for selecting the compliant components needed to achieve a desired set of degrees and freedom. Given that the hip joint itself inherently constrains translations, only rotations are considered.

The functional needs analysis provided in Section 3.3 identified the need for one rotational constraint to restrict adduction, and one rotational degree of freedom to allow flexion/extension. The third rotation, for internal/external rotation of the hip joint, is indifferent. Therefore, freedom systems with either one or two rotational degrees of freedom are selected from the FACT table illustrated in Figure 2.14. Their corresponding constraint systems are created using leaf and wire flexures.

This has resulted in nine concepts, shown in Figures 5.1 through 5.9. In each figure, subfigure (a) shows the mechanism and its orientation relative to the patient's body. Subfigures (b) and (c) display the corresponding constraint and freedom systems. Subfigure (d) shows the mechanism again, together with the part of the freedom system that intersects the hip joint, thereby illustrating the hip joint movements allowed by the mechanism.

Among these concepts, Concept 4 represents the concept of the previously researched design introduced in Section 2.4.

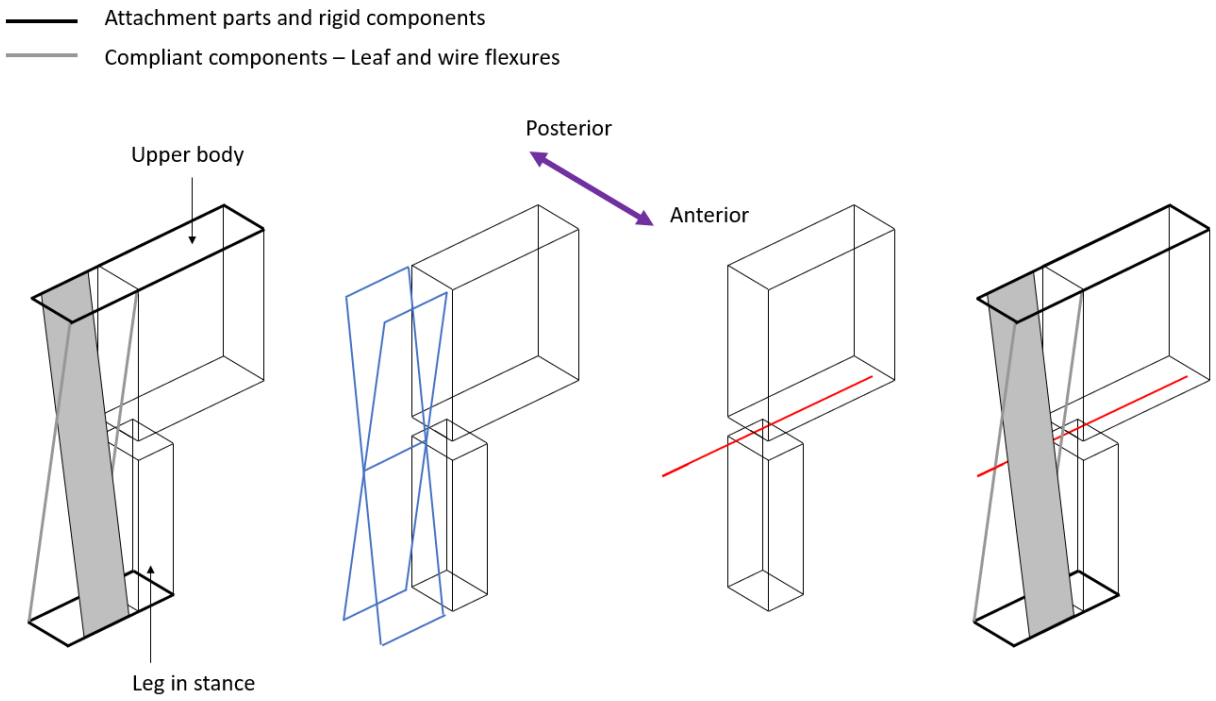

(a) Concept 1.

(b) Constraint system of Concept 1.

(c) Freedom system of Concept 1.

(d) Concept 1 and the portion of its freedom system intersecting the hip joint.

Figure 5.1

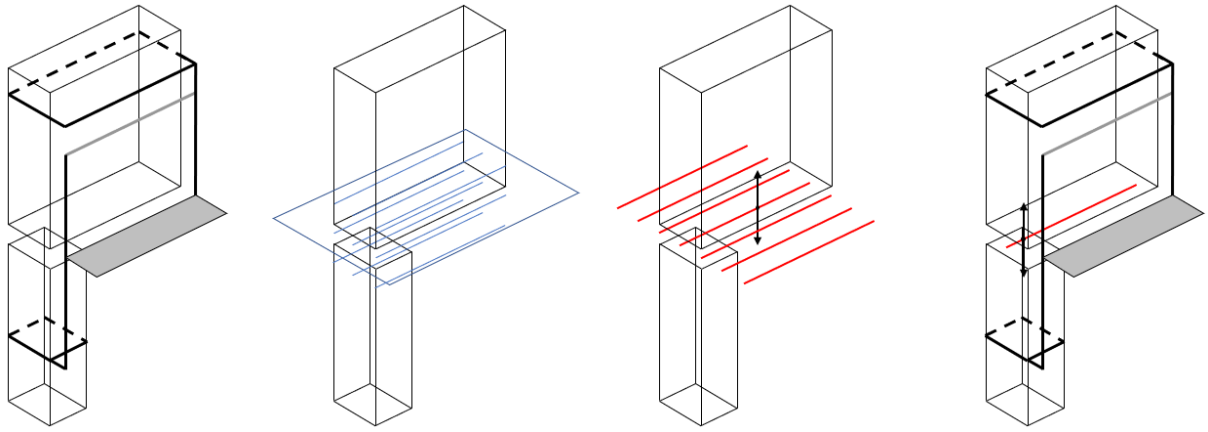

(a) Concept 2.

(b) Constraint system of Concept 2.

(c) Freedom system of Concept 2.

(d) Concept 2 and the portion of its freedom system intersecting the hip joint.

Figure 5.2

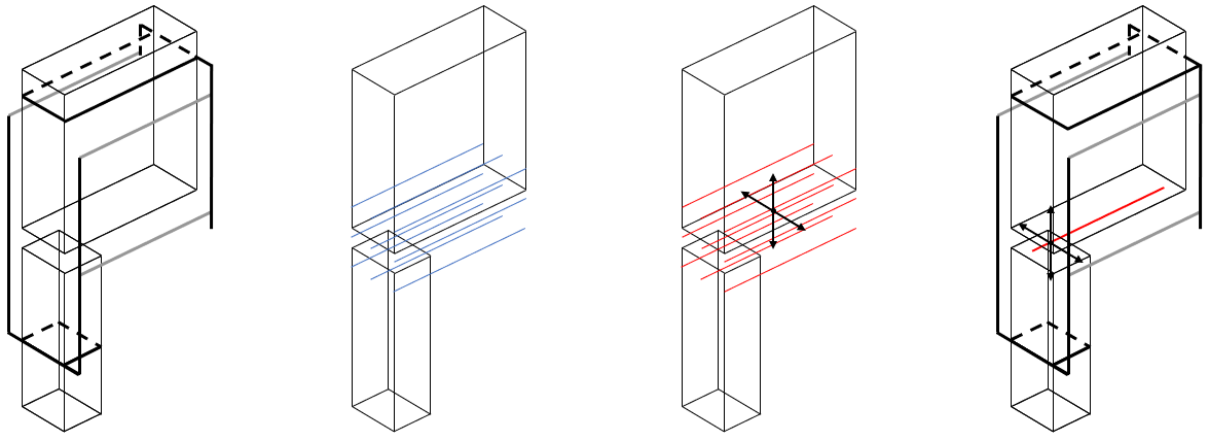

(a) Concept 3.

(b) Constraint system of Concept 3.

(c) Freedom system of Concept 3.

(d) Concept 3 and the portion of its freedom system intersecting the hip joint.

Figure 5.3

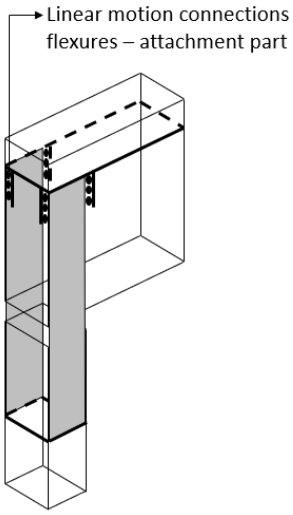

(a) Concept 4, representing the concept of the previously researched design.

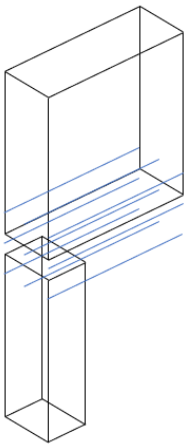

(b) Constraint system of Concept 4.

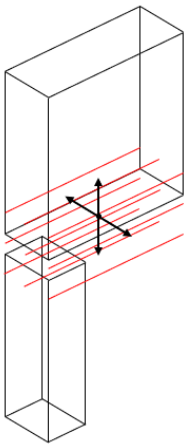

(c) Freedom system of Concept 4.

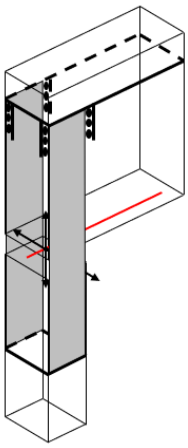

(d) Concept 4 and the portion of its freedom system intersecting the hip joint.

Figure 5.4

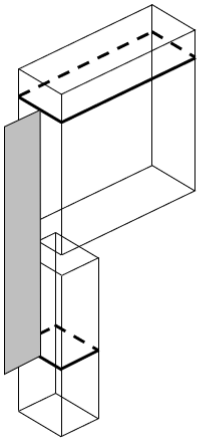

(a) Concept 5.

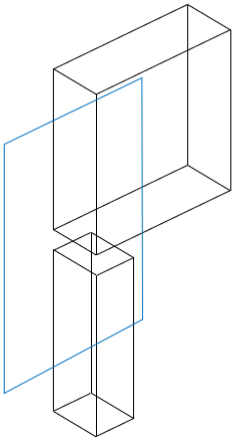

(b) Constraint system of Concept 5.

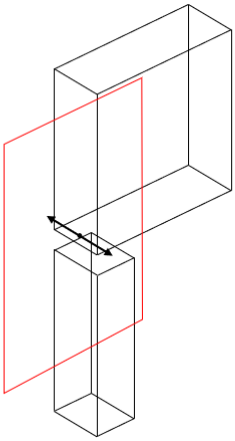

(c) Freedom system of Concept 5.

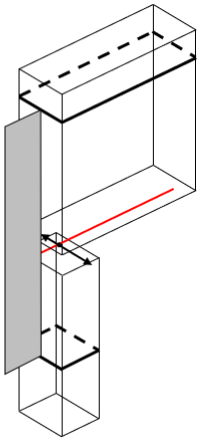

(d) Concept 5 and the portion of its freedom system intersecting the hip joint.

Figure 5.5

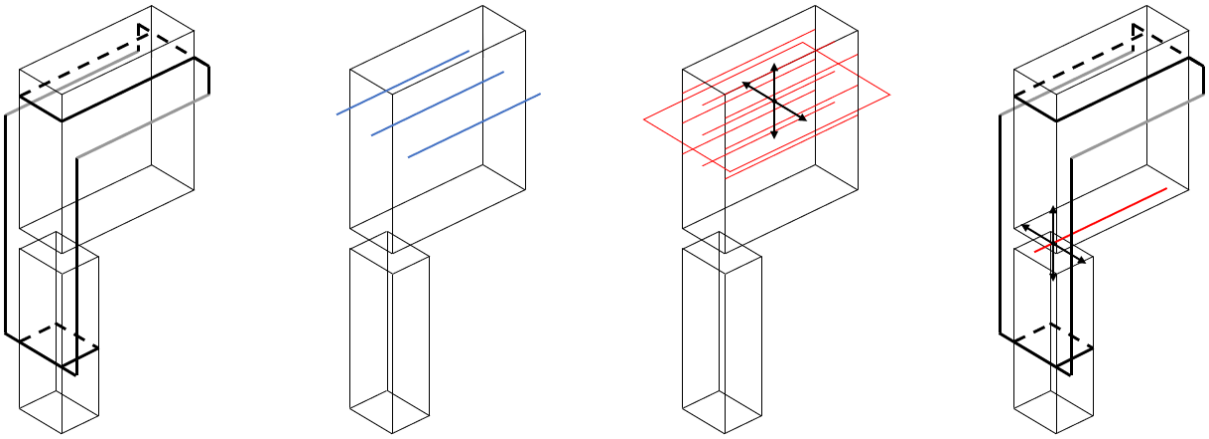

(a) Concept 6.

(b) Constraint system of Concept 6.

(c) Freedom system of Concept 6.

(d) Concept 6 and the portion of its freedom system intersecting the hip joint.

Figure 5.6

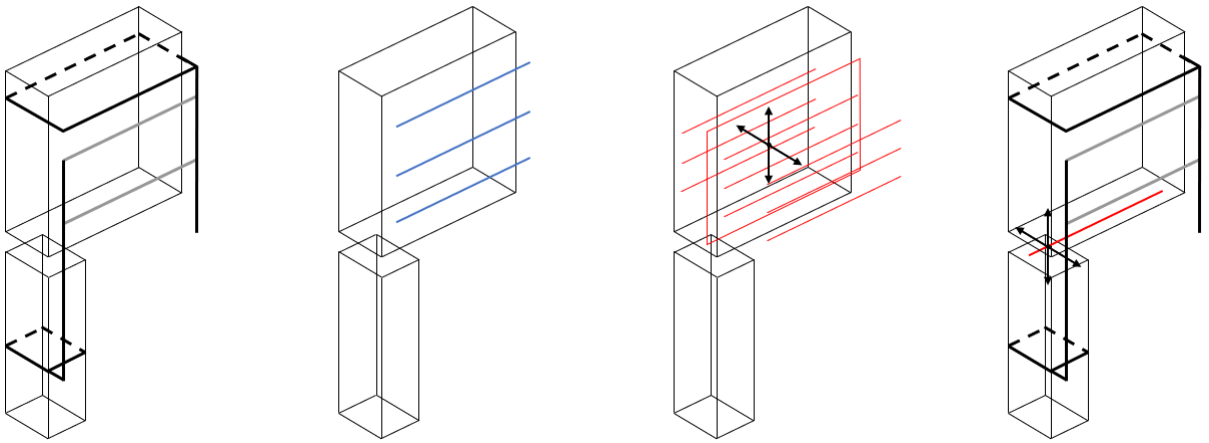

(a) Concept 7.

(b) Constraint system of Concept 7.

(c) Freedom system of Concept 7.

(d) Concept 7 and the portion of its freedom system intersecting the hip joint.

Figure 5.7

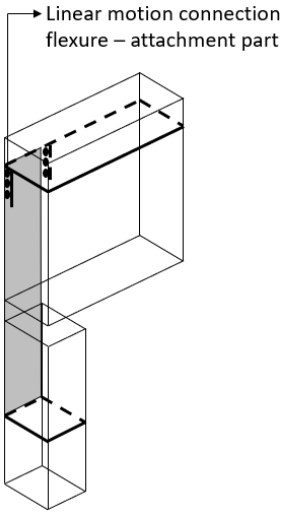

(a) Concept 8.

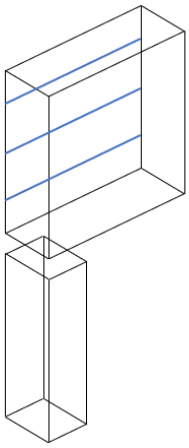

(b) Constraint system of Concept 8.

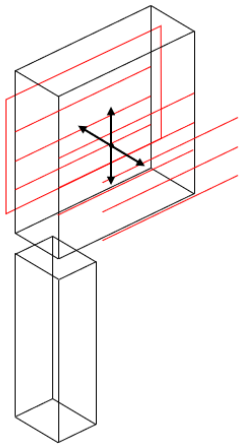

(c) Freedom system of Concept 8.

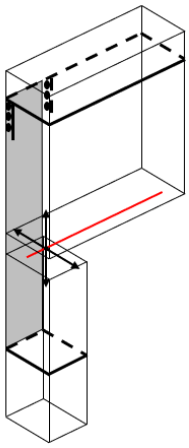

(d) Concept 8 and the portion of its freedom system intersecting the hip joint.

Figure 5.8

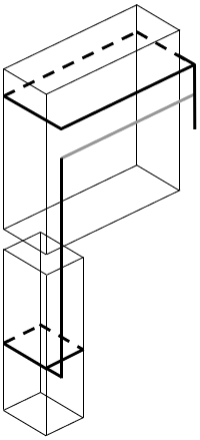

(a) Concept 9.

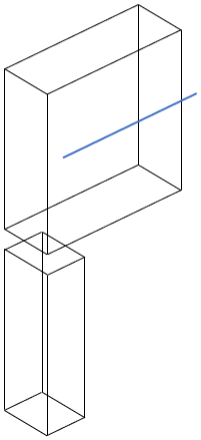

(b) Constraint system of Concept 9.

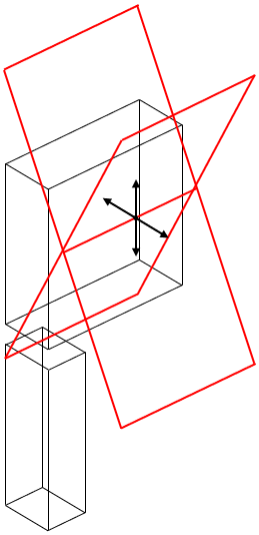

(c) Freedom system of Concept 9.

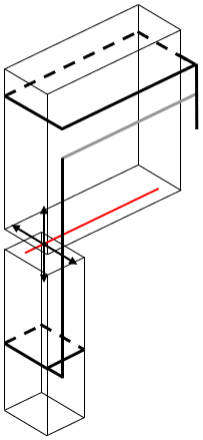

(d) Concept 9 and the portion of its freedom system intersecting the hip joint.

Figure 5.9

5.3 Qualitative concept evaluation

In this section, the most promising concepts are identified through a qualitative evaluation process.

In Concepts 2, 3, 6, 7, and 9, the compliant components are connected to rigid components crossing the hip joint. Upon hip flexion/extension, the kinematic path of these rigid components interferes with the patient's body. Therefore, they must be replaced by compliant components that provide flexion/extension freedom.

Since the new compliant components are placed in series with the original ones, they must also provide the necessary adduction constraint. As a result, the full functionality of the original compliant components – constraining adduction while allowing flexion/extension – is taken over by the new components, making the original compliant components redundant. Therefore, these concepts are eliminated.

Among Concepts 1, 4, 5, and 8, Concepts 4 and 8 offer the most potential for a compact design due to their flat orientation relative to the human body. Therefore, these are considered the most promising solutions.

5.4 Quantitative evaluation of Concepts 4 and 8

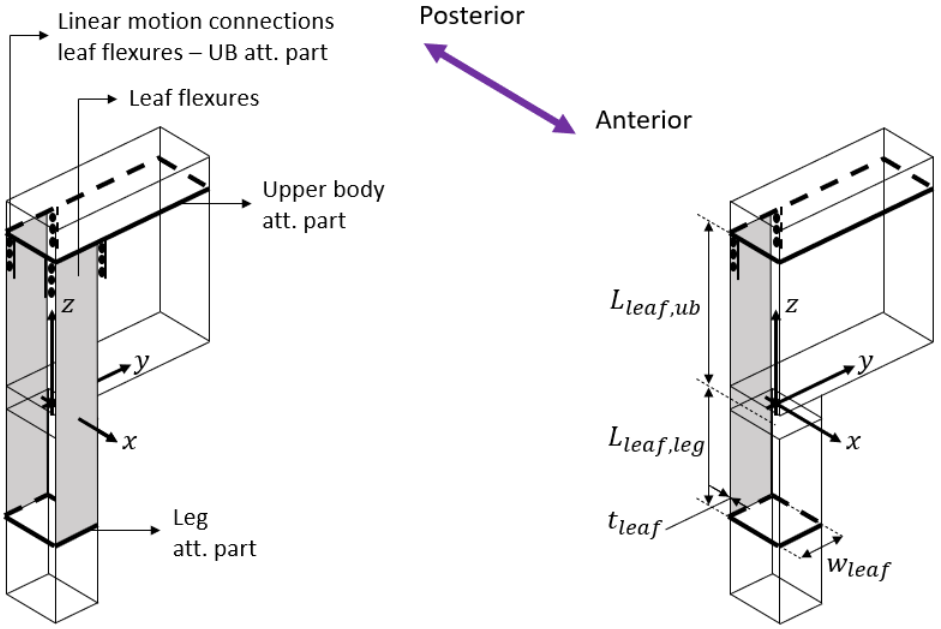

(a) Concept 4, representing the concept of the previously researched design.

(b) Concept 8.

Figure 5.10: The two concepts selected for quantitative evaluation.

Section 5.3 identified Concepts 4 and 8 as the most promising solutions. Concept 4 features two leaf flexures, one anterior and one posterior to the patient's body, whereas Concept 8 contains only one leaf flexure on the posterior side. Both concepts incorporate a linear motion connection between the top ends of the leaf flexures and the upper body attachment part of the orthosis. The bottom ends are fixed to the leg attachment part.

This section quantitatively evaluates these concepts by developing a preliminary design for each and evaluating its performance. Simplifications and straightforward modeling techniques are used during the design and evaluation process to provide a rough, yet informative approximation of each concept's potential.

5.4.1 Preliminary design approach

The development and evaluation of the preliminary designs is guided by Table 5.1, representing a refined and simplified version of the requirements outlined in Section 3.4.

The *refinement* lies in determination of the mechanism's maximum allowable mass and thickness. Requirements 3a and 3b specify the maximum allowable mass and thickness of the orthosis as a whole. By subtracting the mass and thickness of the preliminary attachment parts design, presented in Chapter 4, the maximum allowable values for the mechanism alone are determined.

The *simplification* concerns the evaluation position for adduction stiffness and von Mises stress. Requirements 1a and 1c state that these properties must be evaluated across the entire range of motion, from 8° extension to 30° flexion. In this phase, the 30° flexion position is assumed to be critical within this range and is therefore used for evaluation.

The mechanism design must satisfy all **must** statements in this table. Additionally, optimization for the **should** statements is encouraged to improve its performance. Based on expert advice from Simone Schoon [19], flexion stiffness minimization is prioritized, as this is expected to have the most significant impact on patient walking experience

Property	**Req**	**Must**	**Should**
Adduction stiffness	1a	$\theta_{add} \mid_{\theta_{flex}=30°}^{M_{add}=57\,\mathrm{Nm}} < 1.0°$	
Flexion stiffness	1b	$M_{flex} \mid_{\theta_{flex}=30°} < 43\,\mathrm{Nm}$	Min $M_{flex} \mid_{\theta_{flex}=30°}$
Von Mises stress	1c	$\sigma_{VM,max} \mid_{\theta_{flex}=30°}^{M_{add}=57\,\mathrm{Nm}} < \sigma_f$	
Mass	3a	$m_{mech} < 2.5$ kg	Min m_{mech}
Thickness	3b	$t_{mech} < 4.5$ cm	Min t_{mech}
Surface area	3c		Min A_{mech}

Table 5.1: Refined and simplified requirements for the preliminary design of Concepts 4 and 8.

5.4.2 Assumptions

The following assumptions were made during the development and evaluation of the preliminary designs:

- The design process focuses exclusively on the design of the leaf flexures in both concepts, excluding the design or selection of a linear motion connections between the leaf flexures and the upper body attachment part. The *functionality* of the linear motion connections is taken into account for the leaf flexure design, assuming zero friction in the direction of linear motion, and infinite stiffness in all other directions. Any additional influence is neglected.

- The design process involves selection of the optimal dimensions and material for the leaf flexures in both concepts.

- The leaf flexures are considered rectangular with the following dimensional parameters: a total length that is subdivided into a leg portion ($L_{leaf,leg}$) and an upper body portion ($L_{leaf,ub}$), a width (w_{leaf}), and a thickness (t_{leaf}). These parameters are visualized in Figure 5.11.
- The dimensional parameter resolution – the step size by which they can be adjusted during the design process – for $L_{leaf,leg}$, $L_{leaf,ub}$, and w_{leaf} is set to 1.0 cm. For t_{leaf}, this is 0.10 mm.
- The anterior and posterior leaf flexures in Concept 4 are considered identical.
- The leaf flexures are assumed to adapt perfectly to the curves of the human body with no clearance.

5.4.3 Preliminary design of Concept 4

Design objective

As stated in Section 5.4.1, the design process focuses on minimizing the flexion stiffness. In doing so, it is crucial to ensure that all **must** statements, as specified in Table 5.1, are met.

Flexion stiffness is inherently linked to adduction stiffness, as both are determined by the same compliant mechanism. Therefore, the initial objective is to minimize the flexion stiffness while ensuring sufficient adduction stiffness. The performance of the resulting design is evaluated with respect to all requirements as outlined in Table 5.1. If any of the **must** statements are not met, the design will be adjusted in subsequent steps.

Design space definition

First, the design space for the dimensional parameters of the leaf flexures is defined to guide the parameter selection process.

To avoid non-existent geometry, the length, width and thickness of the leaf flexures must be strictly positive. For w_{leaf} and t_{leaf}, the lower boundaries are set equal to the parameter resolutions defined in Section 5.4.2, as these are the smallest feasible positive values. For $L_{leaf,ub}$, the lower boundary is set to 0.10 m, to accommodate downward displacement of the top end of the posterior leaf flexure during hip flexion. Since this ensures a positive leaf flexure length for all non-negative values of $L_{leaf,leg}$, the lower boundary for this parameter is set to 0.00 m.

The upper boundaries for $L_{leaf,leg}$ and $L_{leaf,ub}$ are set equal to the lengths of the upper leg and upper body of the hypothetical patient introduced in Section 3.2, respectively. The upper boundary for w_{leaf} is set to half the hip breadth. The upper boundary for t_{leaf} is implicitly specified through the maximum allowable mechanism thickness defined in Table 5.1. Given the assumption that the leaf flexures adapt perfectly to the curves of the human body with no clearance, as stated in Section 5.4.2, the upper boundary of t_{leaf} is set equal to the maximum allowable mechanism thickness.

An overview of the resulting design space is provided in Table 5.2.

Parameter	Lower boundary	Upper boundary
$L_{leaf,leg}$	0.00 m	0.35 m
$L_{leaf,ub}$	0.10 m	0.45 m
w_{leaf}	0.010 m	0.20 m
t_{leaf}	0.10 mm	45 mm

Table 5.2: Design space for the dimensional parameters of the leaf flexures.

Initial selection of dimensions and material

The objective of minimizing flexion stiffness while ensuring sufficient adduction stiffness suggests that maximizing the stiffness ratio between adduction and flexion is desirable. Given the complexity of compliant mechanisms, a simplified approach is adopted in this phase, where linear beam theory is used to predict the influence of the dimensional parameters of the leaf flexures on this stiffness ratio. This analysis results in an initial selection of dimensions and material for the leaf flexures.

Considering the flexures as cantilever beams with an endpoint moment, the adduction and flexion stiffness are given by:

$$k_{add} = \frac{EI_{add}}{L_{leaf,leg} + L_{leaf,ub}}, \quad \text{and} \quad k_{flex} = \frac{EI_{flex}}{L_{leaf,leg} + L_{leaf,ub}}$$

Here, $I_{flex} = \frac{w_{leaf} t_{leaf}^3}{12}$ and $I_{add} = \frac{t_{leaf} w_{leaf}^3}{12}$ [53]. Substituting these into the stiffness equations and simplifying yields the following relation for the adduction-to-flexion stiffness ratio:

$$\frac{k_{add}}{k_{flex}} = \frac{w_{leaf}^2}{t_{leaf}^2}$$

Maximization of this stiffness ratio requires maximization of w_{leaf} and minimization of t_{leaf}. Given the design space outlined in Table 5.2, $w_{leaf} = 0.20$ m and $t_{leaf} = 0.10$ mm are selected.

$L_{leaf,leg}$, $L_{leaf,ub}$, and E (Young's modulus) canceled out of the equation, suggesting they have no direct influence on the stiffness ratio. Therefore, $L_{leaf,leg} = 0.20$ m and $L_{leaf,ub} = 0.20$ m are selected as these are moderate values within the design space of these parameters. Although the Young's modulus may not affect the stiffness ratio, selecting a material with a high value for this parameter enables more compact design. Steel is chosen as it combines a high Young's modulus with high strength, which is advantageous for satisfying the fatigue criterion defined in Requirement 1c.

The resulting initial selection of dimensions and material for the leaf flexures, based on this theoretical stiffness analysis, is summarized in Table 5.3. The material properties for steel were derived from material database Granta EduPack [52].

Dimensions		**Material**	
$L_{leaf,leg}$	$= 0.20$ m	Type	= Steel
$L_{leaf,ub}$	$= 0.20$ m	E	$= 210$ GPa
w_{leaf}	$= 0.20$ m	ρ	$= 7.8 \cdot 10^3$ kg/m^3
t_{leaf}	$= 0.10$ mm	ν	$= 0.28$
		σ_f	$= 500$ MPa

Table 5.3: Initial selection of dimensions and material for the leaf flexures.

Final selection of dimensions and material

The dimensions and material presented in Table 5.3 were selected for maximization of the adduction-to-flexion stiffness ratio. However, it needs to be verified whether whether the minimum required adduction stiffness, as specified in Table 5.1, is met. The table states that the adduction stiffness is evaluated through measurement of the adduction angle resulting from a 57 Nm adduction moment applied at a 30° flexion angle. A SolidWorks FEM model is developed to analyze this problem.

Figure 5.11 shows the model's geometry. The distance between the hip joint and the leaf flexures is set to 0.15 m, based on the measurements of the hypothetical patient introduced in Section 3.2.

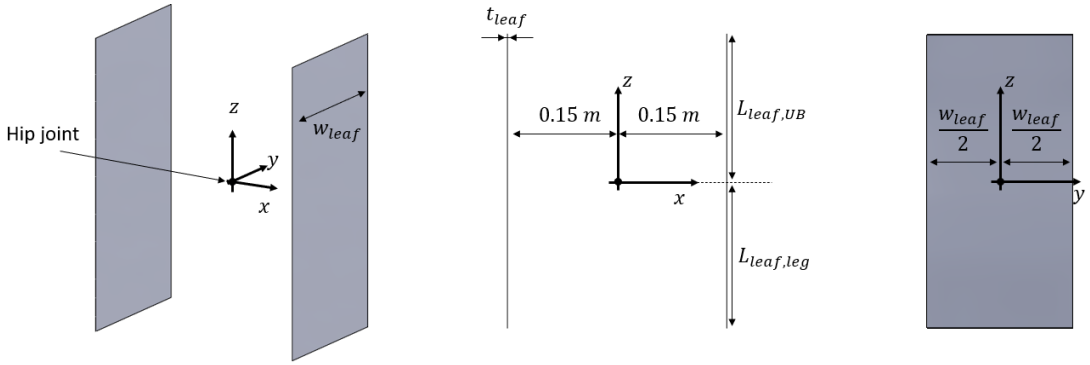

Figure 5.11: Geometry of the SolidWorks FEM model used for the preliminary design of Concept 4.

In this model, hip flexion is simulated by leg movement, while adduction is simulated by upper body movement. To model a 30° flexion angle, a 30° rotation about the negative y-axis is prescribed to the bottom ends of the leaf flexures. To model a 57 Nm adduction moment, the top ends of the leaf flexures are subjected to a 57 Nm moment about the negative x-axis. To accurately simulate leaf flexure deformation upon hip adduction, the top ends of the leaf flexures should be constrained to movement on a circle about the x-axis. The radius of this circle should be free to vary due to the linear motion connection between the leaf flexures and the upper body attachment part. However, due to limitations of SolidWorks, this boundary condition could not be defined. As a result, they are constrained to move freely and independently in the y-z-plane, which serves as a sufficient approximation for this phase. The resulting adduction angle is measured as the rotation angle of the top ends of the leaf flexures in negative x-direction.

The standard mesh automatically generated by SolidWorks was used without conducting a mesh convergence study, as time-efficiency is prioritized over optimizing accuracy at this stage. The flexures are modeled as solid bodies resulting in a mesh composed of solid elements. In the study settings, *Large Displacement* is selected, making this a geometrically nonlinear analysis.

A detailed description of the input data for this model can be found in Appendix B.4.

t_{leaf} (mm)	$\theta_{add,ant}$ (°)	$\theta_{add,post}$ (°)
0.10	Error	Error
0.30	31	29
0.50	13	12
0.70	2.4	2.3
0.90	1.3	1.2
1.0	1.1	0.91
1.1	0.84	0.72

Table 5.4: Adduction angles in both leaf flexures resulting from a 57 Nm adduction moment applied at a 30° flexion angle, measured for varying values of t_{leaf}.

Table 5.4 presents the adduction angles in both leaf flexures for varying values of t_{leaf}. According to Table 5.1, the adduction angle must remain below 1.0° to ensure sufficient adduction stiffness. For the initially selected thickness $t_{leaf} = 0.10$ mm, the simulation resulted in an error indicating excessive incremental strain. This suggests that the deformation under adduction is too large, and therefore, the stiffness is insufficient. By incrementally increasing this parameter, it was determined that the adduction stiffness requirement is met at $t_{leaf} = 1.1$ mm. Consequently, the initially selected thickness is adjusted to this value. The final selected dimensions and material for the leaf flexures are summarized in Table 5.5.

Dimensions		**Material**	
$L_{leaf,leg}$	= 0.20 m	Type	= Steel
$L_{leaf,ub}$	= 0.20 m	E	= 210 GPa
w_{leaf}	= 0.20 m	ρ	= $7.8 \cdot 10^3$ kg/m^3
t_{leaf}	= 1.1 mm	ν	= 0.28
		σ_f	= 500 MPa

Table 5.5: Final selection of dimensions and material for the leaf flexures.

Performance measurements

The performance of the preliminary design is measured with respect to all requirements, as stated in Table 5.1.

Requirement 1a: Adduction stiffness

The adduction stiffness is evaluated through measurement of the adduction angle resulting from a 57 Nm adduction moment applied at a 30° flexion angle.

This measurement was already conducted during the design process. Table 5.4 shows that the resulting adduction angles are 0.84° and 0.72°, in the anterior and posterior leaf flexure, respectively.

Figure 5.13 illustrates the corresponding deformation, suggesting that adduction deformation occurs mainly due to lateral bending through torsion of the leaf flexures.

Requirement 1b: Flexion stiffness

The flexion stiffness is evaluated through measurement of the hip flexion moment required to achieve a 30° flexion angle.

This measurement is conducted in the same SolidWorks FEM model, by eliminating the applied adduction moment, resulting in simulation of only the 30° flexion angle. Investigation of the reaction forces indicates

a required hip flexion moment of 16 Nm.

Figure 5.12 shows the corresponding deformation, illustrating the kinematics of the mechanism's degree of freedom.

Requirement 1c: Von Mises stress
The von Mises stress is evaluated through measurement of its maximum, resulting from a 57 Nm adduction moment applied at a 30° flexion angle.

Figure 5.14 illustrates the stress distribution across the leaf flexures under these conditions, retrieved from the SolidWorks FEM model. The maximum von Mises stress is 406 MPa.

Requirement 3a: Mass
Given the assumption that any influence of the linear motion connections between the leaf flexures and the upper body attachment part is neglected in this design, the mass of the mechanism equals the mass of the leaf flexures. Based on the dimensions and material outlined in Table 5.5, the resulting mass is 1.4 kg.

Requirement 3b: Thickness
Given the assumption that the leaf flexures adapt perfectly to the curves of the human body with no clearance, and that any influence of the linear motion connections is neglected, the mechanism thickness equals the leaf flexure thickness of 1.1 mm.

Requirement 3c: Surface area
Given the assumption that any influence of the linear motion connections is neglected, the mechanism's surface area equals that of the leaf flexures, which is 0.16 m^2.

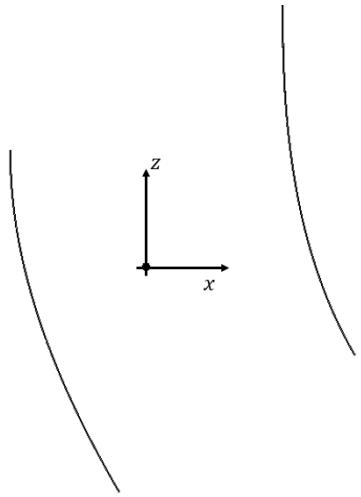

Figure 5.12: Lateral view of the deformation of the leaf flexures resulting from a 30° prescribed flexion angle.

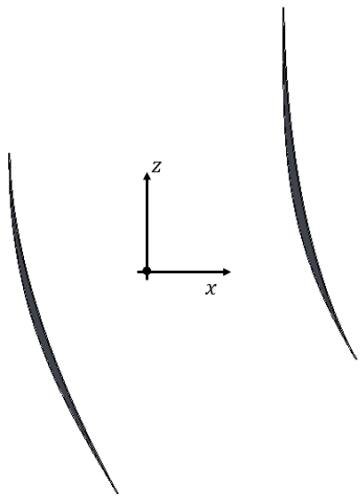

Figure 5.13: Lateral view of the deformation of the leaf flexures resulting from a 57 Nm adduction moment applied at a 30° flexion angle.

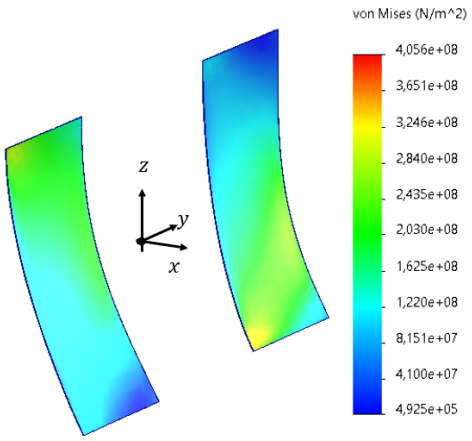

Figure 5.14: Von Mises stress distribution on the leaf flexures resulting from a 57 Nm adduction moment applied at a 30° flexion angle.

Performance evaluation
The performance measurements presented above have been incorporated into Table 5.1 to evaluate the performance of the preliminary design. The results are shown in Table 5.6.

The design objective was to minimize the flexion stiffness while ensuring sufficient adduction stiffness. The resulting preliminary design requires a 16 Nm hip flexion moment to achieve a 30° flexion angle. The table also shows that, in addition to the minimum required adduction stiffness, the design satisfies the **must** statements in all other requirements. Therefore, this preliminary design is accepted as a satisfactory solution, meaning that no adjustments are necessary.

Property	Req	Must	Should	Performance
Adduction stiffness	1a	$\theta_{add} \mid_{\theta_{flex}=30°}^{M_{add}=57\,\text{Nm}} < 1.0°$		$\theta_{add,ant} = 0.84°$ $\theta_{add,post} = 0.72°$
Flexion stiffness	1b	$M_{flex} \mid_{\theta_{flex}=30°} < 43\,\text{Nm}$	Min $M_{flex} \mid_{\theta_{flex}=30°}$	$M_{flex} = 16$ Nm
Von Mises stress	1c	$\sigma_{VM,max} \mid_{\theta_{flex}=30°}^{M_{add}=57\,\text{Nm}} < \sigma_f = 500$ MPa		$\sigma_{VM,max} = 406$ MPa
Mass	3a	$m_{mech} < 2.5$ kg	Min m_{mech}	$m_{mech} = 1.4$ kg
Thickness	3b	$t_{mech} < 4.5$ cm	Min t_{mech}	$t_{mech} = 1.1$ mm
Surface area	3c		Min A_{mech}	$A_{mech} = 0.16$ m^2

Table 5.6: Performance evaluation for the preliminary design of Concept 4.

5.4.4 Preliminary design of Concept 8
The development process for the preliminary design of Concept 8 follows the exact same steps as that of Concept 4, with the only difference being the absence of the anterior leaf flexure. To avoid repetition, the design process is not detailed again. Instead, the performance of the resulting preliminary design is measured and evaluated directly. The final selection of dimensions and material for the leaf flexure in Concept 8 are shown in Table 5.7.

The SolidWorks FEM model used for the preliminary design of Concept 8 is detailed in Appendix B.5.

Dimensions		Material	
$L_{leaf,leg}$	= 0.20 m	Type	= Steel
$L_{leaf,ub}$	= 0.20 m	E	= 210 GPa
w_{leaf}	= 0.20 m	ρ	= $7.8 \cdot 10^3$ kg/m^3
t_{leaf}	= 1.3 mm	ν	= 0.28
		σ_f	= 500 MPa

Table 5.7: Final selection of dimensions and material for the leaf flexure.

Performance measurements
Like the design process, the measurement methods for the preliminary design of Concept 8 are identical to those of Concept 4, and are therefore not detailed again. However, to provide insight into its performance, Figures 5.15 through 5.17 show the relevant deformations and stress distribution.

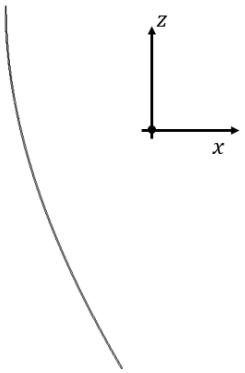

Figure 5.15: Lateral view of the deformation of the leaf flexure resulting from a 30° prescribed flexion angle.

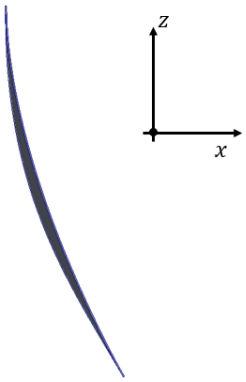

Figure 5.16: Lateral view of the deformation of the leaf flexure resulting from a 57 Nm adduction moment applied at a 30° flexion angle.

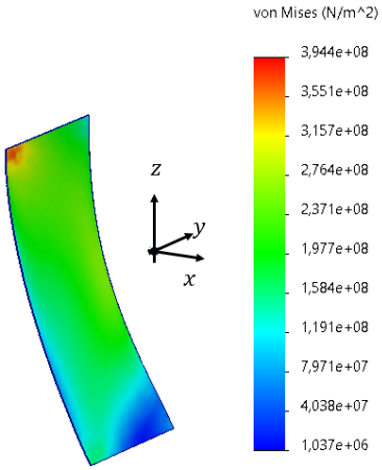

Figure 5.17: Von Mises stress distribution on the leaf flexure resulting from a 57 Nm adduction moment applied at a 30° flexion angle.

Performance evaluation

Table 5.8 shows the performance evaluation for the preliminary design of Concept 8.

The design objective was to minimize the flexion stiffness while ensuring sufficient adduction stiffness. The resulting preliminary design requires a 13 Nm hip flexion moment to achieve a 30° flexion angle. The table also shows that, in addition to the minimum required adduction stiffness, the design satisfies the **must** statements in all other requirements. Therefore, this preliminary design is accepted as a satisfactory solution, meaning that no adjustments are necessary.

Property	Req	Must	Should	Performance
Adduction stiffness	1a	$\theta_{add}\,\vert^{M_{add}=57\,\text{Nm}}_{\theta_{flex}=30°} < 1.0°$		$\theta_{add} = 0.89°$
Flexion stiffness	1b	$M_{flex}\,\vert_{\theta_{flex}=30°} < 43\,\text{Nm}$	Min $M_{flex}\,\vert_{\theta_{flex}=30°}$	$M_{flex} = 13$ Nm
Von Mises stress	1c	$\sigma_{VM,max}\,\vert^{M_{add}=57\,\text{Nm}}_{\theta_{flex}=30°} < \sigma_f = 500$ MPa		$\sigma_{VM,max} = 394$ MPa
Mass	3a	$m_{mech} < 2.5$ kg	Min m_{mech}	$m_{mech} = 0.81$ kg
Thickness	3b	$t_{mech} < 4.5$ cm	Min t_{mech}	$t_{mech} = 1.3$ mm
Surface area	3c		Min A_{mech}	$A_{mech} = 0.080$ m^2

Table 5.8: Performance evaluation for the preliminary design of Concept 8.

5.5 Concept selection

Section 5.4 presented a quantitative evaluation of Concepts 4 and 8 by developing a preliminary design for each and assessing its performance. In this section, the performance of the two preliminary designs is compared to determine which of the corresponding concepts is most promising. This concept is then taken forward into the design phase.

The performance comparison is summarized in Table 5.9. Both preliminary designs satisfy all **must** statements outlined in this table, indicating that both are viable solutions. Their performance with respect to the **should** statements is used to determine which performs best.

Among all **should** statements, flexion stiffness minimization was prioritized during the design process. For this property, the preliminary design of Concept 8 outperforms that of Concept 4, requiring a 13 Nm hip flexion moment to achieve a 30° flexion angle, compared to 16 Nm for the preliminary design of Concept 4. Additionally, its mass and surface area are substantially smaller. In contrast, the preliminary design of Concept 4 has smaller thickness. However, relative to the maximum allowable thickness, the difference between the two values is marginal.

Based on these observations, Concept 8 is considered to offer more potential for flexion stiffness minimization, as well as for enabling a lightweight and compact design, and is therefore taken forward into the design phase. As a result, this thesis does not continue working with the previously researched design introduced in Section 2.4, which was represented by Concept 4.

Property	**Req**	**Must**	**Should**	**Performance Prelim. design Concept 4**	**Performance Prelim. design Concept 8**
Adduction stiffness	1a	$\theta_{add}\,\vert^{M_{add}=57\,\text{Nm}}_{\theta_{flex}=30°} < 1.0°$		$\theta_{add,ant} = 0.84°$ $\theta_{add,post} = 0.72°$	$\theta_{add} = 0.89°$
Flexion stiffness	1b	$M_{flex}\,\vert_{\theta_{flex}=30°} < 43\,\text{Nm}$	Min $M_{flex}\,\vert_{\theta_{flex}=30°}$	$M_{flex} = 16$ Nm	$M_{flex} = 13$ Nm
Von Mises stress	1c	$\sigma_{VM,max}\,\vert^{M_{add}=57\,\text{Nm}}_{\theta_{flex}=30°} < \sigma_f = 500$ MPa		$\sigma_{VM,max} = 406$ MPa	$\sigma_{VM,max} = 394$ MPa
Mass	3a	$m_{mech} < 2.5$ kg	Min m_{mech}	$m_{mech} = 1.4$ kg	$m_{mech} = 0.81$ kg
Thickness	3b	$t_{mech} < 4.5$ cm	Min t_{mech}	$t_{mech} = 1.1$ mm	$t_{mech} = 1.3$ mm
Surface area	3c		Min A_{mech}	$A_{mech} = 0.16$ m^2	$A_{mech} = 0.080$ m^2

Table 5.9: Performance comparison of the preliminary designs of Concepts 4 and 8. Green circles indicate the best performing preliminary design with respect to the **should** statements in the requirements.

5.6 Scale model for concept validation

Before advancing to the design phase, the working principle of the selected concept (Concept 8) was validated using the scale model shown in Figure 5.18.

The scale model demonstrates significantly higher adduction stiffness than flexion/extension stiffness, confirming the intended degrees of freedom and constraints. Additionally, the deformation of the leaf flexure during hip flexion, as well as under an applied adduction moment at a prescribed flexion angle, closely resembles the deformations observed in SolidWorks simulations of the preliminary design (see Figures 5.15 and 5.16).

These observations build confidence in the selected concept and support the decision to proceed with its further development in the design phase.

Note that in this scale model, flexion/extension is illustrated through upper body movement, whereas in SolidWorks this was simulated by leg movement. Also, the scale model allows linear motion of the top end of the leaf flexure using a slot through which the flexure can slide, causing its effective length to change during hip flexion/extension. In contrast, the SolidWorks model used a boundary condition that enabled linear motion without affecting the leaf flexure length.

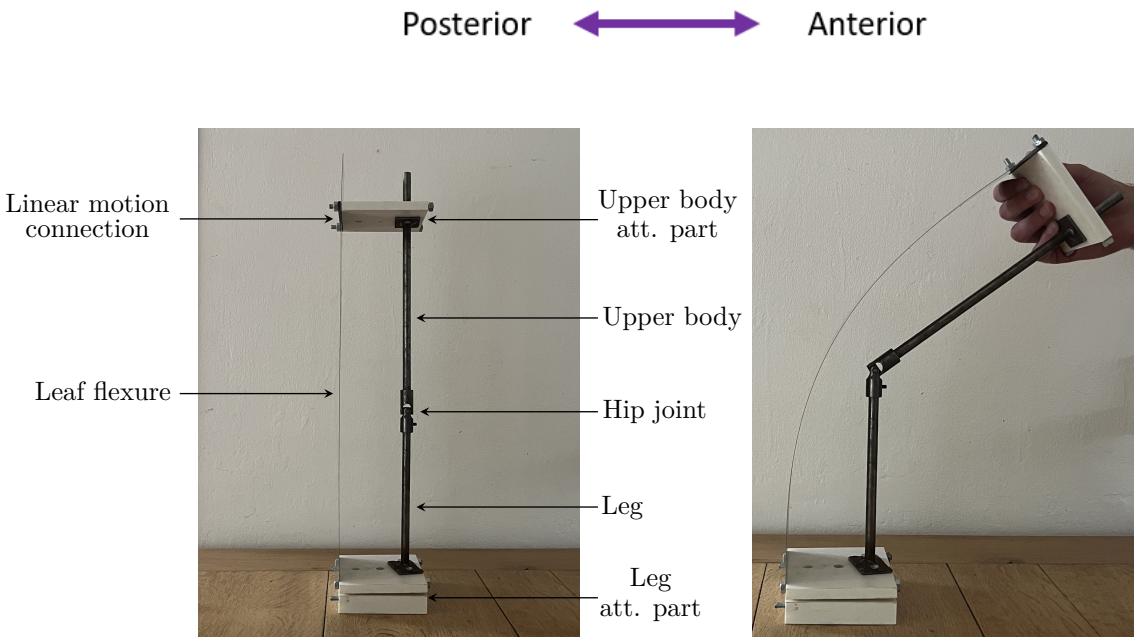

(a) Neutral position.

(b) Hip flexion.

(c) Hip extension.

(d) Adduction moment applied at a prescribed flexion angle.

Figure 5.18: Lateral view of the scale model in four different configurations.

6 Orthosis mechanism design phase

6.1 Introduction

Chapter 5 presented the concept phase for the orthosis mechanism. Based on a quantitative evaluation of the preliminary designs of Concepts 4 and 8, Concept 8 was selected for further development in the design phase.

This chapter details the design phase for the orthosis mechanism. Section 6.2 begins by selecting suitable FEM software for the design process. Section 6.3 then presents a mechanism design using a conventional leaf flexure. Finally, Section 6.4 introduces an alternative design using a leaf flexure incorporating warping constraints, as introduced in Section 2.5.

6.2 FEM software selection

In the concept phase, the SolidWorks FEM package was used for development and evaluation of the preliminary designs of Concepts 4 and 8 (see Section 5.4). However, several limitations were encountered, highlighting the need for a more capable tool in the design phase.

Therefore, this section discusses the limitations of SolidWorks, evaluates alternative FEM software packages, and selects the most suitable option for use in the design phase.

6.2.1 Limitations of the SolidWorks FEM package

The following limitations of the SolidWorks FEM package were encountered:

Boundary conditions
SolidWorks offers limited options for defining boundary conditions. As a result, simplified boundary conditions had to be used that require refinement for the design phase.

Parameter studies
SolidWorks does not facilitate automated parameter studies. Therefore, linear beam theory was used to predict influence of the dimensional parameters on the adduction-to-flexion stiffness ratio. In the design phase, parametric influence must be evaluated using FEM-obtained data.

Custom meshing
SolidWorks does not support custom meshing. This lack of mesh control can result in non-optimized meshes that require long computation times to obtain accurate results.

Static study limitations
Static studies were conducted with *Large Displacement* enabled to account for geometric nonlinearity. This study type does not provide access to intermediate solution step results, limiting interpretability of the final outcome and complicating troubleshooting of aborted simulations. Additionally, it does not allow control over the number of solution steps, which is one of the most useful tools for improving robustness. The fully nonlinear study type addresses these limitations, but is underdeveloped and prone to unexplained errors, making it a highly unreliable tool.

These limitations highlight the need for more capable FEM software for the design phase of the orthosis mechanism.

6.2.2 Evaluation of alternative FEM software

Two alternative FEM software packages are considered: a MATLAB Beam Code developed by Giuseppe Radaelli [54], and COMSOL Multiphysics. The Beam Code is specialized software based on Euler-Bernoulli beam theory, specifically written for nonlinear analysis of flexures. COMSOL is more traditional FEM software that, in addition to its strengths in multiphysics simulations, is also highly capable in single-physics domains such as structural mechanics. Unlike SolidWorks, which primarily focuses on CAD with an added FEM package, these two are dedicated FEM tools. As a result, they offer a wide range of advanced analysis options, addressing the limitations encountered in the SolidWorks FEM package.

To determine whether the alternative FEM software packages can provide accurate results for the design phase, a comparative evaluation is performed. In the concept phase, SolidWorks was used to evaluate the adduction stiffness, flexion stiffness, and von Mises stress of the preliminary design of Concept 8. Since similar analyses will be required in the design phase, the SolidWorks model is recreated in both the Beam Code and COMSOL, and the same properties are re-evaluated. The resulting values are compared with each other and with the original SolidWorks results. While SolidWorks is not considered a viable option for the design phase, its results serve as an additional point of reference that may offer insight into the relative accuracy of the other two tools. The measurement results across all three software packages are presented in Table 6.1.

As in the SolidWorks model, default meshes and settings are used, as the goal is to efficiently obtain approximate comparative results. A detailed description of the input data for the Beam Code and COMSOL model can be found in appendices B.6 and B.7, respectively.

Property	Req	Measurement	SolidWorks	Beam Code	COMSOL
Adduction stiffness	1a	$\theta_{add}\,\vert_{\theta_{flex}=30°}^{M_{add}=57\,\mathrm{Nm}}$	0.89°	0.0079°	1.0°
Flexion stiffness	1b	$M_{flex}\,\vert_{\theta_{flex}=30°}$	13 Nm	12 Nm	13 Nm
Von Mises stress	1c	$\sigma_{VM,max}\,\vert_{\theta_{flex}=30°}^{M_{add}=57\,\mathrm{Nm}}$	394 MPa	N/A	552 MPa

Table 6.1: Evaluations of adduction stiffness, flexion stiffness and von Mises stress for the preliminary design of Concept 8, as obtained through SolidWorks, the Beam Code and COMSOL.

Requirement 1b: Flexion stiffness

The three software packages yield nearly identical results for flexion stiffness. This consistency indicates that all three are accurate for evaluation of this property.

Requirement 1c: Von Mises stress

The Beam Code does not support von Mises stress analysis, so only SolidWorks and COMSOL are compared. These two software packages yield significantly different results, with COMSOL suggesting a peak von Mises stress of 40% higher than SolidWorks. However, this is a local result, which can be sensitive to singularities and mesh quality. Since default meshes were used and no mesh convergence studies were conducted, this likely explains the discrepancy.

To better assess global agreement, the full von Mises stress distributions are compared in Figure 6.1. The figure reveals a high degree of similarity between the SolidWorks and COMSOL models, indicating that both provide accurate global stress results. Local discrepancies can be solved through mesh refinement and singularity elimination.

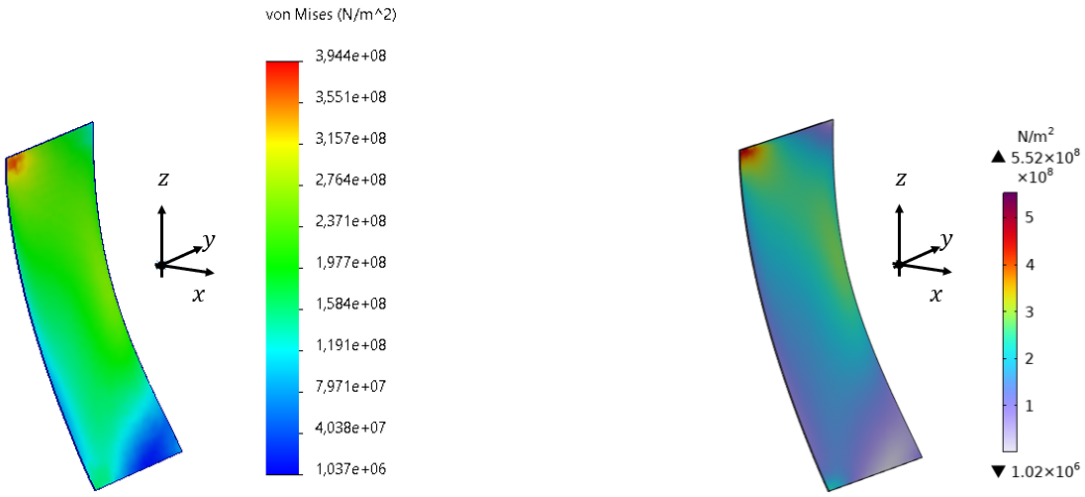

(a) SolidWorks.

(b) COMSOL.

Figure 6.1: Von Mises stress distribution resulting from a 57 Nm adduction moment applied at a 30° flexion angle, as retrieved from SolidWorks and COMSOL.

Requirement 1a: Adduction stiffness
For the adduction stiffness evaluation, SolidWorks and COMSOL show very similar results, while the Beam Code suggests significantly higher adduction stiffness. Being the clear outlier, the Beam Code result is considered inaccurate. To better understand the discrepancy, the deformation behavior in all models is compared in Figure 6.2. In order to achieve a visually comparable adduction angle in the Beam Code, the applied moment had to be increased from 57 Nm to 10 kNm.

The deformation patterns observed in SolidWorks and COMSOL show that adduction occurs primarily due to lateral bending through torsion of the leaf flexure. Conversely, the Beam Code model shows mainly in-plane bending of the leaf flexure. The deformations in SolidWorks and COMSOL align with those observed in the physical scale model shown in Figure 5.18. These observations further confirm accuracy of SolidWorks and COMSOL, and inaccuracy of the Beam Code.

The inaccuracy of the Beam Code for adduction analyses can be attributed to the element type it uses. As it is based on Euler-Bernoulli beam theory, the beam code does not account for shear and warping effects, which are the main contributors to torsional deformation. As a result, the Beam Code is unable to capture lateral bending through torsion, leading to a significant overestimation of adduction stiffness [55, 56].

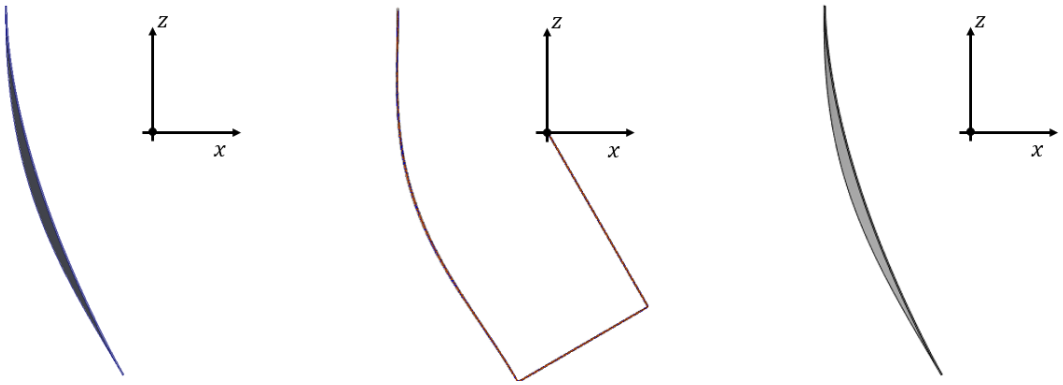

(a) SolidWorks. (b) Beam Code. (c) COMSOL.

Figure 6.2: Lateral view of the deformations of the leaf flexure resulting from a 57 Nm adduction moment applied at a 30° flexion angle, as retrieved from SolidWorks, the Beam Code, and COMSOL.

6.2.3 Selection of alternative FEM software

Given the limitations of the SolidWorks FEM package, two alternative FEM software packages were considered: a MATLAB Beam Code and COMSOL Multiphysics.

Both address the limitations of SolidWorks. However, the Beam Code does not support stress analysis and significantly overestimates adduction stiffness due to its reliance on Euler-Bernoulli beam theory. COMSOL, on the other hand, accurately captures both flexion and adduction behavior and provides reliable stress distributions.

Therefore, COMSOL is selected as the FEM software for the design phase of the orthosis mechanism.

6.3 Mechanism design using a conventional leaf flexure

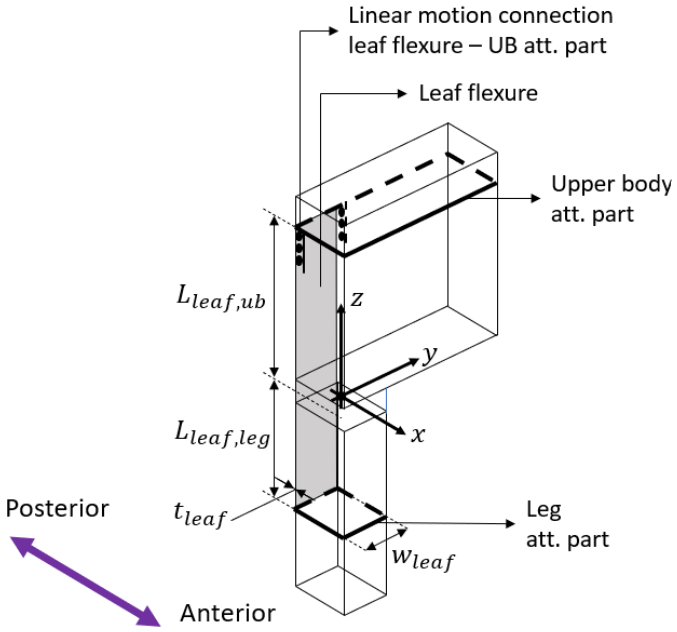

Figure 6.3: Concept 8

In Section 5.5, Concept 8 was selected for further development in the design phase. This concept features a leaf flexure positioned posterior to the patient's body. The bottom end of the leaf flexure is fixed to the leg attachment part, while the top end connects to the upper body attachment part via a connection that allows linear motion.

This section details the mechanism design of this concept using a conventional leaf flexure.

6.3.1 Refinements with respect to the preliminary design

In the concept phase, a preliminary design of Concept 8 was developed and evaluated using several simplifications and assumptions. In the design phase, the most important of these are addressed as follows:

- Requirements 1a and 1c state that the adduction stiffness and von Mises stress must be evaluated across the entire range of motion, from 8° extension to 30° flexion. For the preliminary design, the 30° flexion position was assumed to be critical within this range and was therefore used for evaluation. In the design phase, the entire range of motion is considered.

- The FEM analyses for the preliminary design were conducted in SolidWorks, using simplified boundary conditions and an automatically generated standard mesh, without conducting a mesh convergence study. These factors may have affected result accuracy and are addressed in the design phase.

- In an attempt to minimize flexion stiffness while maintaining sufficient adduction stiffness in the preliminary design, linear beam theory was used to predict parametric influence on the adduction-to-flexion stiffness ratio. In the design phase, parametric influence is assessed through FEM-obtained data.

6.3.2 Design approach

The development and evaluation of the design are guided by Table 6.2, representing a refined version of the requirements outlined in Section 3.4.

The refinement lies in determination of the mechanism's maximum allowable mass and thickness. Requirements 3a and 3b specify the maximum allowable mass and thickness of the orthosis as a whole. By subtracting the mass and thickness of the preliminary attachment parts design, presented in Chapter 4, the maximum allowable values for the mechanism alone are determined.

The mechanism design must satisfy all **must** statements in this table. Additionally, optimization for the **should** statements is encouraged to improve its performance. Based on expert advice from Simone Schoon [19], flexion stiffness minimization is prioritized, as this is expected to have the most significant impact on patient walking experience

Property	**Req**	**Must**	**Should**
Adduction stiffness	1a	$\theta_{add} \mid_{\theta_{flex} \in [-8°,\ 30°]}^{M_{add}=57\,\mathrm{Nm}} < 1.0°$	
Flexion stiffness	1b	$M_{flex} \mid_{\theta_{flex}=30°} < 43\,\mathrm{Nm}$	Min $M_{flex} \mid_{\theta_{flex}=30°}$
Von Mises stress	1c	$\sigma_{VM,max} \mid_{\theta_{flex} \in [-8°,\ 30°]}^{M_{add}=57\,\mathrm{Nm}} < \sigma_f$	
Mass	3a	$m_{mech} < 2.5$ kg	Min m_{mech}
Thickness	3b	$t_{mech} < 4.5$ cm	Min t_{mech}
Surface area	3c		Min A_{mech}

Table 6.2: Refined requirements for the mechanism design phase.

6.3.3 Assumptions

Although the design in this phase is refined with respect to the preliminary design in the concept phase, the following simplifications and assumptions remain:

- The design process focuses exclusively on the design of the leaf flexure, excluding the design or selection of a linear motion connection between the leaf flexure and the upper body attachment part. The *functionality* of the linear motion connection is taken into account for the leaf flexure design, assuming zero friction in the direction of linear motion, and infinite stiffness in all other directions. Any additional influence is neglected.

- The design process exclusively involves the selection of the optimal dimensional parameters for the leaf flexure, using the same material as selected for the preliminary design.

- The leaf flexure is considered rectangular, characterized by the following dimensional parameters: a total length that is subdivided into a leg portion ($L_{leaf,leg}$) and an upper body portion ($L_{leaf,ub}$), a width (w_{leaf}), and a thickness (t_{leaf}). These parameters are visualized in Figure 6.4.

- The dimensional parameter resolution – the step size by which they can be adjusted during the design process – for $L_{leaf,leg}$, $L_{leaf,ub}$, and w_{leaf} is set to 1.0 cm. For t_{leaf}, this is 0.10 mm.

- The leaf flexure is assumed to adapt perfectly to the curves of the human body with no clearance.

6.3.4 COMSOL FEM model setup

In Section 6.2, COMSOL was selected as the FEM software for the design phase. This section describes the setup of the COMSOL model that will be used for development and evaluation of the design. For a detailed description of the input data of this model, see Appendix B.8.

Geometry

As stated in the assumptions in Section 6.3.3, the design process focuses exclusively on the leaf flexure design, excluding the design or selection of a linear motion connection between the leaf flexure and the upper body attachment part. Consequently, only the geometry of the leaf flexure is implemented in the model. Figure 6.4 illustrates the geometry, as defined by the leaf flexure's dimensional parameters. In this figure the dimensional parameter values selected for the preliminary design were used. These values serve as placeholders and will be adjusted during the design process.

Based on the measurements of the hypothetical patient introduced in Section 3.2, the distance in x-direction between the leaf flexure and the hip joint is set to 0.15 m. The hip joint coincides with the origin of the coordinate system.

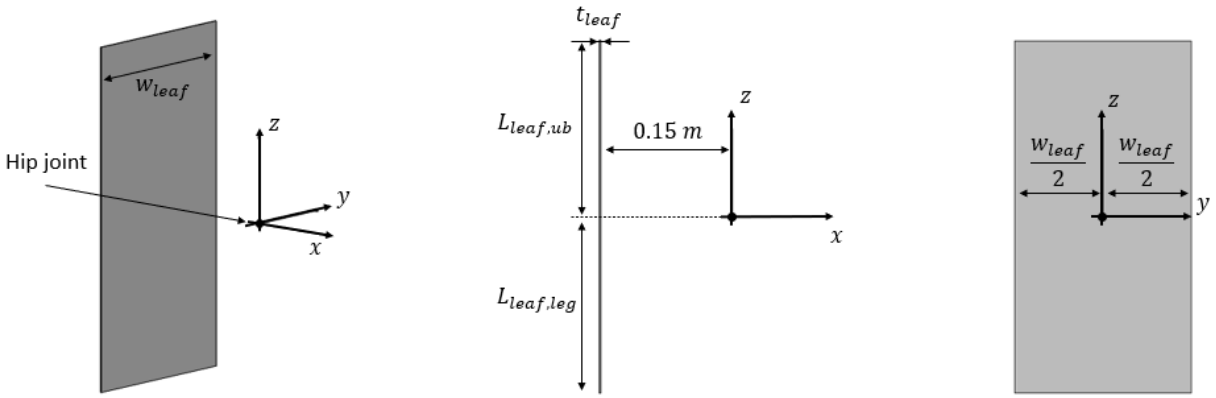

Figure 6.4: Geometry of the COMSOL model.

Material

As stated in the assumptions in Section 6.3.3, the design process focuses on optimizing the dimensional parameters of the leaf flexure, using the same material chosen for the preliminary design. This material is an unspecified steel type with the following properties:

- Young's modulus: $E = 210$ GPa
- Density: $\rho = 7.8 \cdot 10^3$ kg/m^3
- Poisson's ratio: $\nu = 0.28$
- Fatigue limit: $\sigma_f = 500$ MPa

COMSOL requires input of the Young's modulus, density, and Poisson's ratio. These properties are implemented, along with a linear elastic and isotropic material model. The material's fatigue limit is not used as an input in the model, but is considered during evaluation of Requirement 1c, which specifies that the maximum von Mises stress must remain below this limit at all times.

Physics
Within the structural mechanics module, COMSOL offers the option to use solid, shell, or beam elements. Shell and beam elements are generally more computationally efficient than solid elements. However, they only provide accurate results when their underlying assumptions are valid.

In Section 6.2, it was concluded that beam elements based on Euler-Bernoulli beam theory cannot accurately capture adduction deformation. These elements neglect shear and warping deformations, leading to overestimation of the leaf flexure's torsion stiffness. As lateral bending through torsion of the leaf flexure is the main deformation mode for adduction, adduction stiffness is also greatly overestimated.

In addition to Euler-Bernoulli beam theory, COMSOL provides the option to use beam elements based on Timoshenko beam theory. These elements do incorporate shear and warping effects and may therefore address the limitations of Euler-Bernoulli beam theory for modeling adduction. However, due to their 1-dimensional nature, obtaining detailed results such as stress distributions across the width of the leaf flexure is impractical and potentially inaccurate.

Shell elements in COMSOL are based on Reissner-Mindlin plate theory. These elements incorporate shear and warping deformation, making them likely suitable for modeling adduction. Additionally, their 2-dimensional nature allows for accurate stress distribution results across the width of the leaf flexure.

Given that shell elements are expected to yield accurate results, while being less computationally intensive than solid elements, they are selected for this model. Their accuracy is confirmed at the end of this section, under the heading *Verification of Shell Modeling Accuracy.* [55, 56]

Boundary conditions
The COMSOL model is used for evaluation of the mechanism's adduction stiffness, flexion stiffness, and von Mises stress. Table 6.2 indicates that evaluation of these properties require input flexion/extension angles and adduction moments. In this model, flexion/extension is simulated by leg movement, while adduction is simulated by upper body movement. Figure 6.5 schematically illustrates the boundary conditions in the model.

The bottom end of the leaf flexure is free to move along a circular path about the y-axis, with its rotation angle matching the arc angle of the path. The radius of this circle is constant, as the bottom end of the leaf flexure is fixed to the leg attachment part. This boundary condition models the degree of freedom for flexion/extension of the hip joint.

The top end of the leaf flexure is free to move along a circular path about the x-axis, with its rotation angle matching the arc angle of the path. Additionally, the radius of this circle is free to vary in length. These boundary conditions capture both the abduction/adduction freedom of the hip joint, and the translational degree of freedom of the linear motion connection between the top end of the leaf flexure and the upper body attachment part of the orthosis.

The input parameters θ_{flex} and M_{add} are defined to prescribe angles of flexion/extension and to apply adduction moments.

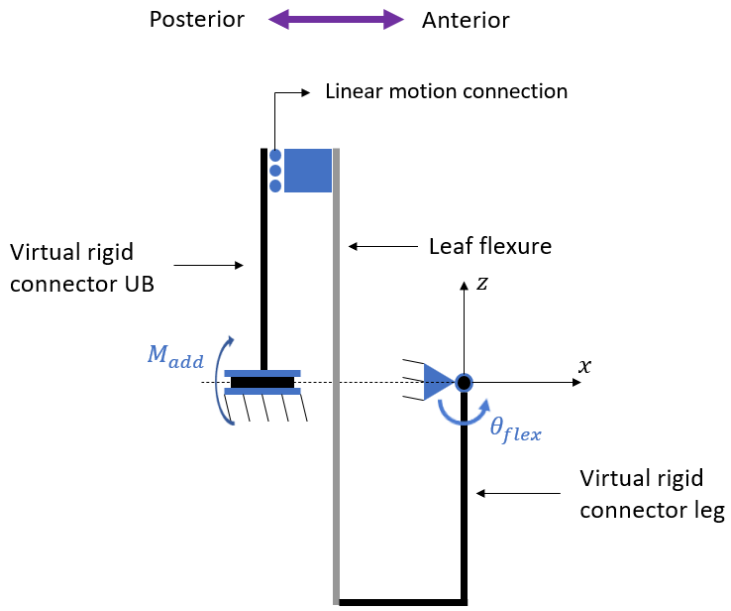

Figure 6.5: Schematic illustration of the model's boundary conditions.

Mesh

A custom mesh is created using quadrilateral elements. The mesh incorporates mesh refinement faces in all corners of the leaf flexure, as these are the regions where peak stress is expected to occur. The refinement faces have a width of $\frac{w_{leaf}}{8}$ and a height of $\frac{w_{leaf}}{16}$. The element size can be controlled both globally, for the entire mesh, and locally, within the refinement faces. To ensure consistency when adjusting the dimensional parameters of the leaf flexure, element sizes are defined as fractions of the leaf flexure's width. Figure 6.6 illustrates a mesh example where the global element size is set to $\frac{w_{leaf}}{16}$, while the local element size in the refinement faces is set to $\frac{w_{leaf}}{64}$.

To ensure results accuracy, a mesh convergence study is conducted for each measurement, iteratively refining the mesh by halving the element size. Convergence is considered achieved once further halving results in less than a 1.0% change in the measurement outcome.

For measurements of adduction stiffness and flexion stiffness, mesh refinement is performed globally. For von Mises stress measurements, the global mesh refinement is followed by local mesh refinement, focusing on the region where peak stress occurs.

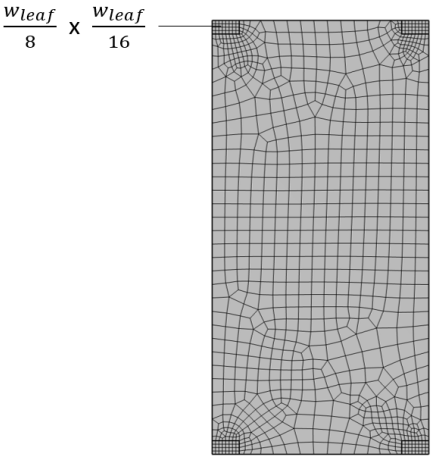

Figure 6.6: Mesh example where the global element size is set to $\frac{w_{leaf}}{16}$, and the local element size in the mesh refinement faces is set to $\frac{w_{leaf}}{64}$.

Study

A stationary study is used to apply the input parameters, θ_{flex} and M_{add}, for evaluation of the adduction stiffness, flexion stiffness, and von Mises stress. The *Include geometric nonlinearity* option is selected to take into account large displacement effects.

The input parameters are introduced sequentially across multiple study steps. Within each step, the input is incrementally applied using auxiliary sweeps. This strategy improves convergence and facilitates analysis of moment-angle relationships.

Solver settings may vary slightly between study steps. The configuration aims to reduce computation time while maintaining robust convergence. The following considerations can be made to strike a balance between efficiency and robustness:

- The *number of steps* in the auxiliary sweeps for the input parameters, θ_{flex} and M_{add}, can be adjusted. Fewer steps reduce computation time but may impair robustness, while more steps improve robustness at the cost of time.

- *Continuation* within auxiliary sweeps can be enabled to improve robustness by allowing COMSOL to insert intermediate auxiliary sweep values if a step fails to converge. Disabling continuation may speed up the simulation but increases the risk of solver failure in nonlinear problems.

- The *nonlinear method* can be set to either Automatic (Newton) or Constant (Newton). Constant (Newton) is more aggressive as it does not introduce damping and makes larger updates. Consequently, it is more time-efficient, but also more likely to diverge. This iteration scheme is particularly suitable in moderately nonlinear problems. Automatic (Newton) on the other hand, is a more conservative approach that introduces damping and makes smaller updates, making it less time-efficient but more robust. This iteration scheme is particularly suitable in highly nonlinear and unstable problems. In this application, a typical example is in cases where the leaf flexure (almost) reaches the mode of lateral torsional buckling under the applied adduction moment [57].

- The *maximum number of Newton iterations* can be increased. Although this does not directly affect computation time, a larger maximum allows the solver more time to compute.

Measurements

Table 6.2 indicates that evaluation of the adduction stiffness, flexion stiffness, and von Mises stress requires measurement of the adduction angle, flexion moment, and maximum von Mises stress, under the specified input conditions. The measurement methods used in the COMSOL model are as follows:

- The *adduction angle* is measured by evaluating the rotation of the top end of the leaf flexure in the negative x-direction.
- The *flexion moment* is measured by evaluating the reaction moment of the bottom end of the leaf flexure about the negative y-axis.
- The *maximum von Mises stress* is determined using the maximum von Mises stress prompt, which evaluates the highest stress value across the top and bottom faces of the shell. To avoid singularity effects, quarter circle regions with a 1 mm radius are excluded from the stress plot in all corners of the leaf flexure.

Verification of shell modeling accuracy

Under the heading *Physics*, it was reasoned that shell elements are likely to provide a good balance between results accuracy and computational efficiency. This hypothesis is now verified by performing measurements of the adduction stiffness, flexion stiffness, and von Mises stress, in both a solid and shell model. The corresponding mesh convergence graphs will provide insight into accuracy and efficiency through the values towards which they converge and the rate at which convergence occurs, respectively.

Given that the dimensional parameters for the leaf flexure are yet to be determined, the dimensional parameters selected for the preliminary design are used for this verification analysis. The conclusions drawn from this analysis are also valid for different parameter combinations, as the general shape of the geometry will remain similar.

The measurements are performed as specified in Table 6.2, with the simplification that the adduction stiffness and von Mises stress are evaluated at a 30° flexion angle, rather than across the entire range of motion, from 8° extension to 30° flexion.

Figure 6.7 shows the resulting mesh convergence graphs. For each measurement, solid and shell elements result in convergence toward the same value, confirming measurement accuracy. However, shell elements converge at significantly coarser meshes than solid elements. This confirms the hypothesis that shell elements provide a good balance between results accuracy and computational efficiency, justifying the selection of shell elements in this model.

Additionally, the figure demonstrates that this refined COMSOL model yields significantly different results for the adduction stiffness and von Mises stress measurements than the SolidWorks model used for the preliminary design. The adduction angle and maximum von Mises stress measured in COMSOL are 0.43° and 610 MPa, while SolidWorks measured 0.89° and 394 MPa, respectively. This finding highlights the importance of the refinements made in the design phase. Not only for identifying an optimal solution, but also for ensuring accurate performance evaluation.

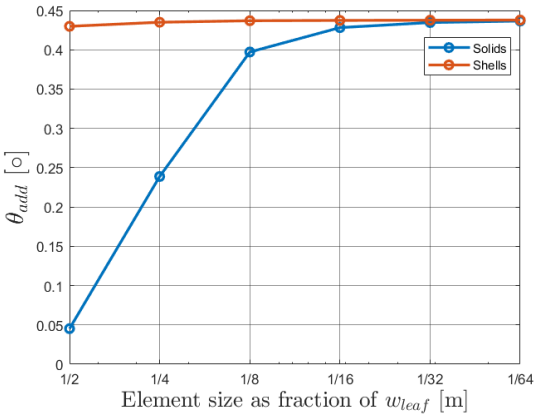

(a) Mesh convergence of the adduction angle resulting from a 57 Nm adduction moment applied at a 30° flexion angle.

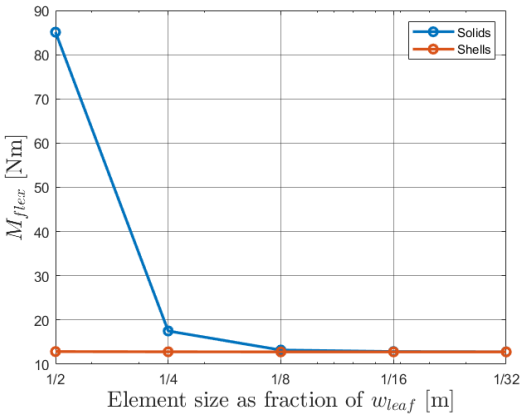

(b) Mesh convergence of the flexion moment required to achieve a 30° flexion angle.

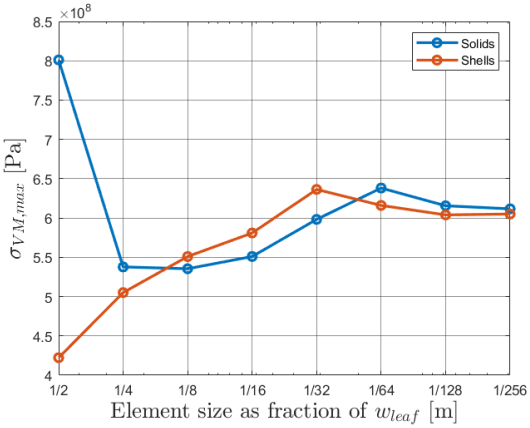

(c) Mesh convergence of the maximum von Mises stress resulting from a 57 Nm adduction moment applied at a 30° flexion angle.

Figure 6.7: Mesh convergence studies revealing the accuracy and efficiency of solid and shell elements for measurements of the adduction stiffness, flexion stiffness and von Mises stress of the leaf flexure.

6.3.5 Dimensional parameter selection

This section aims to select the optimal dimensional parameters for the leaf flexure to minimize the flexion stiffness, while ensuring compliance with all **must** statements outlined in Table 6.2. The design space defined for the preliminary design during the concept phase remains applicable, based on the same underlying rationale as explained in Section 5.4. The resulting design space is summarized in Table 6.3.

Parameter	Lower boundary	Upper boundary
$L_{leaf,leg}$	0.00 m	0.35 m
$L_{leaf,ub}$	0.10 m	0.45 m
w_{leaf}	0.010 m	0.20 m
t_{leaf}	0.10 mm	45 mm

Table 6.3: Design space for the dimensional parameters of the leaf flexure.

The selection process consists of two distinct phases. In Phase 1, parametric sweeps are conducted to iteratively refine the design space towards the region containing the most promising solutions. A relatively coarse mesh is used in this phase to enable efficient evaluation of a large number of parameter combinations. Based on Figure 6.7, a global element size of $\frac{w_{leaf}}{4}$ was selected, with local mesh refinement in the corners of the leaf flexure using an element size of $\frac{w_{leaf}}{16}$. This meshing strategy offers a suitable balance between accuracy and efficiency for the purposes of this phase.

Additionally, although Table 6.2 specifies that adduction stiffness and von Mises stress must be evaluated across the entire range of motion, from 8° extension to 30° flexion, this phase only considers the 30° flexion position. This simplification significantly reduces computational effort, and since 30° flexion is expected to be critical within the range, it is likely to effectively filter out most solutions that do not comply with the minimum required adduction stiffness and maximum allowable von Mises stress. However, due to the coarse mesh and single-angle evaluation of adduction stiffness and von Mises stress, some false-feasible solutions may still remain.

In Phase 2, the most promising solutions from Phase 1 are re-evaluated by assessing adduction stiffness and von Mises stress across the entire range of motion, from 8° extension to 30° flexion, using a refined mesh obtained through a mesh convergence study. This eliminates the false-feasible solutions and identifies the optimal parameter combination that is truly feasible.

This phased approach ensures efficient use of computational resources while providing high confidence in the selected parameter combination.

Phase 1: Iterative design space refinement through parametric sweeps

Since the objective is to minimize flexion stiffness, the corresponding performance indicator – the hip flexion moment required to achieve a 30° flexion angle – is used to evaluate the solutions within the parametric sweeps. Figure 6.8 illustrates the relationship between this indicator and the dimensional parameters of the leaf flexure through scatter plots of the sweeps conducted in this phase. Each scatter point in these plots represents a unique combination of dimensional parameters. Jittering was applied to introduce small random horizontal perturbations, improving the visual distinction between individual solutions. Solutions that do not comply with all **must** statements outlined in Table 6.2 are filtered out, leaving only feasible solutions for evaluation. The individual parametric sweeps are discussed in detail below the figure.

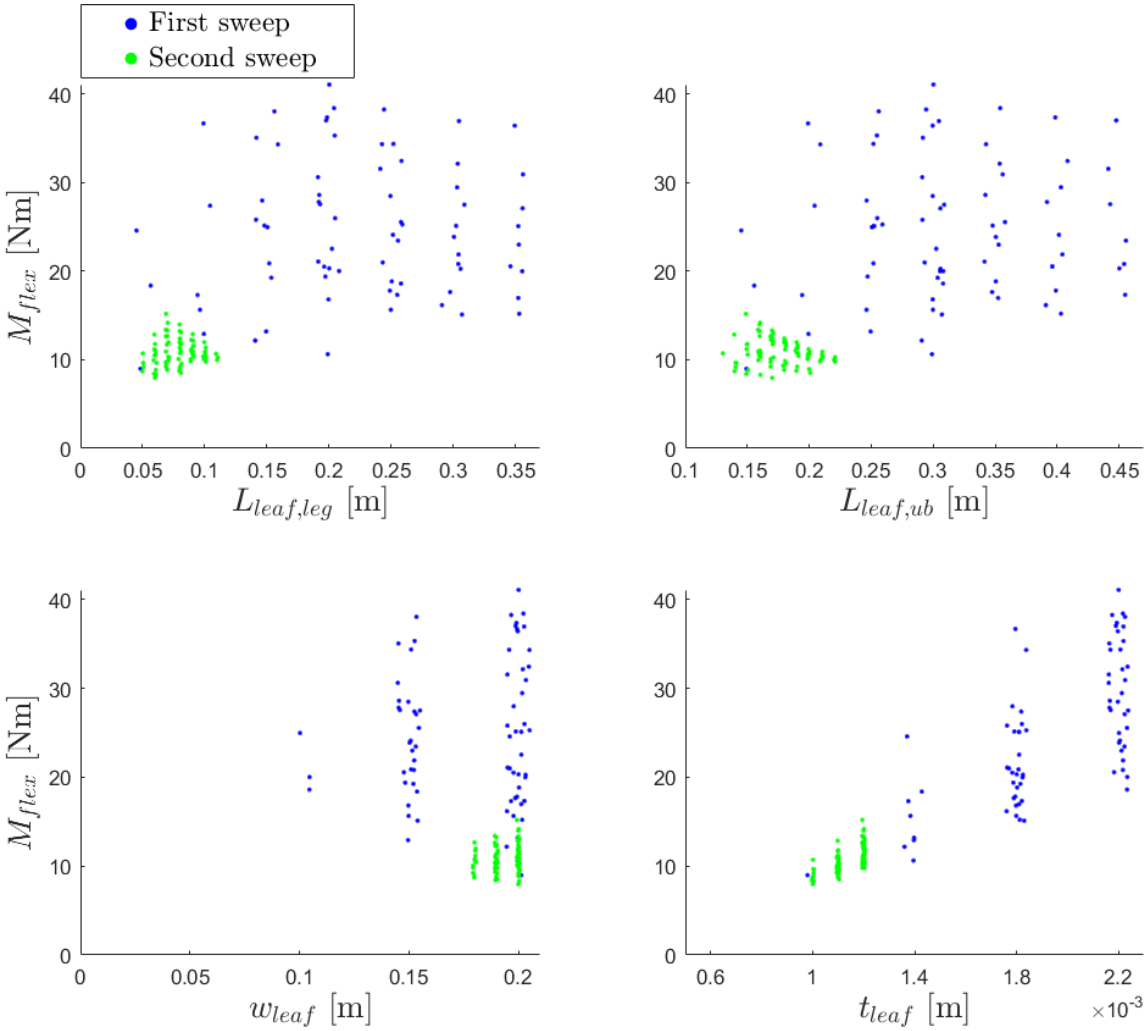

Figure 6.8: Scatter plots showing the relationship between the dimensional parameters of the leaf flexure and the hip flexion moment required to achieve a 30° flexion angle.

First parametric sweep

The first parametric sweep aimed to explore the entire design space of the dimensional parameters. For the leaf flexure thickness, only the region surrounding the value selected for the preliminary design ($t_{leaf} = 1.3$ mm) was explored. Table 6.4 outlines the exact values investigated for each parameter.

Parameter	**Value range**	**Step size**
$L_{leaf,leg}$	0.00 – 0.35 m	0.050 m
$L_{leaf,ub}$	0.10 – 0.45 m	0.050 m
w_{leaf}	0.050 – 0.20 m	0.050 m
t_{leaf}	0.60 – 2.2 mm	0.40 mm

Table 6.4: Dimensional parameter values explored in the first parametric sweep.

Figure 6.8 reveals the following trends among the first parametric sweep results:

- Both $L_{leaf,leg}$ and $L_{leaf,ub}$ show slightly more potential for minimizing the flexion stiffness at smaller values. However, in both cases, this is accompanied by a reduction in the number of feasible solutions.

- w_{leaf} shows a strong trend where increasing its value significantly enhances the potential for minimizing flexion stiffness. Additionally, a larger w_{leaf} leads to an increase in the number of feasible solutions.

- t_{leaf} shows a strong trend where decreasing its value significantly enhances the potential for minimizing flexion stiffness. However, this is accompanied by a reduction in the number of feasible solutions.

These observations indicate that maximizing w_{leaf} and minimizing t_{leaf} are desirable for reducing flexion stiffness. While the influence of $L_{leaf,leg}$ and $L_{leaf,ub}$ is less pronounced, lower values still appear favorable. Additionally, this contributes to a more compact and lightweight design, aligning well with the overall design objectives.

Based on these insights, a second parametric sweep was conducted to zoom in on the regions of the design space with the most promising solutions.

Second parametric sweep
Table 6.5 outlines the parameter values explored in the second parametric sweep.

Parameter	**Value range**	**Step size**
$L_{leaf,leg}$	0.030 – 0.12 m	0.010 m
$L_{leaf,ub}$	0.13 – 0.22 m	0.010 m
w_{leaf}	0.18 – 0.20 m	0.010 m
t_{leaf}	0.90 – 1.2 mm	0.10 mm

Table 6.5: Dimensional parameter values explored in the second parametric sweep.

Figure 6.8 reveals the following trends among the second parametric sweep results:

- Both $L_{leaf,leg}$ and $L_{leaf,ub}$ show convex trends, indicating that the solution with lowest flexion stiffness is encompassed within the explored range.

- w_{leaf} and t_{leaf} show the same trends as in the first parametric sweep, where increasing w_{leaf} and decreasing t_{leaf} enhances the potential for minimizing flexion stiffness. However, further reduction of t_{leaf} yields only infeasible solutions, and further increase of w_{leaf} is not possible due to the upper limit of its design space.

These results confirm that the second parametric sweep successfully targeted the most promising regions of the design space. Since this sweep already achieves the parameter resolution defined in the assumptions in Section 6.3.3, no further refinement step is possible. Therefore, this second parametric sweep concludes Phase 1 of the dimensional parameter selection process.

Phase 2: Refined evaluation of most promising solutions

In Phase 1, parameter combinations that did not comply with all **must** statements outlined in Table 6.2 were filtered out. However, for efficiency purposes, a coarse mesh was used and the adduction stiffness and von Mises stress were evaluated only in the 30° flexion position rather than across the entire range of motion, from 8° extension to 30° flexion. This may result in false-feasible solutions.

To address this, Phase 2 re-evaluates the adduction stiffness and von Mises stress in the most promising solutions from Phase 1. This evaluation considers the full range of motion, and results are obtained through a mesh convergence study. This ensures that the selected solution is truly feasible.

For the solution with the lowest flexion stiffness from Phase 1, Figure 6.9 shows the full range of motion measurements of adduction stiffness and von Mises stress. The adduction angle and von Mises stress remain below 1.0° and 500 MPa at all times, respectively, proving compliance with the minimum required adduction stiffness and maximum allowable von Mises stress, as defined in able 6.2.

Therefore, this solution is selected as the optimal dimensional parameter combination.

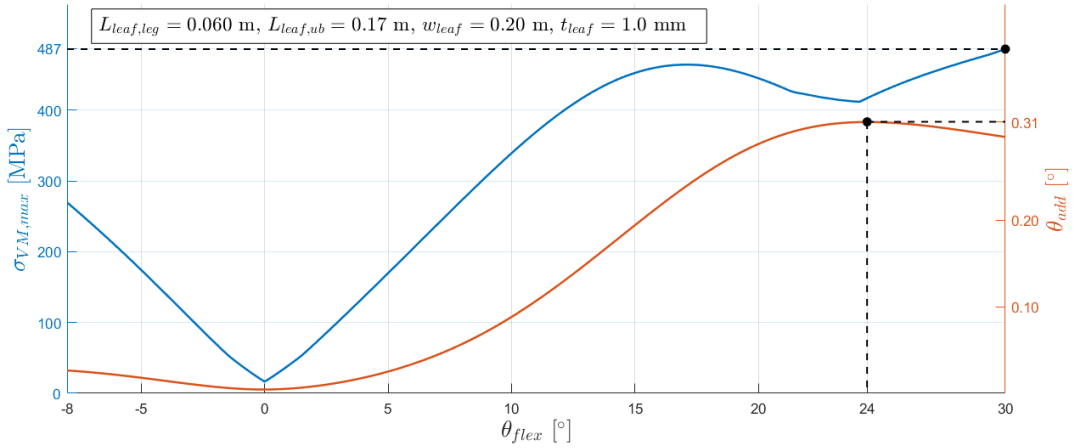

Figure 6.9: Measurement of the adduction angle and maximum von Mises stress resulting from a 57 Nm adduction moment applied throughout the entire range of motion, from 8° extension to 30° flexion, for the selected parameter combination.

6.3.6 Design evaluation

In Section 6.3.5, the optimal dimensional parameters were selected for the leaf flexure to minimize the flexion stiffness while ensuring compliance with all **must** statements in Table 6.2. Since this design uses the same material as selected for the preliminary design, the design process is considered complete. Table 6.6 summarizes the selected dimensions and material for the leaf flexure.

This section presents the evaluation of the resulting design, including performance measurements, a performance evaluation, and an artist impression representing the leaf flexure in motion.

Dimensions		**Material**	
$L_{leaf,leg}$	= 0.060 m	Type	= Steel
$L_{leaf,ub}$	= 0.17 m	E	= 210 GPa
w_{leaf}	= 0.20 m	ρ	= $7.8 \cdot 10^3$ kg/m^3
t_{leaf}	= 1.0 mm	ν	= 0.28
		σ_f	= 500 MPa

Table 6.6: Dimensions and material selected for the leaf flexure.

Performance measurements

The first step in evaluating the design is to quantify its performance. This is done by conducting the relevant measurements for each requirement, as outlined in Table 6.2.

Requirement 1a: Adduction stiffness

The adduction stiffness is evaluated through measurement of the adduction angle resulting from a 57 Nm adduction moment applied throughout the entire range of motion, from 8° extension to 30° flexion.

Figure 6.9 presents the full range of motion measurement and reveals that the peak adduction angle within this range is 0.31°, occurring at a 24° flexion angle. Figure 6.11 illustrates the corresponding deformation.

Requirement 1b: Flexion stiffness

The flexion stiffness is evaluated through measurement of the hip flexion moment required to achieve a 30° flexion angle.

The COMSOL model indicates a required hip flexion moment of 7.9 Nm. Figure 6.10 illustrates the corresponding deformation.

Requirement 1c: Von Mises stress

The von Mises stress is evaluated through measurement of its maximum, resulting from a 57 Nm adduction moment applied throughout the entire range of motion, from 8° extension to 30° flexion.

Figure 6.9 presents the full range of motion measurement and reveals that the peak von Mises stress within this range is 487 MPa, occurring at a 30° flexion angle. Figure 6.12 illustrates the corresponding stress distribution on the leaf flexure.

Requirement 3a: Mass

Given the assumption that any influence of the linear motion connection between the leaf flexure and the upper body attachment part is neglected in this design, the mechanism's mass equals that of the leaf flexure. Based on the dimensions and material outlined in Table 6.6, the resulting mass is 0.36 kg.

Requirement 3b: Thickness
Given the assumption that the leaf flexure adapts perfectly to the curves of the human body with no clearance, and that any influence of the linear motion connection is neglected, the mechanism thickness equals the leaf flexure thickness of 1.0 mm.

Requirement 3c: Surface area
Given the assumption that any influence of the linear motion connection is neglected, the mechanism's surface area equals that of the leaf flexure, which is 0.046 m^2.

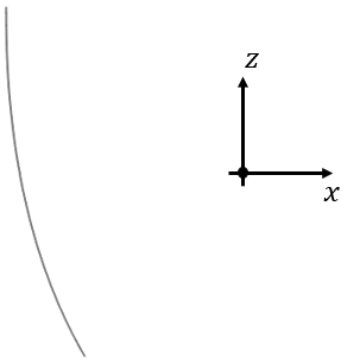

Figure 6.10: Lateral view of the deformation of the leaf flexure resulting from a 30° prescribed flexion angle.

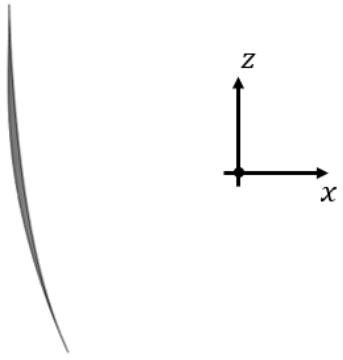

Figure 6.11: Lateral view of the deformation of the leaf flexure resulting from a 57 Nm adduction moment applied at a 24° flexion angle.

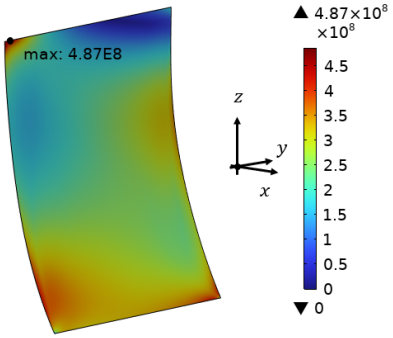

Figure 6.12: Von Mises stress distribution on the leaf flexure resulting from a 57 Nm adduction moment applied at a 30° flexion angle.

Performance evaluation

The results of the performance measurements conducted in the previous section have been incorporated into Table 6.2 to evaluate the design's performance. The results are presented in Table 6.7.

The design objective was to minimize the flexion stiffness while ensuring compliance with all **must** statements outlined in Table 6.2. As shown in Table 6.7, the resulting design requires a 7.9 Nm hip flexion moment to achieve a 30° flexion angle. Moreover, the design satisfies all **must** statements, confirming that it is a satisfactory solution.

Property	Req	Must		Should	Performance	
Adduction stiffness	1a	$\theta_{add}\ \vert^{M_{add}=57\,\text{Nm}}_{\theta_{flex}\in[-8°,\ 30°]}$	$< 1.0°$		θ_{add}	$\leq 0.31°$
Flexion stiffness	1b	$M_{flex}\ \vert_{\theta_{flex}=30°}$	$< 43\,\text{Nm}$	Min $M_{flex}\ \vert_{\theta_{flex}=30°}$	M_{flex}	$= 7.9$ Nm
Von Mises stress	1c	$\sigma_{VM,max}\ \vert^{M_{add}=57\,\text{Nm}}_{\theta_{flex}\in[-8°,\ 30°]}$	$< \sigma_f$ $= 500$ MPa		$\sigma_{VM,max}$	≤ 487 MPa
Mass	3a	m_{mech}	< 2.5 kg	Min m_{mech}	m_{mech}	$= 0.36$ kg
Thickness	3b	t_{mech}	< 4.5 cm	Min t_{mech}	t_{mech}	$= 1.0$ mm
Surface area	3c			Min A_{mech}	A_{mech}	$= 0.046$ m^2

Table 6.7: Performance evaluation for the mechanism design using a conventional leaf flexure.

Artist impression

Figure 6.13 provides an artist impression of the leaf flexure design, illustrating its scale and placement relative to the human body, as well as its function in enabling flexion/extension freedom.

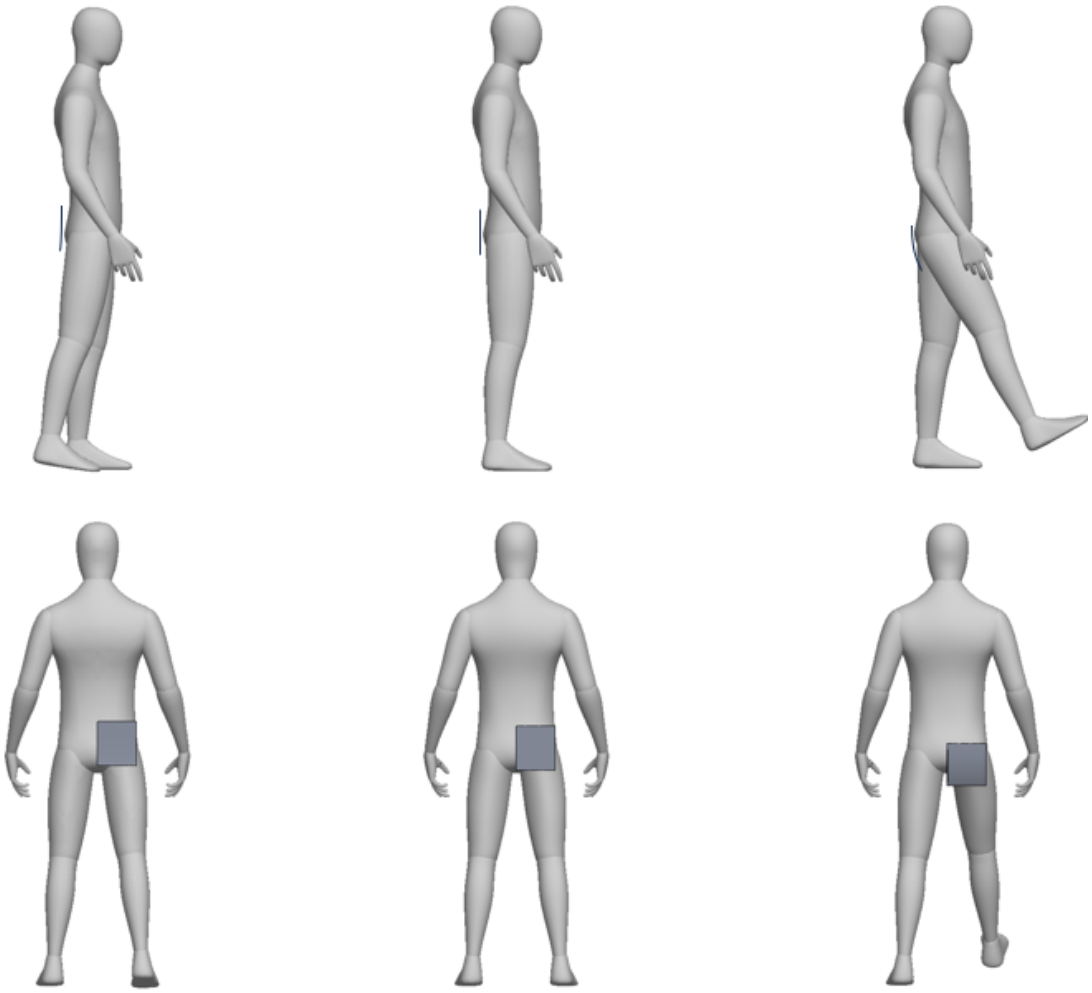

(a) 8° extension. (b) Neutral position. (c) 30° flexion.

Figure 6.13: Artist impression of the conventional leaf flexure design.

6.4 Mechanism design using a leaf flexure incorporating warping constraints

Section 6.3 presented a mechanism design using a conventional leaf flexure, focused on minimizing flexion stiffness. One of the main factors limiting flexion stiffness minimization was the need to comply with the minimum required adduction stiffness, as specified in Requirement 1a.

Analysis of the leaf flexure's deformation behavior revealed that the dominant deformation mode for adduction is lateral bending through torsion of the leaf flexure. Section 2.5 introduced two methods for increasing torsion stiffness in leaf flexures without significantly affecting bending stiffness: triangular reinforcement structures, and warping constraints. Implementation of these methods into the mechanism design is expected to enable further reduction of the flexion stiffness while preserving the required adduction stiffness.

As discussed in Section 2.5, the effectiveness of triangular reinforcement structures is more established in literature. However, warping constraints offer a significantly more compact solution. As the mechanism design using a conventional leaf flexure already complies with the maximum allowable flexion stiffness by a significant margin, the lower space efficiency of triangular reinforcement structures is not an acceptable tradeoff for further reduction of the flexion stiffness. Therefore, warping constraints are considered the more suitable solution.

This section details an alternative mechanism design using a leaf flexure incorporating warping constraints. For conciseness, only the aspects that differ from the design process of the mechanism using a conventional leaf flexure are detailed.

6.4.1 Design approach

Like the mechanism design using a conventional leaf flexure, the development and evaluation of this design are guided by Table 6.2. The design process again focuses on minimizing flexion stiffness while ensuring compliance with all **must** statements outlined in this table.

The mechanism design using a conventional leaf flexure serves as the basis for this design. Warping constraints are added to the leaf flexure to selectively enhance its torsion stiffness, and thereby also the adduction stiffness. This modification is expected to reduce the thickness needed to meet the minimum required adduction stiffness, enabling further reduction of the flexion stiffness. The length and width of the leaf flexure will remain unchanged from the mechanism design using a conventional leaf flexure.

6.4.2 Assumptions

The simplifications and assumptions for this design largely follow those applied in the mechanism design using a conventional leaf flexure. The following simplifications and assumptions remain unchanged:

- The design process focuses exclusively on the design of the leaf flexure, excluding the design or selection of a linear motion connection between the leaf flexure and the upper body attachment part. The *functionality* of the linear motion connection is taken into account for the leaf flexure design, assuming zero friction in the direction of linear motion, and infinite stiffness in all other directions. Any additional influence is neglected.

- The design process exclusively involves the selection of the optimal dimensional parameters for the leaf flexure, using the same material as selected for the preliminary design.

- The leaf flexure is assumed to adapt perfectly to the curves of the human body with no clearance.

The following simplifications and assumptions have been modified or added due to the incorporation of warping constraints:

- The base geometry of the leaf flexure remains rectangular, defined by a total length subdivided into a leg portion ($L_{leaf,leg}$) and an upper body portion ($L_{leaf,ub}$), a width (w_{leaf}), and a thickness (t_{leaf}). In addition, rectangular warping constraints are integrated, characterized by the following dimensional parameters: a number of warping constraints (n_{wc}), a thickness (t_{wc}), and a depth (d_{wc}). These warping constraints are evenly distributed along the length of the leaf flexure and span its full width. The dimensional parameters are visualized in Figure 6.14.

- As stated in the design approach in Section 6.4.1, the length and width of the leaf flexure remain unchanged from the mechanism design using a conventional leaf flexure. The resolution of the *adjustable* dimensional parameters is set to 1 for n_{wc}, 1.0 mm for both t_{wc} and d_{wc}, and 0.10 mm for t_{leaf}.

6.4.3 COMSOL FEM model setup

The COMSOL model developed for the mechanism design using a conventional leaf flexure is reused for this design, with the geometry modified to incorporate the warping constraints. The adjusted geometry necessitates different physics and mesh configuration. However, the material properties, boundary conditions, study settings, and measurement methods remain unchanged. For a detailed description of the input data of this model, see Appendix B.9.

Geometry

The geometry of the COMSOL model developed for the mechanism design using a conventional leaf flexure is modified for this design by the adding warping constraints. Figure 6.14 illustrates the resulting geometry, as defined by the dimensional parameters of both the leaf flexure and the warping constraints.

In this figure, the dimensional parameter values selected for the leaf flexure in the mechanism design using a conventional leaf flexure were used for the base geometry of the leaf flexure. For the warping constraints, $n_{wc} = 10$, $t_{wc} = 5.0$ mm and $d_{wc} = 5.0$ mm were selected. As stated in the assumptions in Section 6.4.2, the length and width of the leaf flexure remain unchanged from the mechanism design using a conventional leaf flexure. However, the dimensional parameter values for the warping constraints and the leaf flexure thickness used here serve as placeholders and will be adjusted during the design process.

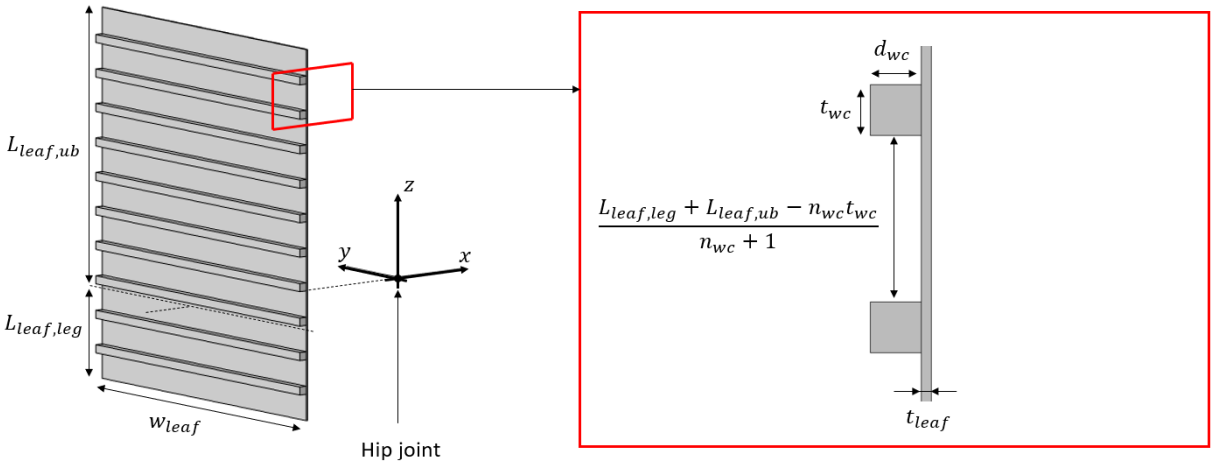

Figure 6.14: Geometry of the COMSOL model.

Physics
In the original model, shell elements were used to facilitate efficient yet accurate analysis of the leaf flexure. However, the added warping constraints cannot be accurately represented using shell elements due to their three-dimensional geometry. Therefore, these components are modeled using solid elements.

To maintain high computational efficiency for the leaf flexure, the model combines shell elements (for the base geometry of the leaf flexure) with solid elements (for the warping constraints).

Interaction between the two domains is enabled using the *Solid–Thin Structure Connection* feature from COMSOL's *Multiphysics* interface. This feature ensures continuity across the shared boundaries of the solid and shell domains.

Mesh
To ensure computational efficiency, an custom mesh with independent control for each geometric component is essential. To achieve this, a custom mesh was built with separate control of the number of elements through the warping constraint thickness, depth and width. The remaining part of the geometry – the sections of the leaf flexure located between the warping constraints – is filled with quadrilateral elements. The size of these elements is defined as a fraction of the leaf flexure's width.

In contrast to the original model, no mesh refinement faces are applied to the regions where peak stress is expected to occur. This is because in this model, no suitable method was found to incorporate mesh refinement faces that automatically adjust to changes in geometry and/or mesh. However, for specific cases that require high-accuracy stress evaluation, mesh refinement faces can still be manually created.

Figure 6.15 shows a mesh example with two elements through the thickness and depth of the warping constraints, four through the width, and a remaining element size of $\frac{w_{leaf}}{4}$.

To ensure results accuracy, a mesh convergence study is conducted for each measurement, iteratively refining the mesh by halving the element size for each mesh parameter. Convergence is considered achieved once further halving results in less than a 1.0% change in the measurement outcome.

For measurements of adduction stiffness and flexion stiffness, mesh refinement is performed globally. For von Mises stress measurements, the global mesh refinement is followed by local mesh refinement, focusing on the region where peak stress occurs.

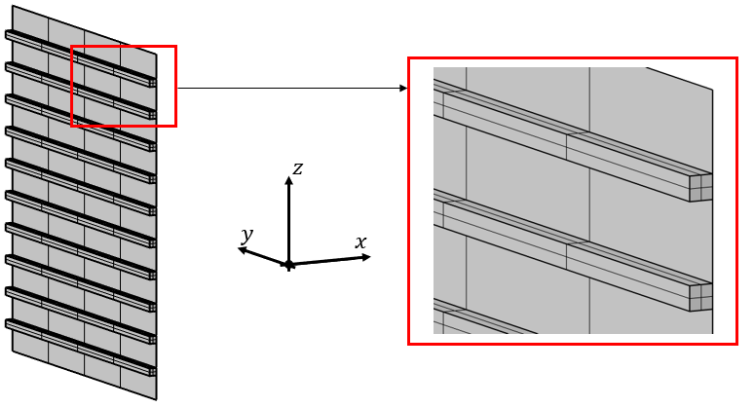

Figure 6.15: Mesh example with two elements through the thickness and depth of the warping constraints, four through the width, and a remaining element size of $\frac{w_{leaf}}{4}$.

6.4.4 Dimensional parameter selection

This section aims to select the optimal dimensional parameters for the warping constraints and leaf flexure thickness to minimize the flexion stiffness, while ensuring compliance with all **must** statements in Table 6.2. The design space for the dimensional parameters is defined as follows:

To avoid non-existent geometries, all dimensional parameters must be strictly positive. The lower boundaries are set equal to the parameter resolution defined in the assumptions in Section 6.4.2, as these are the smallest feasible positive values.

The upper boundaries of the dimensional parameters are interdependent. Specifically, the product of the number of warping constraints (n_{wc}) and their thickness (t_{wc}) must be smaller than the total length of the leaf flexure ($L_{leaf,leg} + L_{leaf,ub}$) to ensure all warping constraints fit along the flexure with space between them. Based on the mechanism design using a conventional leaf flexure, $L_{leaf,leg} + L_{leaf,ub} = 0.060\text{ m} + 0.17\text{ m} = 0.23\text{ m}$. Additionally, the sum of the warping constraint depth (d_{wc}) and leaf flexure thickness (t_{leaf}) must be smaller than 4.5 cm to comply with the maximum allowable mechanism thickness, as defined in Table 6.2.

The resulting design space is summarized in Table 6.8.

Parameter	**Lower boundary**	**Upper boundary**
n_{wc}	1	$n_{wc} \cdot t_{wc} < 0.23$ m
t_{wc}	1.0 mm	$n_{wc} \cdot t_{wc} < 0.23$ m
d_{wc}	1.0 mm	$d_{wc} + t_{leaf} < 4.5$ cm
t_{leaf}	0.1 mm	$d_{wc} + t_{leaf} < 4.5$ cm

Table 6.8: Design space for the dimensional parameters of the warping constraints and leaf flexure thickness.

This section follows the same two-phase approach used for the dimensional parameter selection for the mechanism design using a conventional leaf flexure, as described in Section 6.3.5.

In Phase 1, parametric sweeps are conducted to iteratively refine the design pace towards the region containing the most promising solutions. This phase uses a relatively coarse mesh and only evaluates the adduction stiffness and von Mises stress at 30° flexion, rather than across the entire range of motion, from 8° extension to 30° flexion. This strategy facilitates efficient data collection, but may introduce false-feasible solutions.

In Phase 2, the most promising solutions from Phase 1 are re-evaluated across the full range of motion using a mesh convergence study. This eliminates false-feasible solutions and identifies the optimal parameter combination that is truly feasible.

The mesh used for the parametric sweeps in Phase 1 has two elements through the thickness and depth of the warping constraints, and four elements through their width. For the sections of the leaf flexure between the warping constraints, an element size of $\frac{w_{leaf}}{4}$ is selected.

Phase 1: Iterative design space refinement through parametric sweeps

Since the objective is to minimize flexion stiffness, the corresponding performance indicator – the hip flexion moment required to achieve a 30° flexion angle – is used to evaluate the solutions within the parametric sweeps. Figure 6.16 illustrates the relationship between this indicator, and the dimensional parameters of the warping constraints and the leaf flexure thickness, through scatter plots of the sweeps conducted in this phase. Each scatter point in these plots represents a unique combination of dimensional parameters. Jittering was applied to introduce small random horizontal perturbations, improving the visual distinction between individual solutions. Solutions that do not comply with all **must** statements outlined in Table 6.2 are filtered out, leaving only feasible solutions for evaluation. The individual parametric sweeps are discussed in detail below the figure.

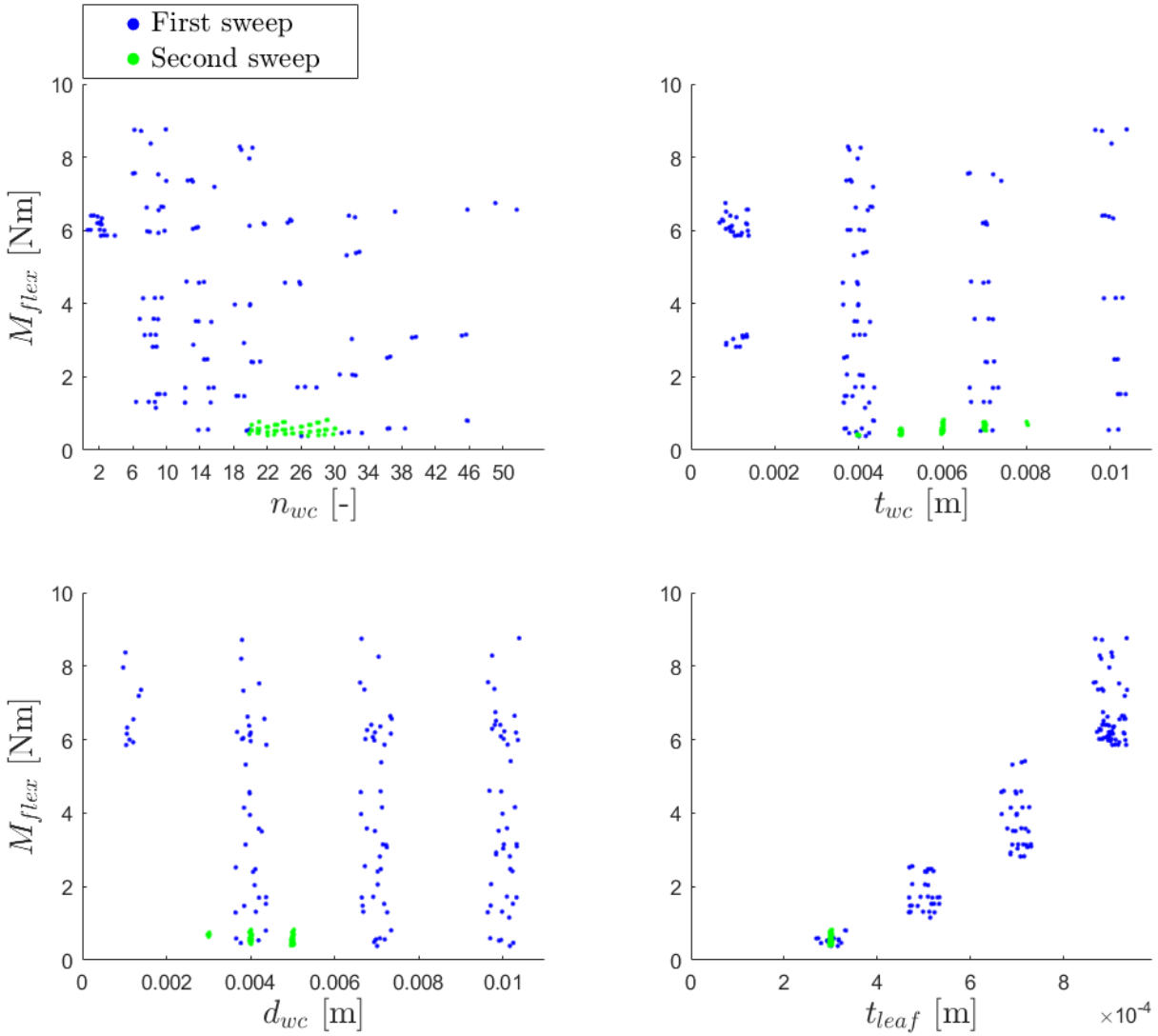

Figure 6.16: Scatter plots showing the relationship between the dimensional parameters of the warping constraints and the leaf flexure thickness, and the hip flexion moment required to achieve a 30° flexion angle.

First parametric sweep
Rather than covering the entire design space, the first parametric sweep targets the region most likely to contain the optimal solution.

For n_{wc}, a range from 2 to 50 was selected based on what were intuitively considered reasonable upper and lower boundaries. For t_{wc} and d_{wc}, values up to 10 mm were explored, as for these parameters further increase beyond a certain threshold was expected to no longer have significant effect on performance. For t_{leaf}, only values smaller than the value selected for the mechanism design using a conventional leaf flexure were considered, as ultimately the goal is to achieve reduction in leaf flexure thickness.

Table 6.9 outlines the exact values investigated for each parameter. Parameter combinations that do not satisfy $n_{wc} \cdot t_{wc} < 0.23$ m were excluded. It should be noted that this sweep covers only a subset of the full design space. If results indicate a promising trend toward the boundaries of this subset, extrapolation remains a viable next step.

Parameter	**Value range**	**Step size**
n_{wc}	2 – 50	6
t_{wc}	1.0 – 10 mm	3.0 mm
d_{wc}	1.0 – 10 mm	3.0 mm
t_{leaf}	0.10 – 0.90 mm	0.20 mm

Table 6.9: Dimensional parameter values explored in the first parametric sweep.

Figure 6.16 reveals the following trends among the first parametric sweep results:

- Reducing t_{leaf} significantly enhances the potential for minimizing flexion stiffness, but is accompanied by a reduction in the number of feasible solutions.

- n_{wc}, t_{wc}, and d_{wc} show relatively consistent potential for minimizing flexion stiffness throughout their respective ranges, as long as a certain threshold value is reached. However, these parameters cannot all be set exactly at this threshold. If one is small, another must be larger to ensure sufficient structural support for facilitating a small t_{leaf}.

These findings suggest that, as long as t_{leaf} is minimized, a wide range of values for n_{wc}, t_{wc}, and d_{wc} can yield similarly low flexion stiffness. Therefore, mass minimization is introduced as a secondary design objective to identify favorable regions within the design space. Figure 6.17 illustrates the relationship between the dimensional parameters of the warping constraints, and the mass of the leaf flexure including the warping constraints, for the subset $t_{leaf} = 0.30$ mm.

This figure shows that within this subset, in contrast to their limited influence on flexion stiffness, the parameters n_{wc}, t_{wc}, and d_{wc} do have a significant effect on mass. A small value for d_{wc}, combined with moderate values for t_{wc} and n_{wc} appears to offer the best potential for mass minimization.

Based on these insights, a second parametric sweep was conducted to zoom in on the regions of the design space with the most promising solutions.

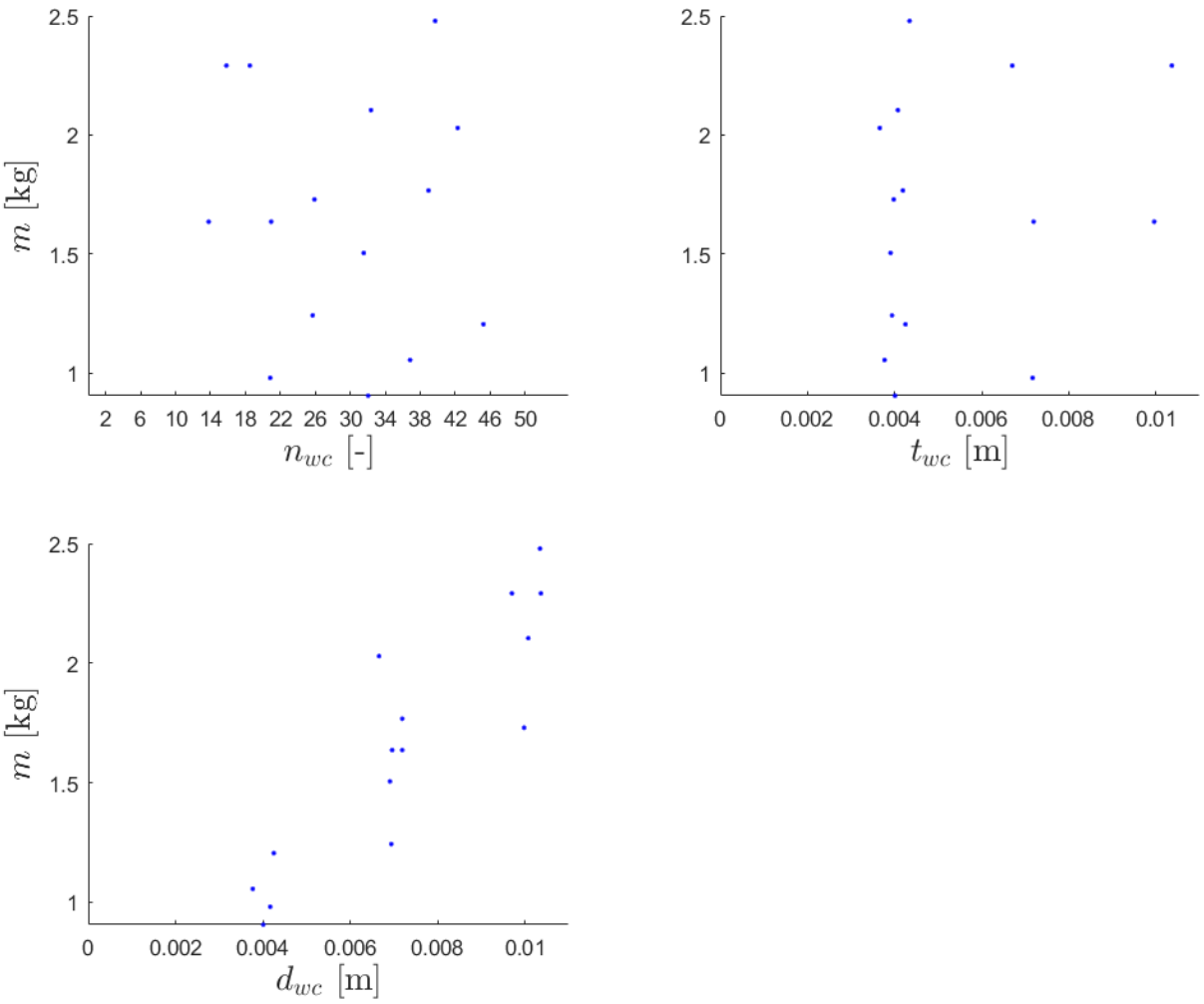

Figure 6.17: Scatter plots showing the relationship between the dimensional parameters of the warping constraints, and the mass of the leaf flexure including the warping constraints, for the subset $t_{leaf} = 0.30$ mm.

Second parametric sweep

Table 6.10 outlines the parameter values explored in the second parametric sweep.

Parameter	**Value range**	**Step size**
n_{wc}	20 – 30	1
t_{wc}	3.0 – 8.0 mm	1.0 mm
d_{wc}	2.0 – 5.0 mm	1.0 mm
t_{leaf}	0.20 – 0.30 mm	0.10 mm

Table 6.10: Dimensional parameter values explored in the second parametric sweep.

All parameter combinations with $t_{leaf} = 0.20$ mm resulted in failure, leaving only feasible solutions with

$t_{leaf} = 0.30$. As expected, Figure 6.16 shows very little variation in flexion stiffness among these remaining solutions. Therefore, the parametric influence on mass is again examined using Figure 6.18.

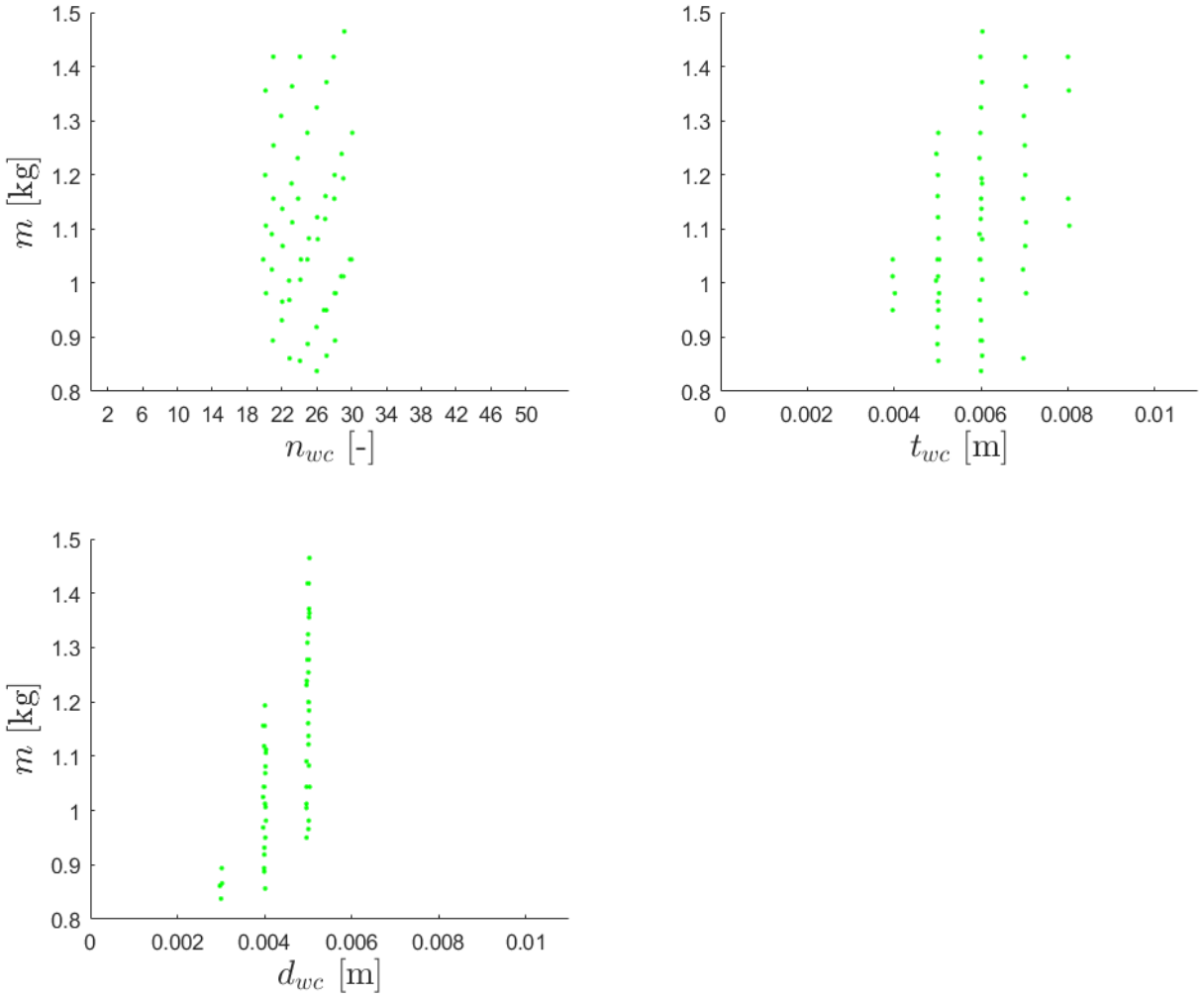

Figure 6.18: Scatter plots showing the relationship between the dimensional parameters of the warping constraints, and the mass of the leaf flexure including the warping constraints.

This figure shows great mass variation between solutions and reveals the following trends:

- n_{wc} and t_{wc} show convex trends, indicating that the solution with lowest mass is encompassed within the explored range.
- d_{wc} and t_{leaf} show the same trends as in the first parametric sweep, where decreasing these parameters enhances the potential for minimizing mass. However, further reduction yields only infeasible solutions.

These results confirm that the second parametric sweep successfully targeted the most promising regions of the design space. Since this sweep already achieves the parameter resolution defined in the assumptions

in Section 6.4.2, no further refinement step is possible. Therefore, this second parametric sweep concludes Phase 1 of the dimensional parameter selection process.

Phase 2

In Phase 1, parameter combinations that did not comply with all **must** statements outlined in Table 6.2 were filtered out. However, for efficiency purposes, a coarse mesh was used and the adduction stiffness and von Mises stress were evaluated only in the 30° flexion position rather than across the entire range of motion, from 8° extension to 30° flexion. This may result in false-feasible solutions.

To address this, Phase 2 re-evaluates the adduction stiffness and von Mises stress in the most promising solutions from Phase 1. This evaluation considers the full range of motion, and results are obtained through a mesh convergence study. This ensures that the selected solution is truly feasible.

The design process focuses in minimizing flexion stiffness. However, all solutions within the second parametric sweep exhibit similar flexion stiffness but show significant variation in mass. Therefore, mass minimization is again considered as the secondary design objective to identify the most promising solutions.

For the lightest solutions, the adduction stiffness and von Mises stress were re-evaluated across the entire range of motion, from 8° extension to 30° flexion, using a mesh convergence study to ensure result accuracy. This revealed that the 14 lightest solutions were false-feasible, with the 15$^{\text{th}}$ lightest solution being the first to prove truly feasible.

Figure 6.19 presents the full range of motion measurements for adduction stiffness and von Mises stress of this parameter combination. The adduction angle remains below 1.0° and the von Mises stress below 500 MPa throughout the entire range, confirming compliance with the minimum required adduction stiffness and maximum allowable von Mises stress, as specified in Table 6.2.

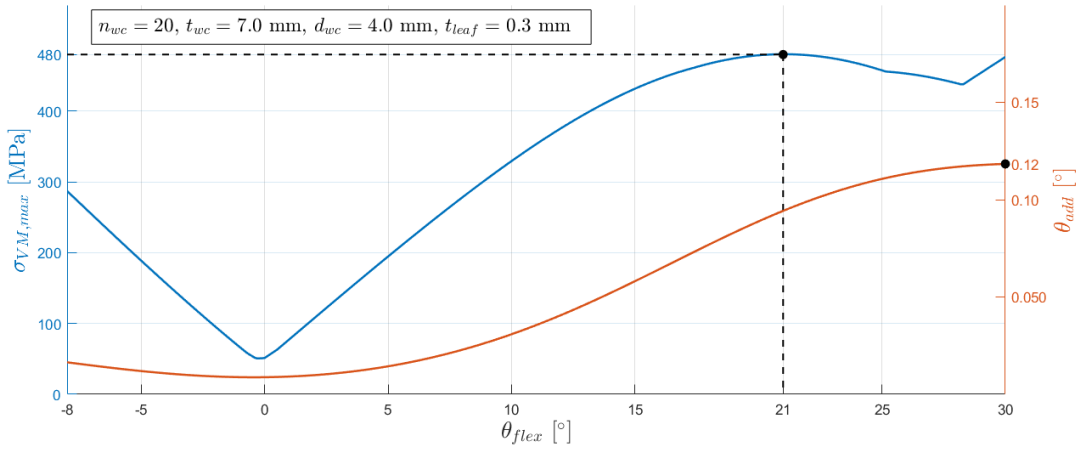

Figure 6.19: Measurement of the adduction angle and maximum von Mises stress resulting from a 57 Nm adduction moment applied throughout the entire range of motion from 8° extension to 30° flexion, for the selected parameter combination.

6.4.5 Design evaluation

In Section 6.4.4, the optimal dimensional parameters were selected for the warping constraints and leaf flexure thickness to minimize the flexion stiffness while ensuring compliance with all **must** statements in Table 6.2. Since the leaf flexure's length, width, and material remain unchanged from the mechanism design using a conventional leaf flexure, the design process is considered complete. Table 6.11 summarizes the selected dimensions and material for the leaf flexure incorporating warping constraints.

This section presents the evaluation of the resulting design, including performance measurements, a performance evaluation, and an artist impression representing the leaf flexure in motion.

Dimensions		**Material**	
$L_{leaf,leg}$	$= 0.060$ m	Type	= Steel
$L_{leaf,ub}$	$= 0.17$ m	E	$= 210$ GPa
w_{leaf}	$= 0.20$ m	ρ	$= 7.8 \cdot 10^3$ kg/m^3
t_{leaf}	$= 0.30$ mm	ν	$= 0.28$
		σ_f	$= 500$ MPa
n_{wc}	$= 20$		
t_{wc}	$= 7.0$ mm		
d_{wc}	$= 4.0$ mm		

Table 6.11: Dimensions and material selected for the leaf flexure incorporating warping constraints.

Performance measurements

The measurement methods for this design are identical to those used for the mechanism design using a conventional leaf flexure, and are therefore not detailed again. However, to provide insight into its performance, Figures 6.20, 6.21, and 6.22 show the relevant deformations and stress distribution.

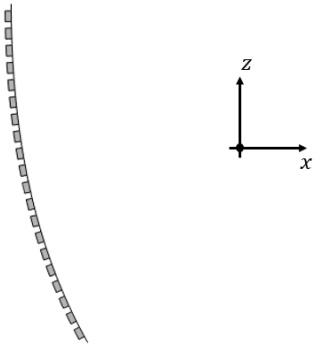

Figure 6.20: Lateral view of the deformation of the leaf flexure resulting from a 30° prescribed flexion angle.

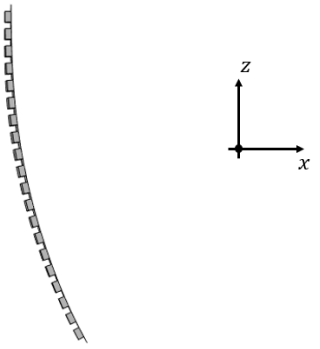

Figure 6.21: Lateral view of the deformation of the leaf flexure resulting from a 57 Nm adduction moment applied at a 30° flexion angle.

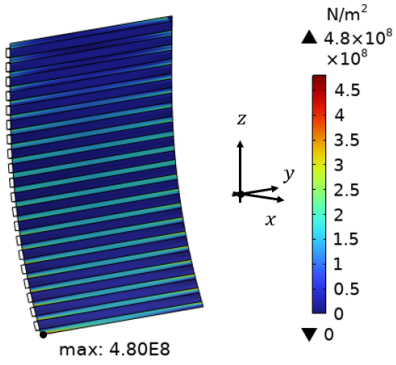

Figure 6.22: Von Mises stress distribution on the leaf flexure resulting from a 57 Nm adduction moment applied at a 21° flexion angle.

Performance evaluation

The results of the performance measurements conducted in the previous section have been incorporated into Table 6.2 to evaluate the design's performance. The results are presented in Table 6.12.

The design objective was to further reduce the flexion stiffness through implementation of warping constraints, while remaining compliance with all **must** statements outlined in Table 6.2, as previously achieved with the conventional leaf flexure. As shown in Table 6.12, the resulting design requires a 0.55 Nm hip flexion moment to achieve a 30° flexion angle. Moreover, the design satisfies all **must** statements, confirming that this is a satisfactory alternative solution.

Property	**Req**	**Must**	**Should**	**Performance**
Adduction stiffness	1a	$\theta_{add} \mid^{M_{add}=57\,\text{Nm}}_{\theta_{flex}\in[-8°,\ 30°]} < 1.0°$		$\theta_{add} \leq 0.12°$
Flexion stiffness	1b	$M_{flex} \mid_{\theta_{flex}=30°} < 43\,\text{Nm}$	Min $M_{flex} \mid_{\theta_{flex}=30°}$	$M_{flex} = 0.55$ Nm
Von Mises stress	1c	$\sigma_{VM,max} \mid^{M_{add}=57\,\text{Nm}}_{\theta_{flex}\in[-8°,\ 30°]} < \sigma_f = 500$ MPa		$\sigma_{VM,max} \leq 480$ MPa
Mass	3a	$m_{mech} < 2.5$ kg	Min m_{mech}	$m_{mech} = 0.98$ kg
Thickness	3b	$t_{mech} < 4.5$ cm	Min t_{mech}	$t_{mech} = 4.3$ mm
Surface area	3c		Min A_{mech}	$A_{mech} = 0.046$ m^2

Table 6.12: Performance evaluation for the mechanism design using a leaf flexure incorporating warping constraints.

Artist impression

Figure 6.23 provides an artist impression of the leaf flexure design, illustrating its scale and placement relative to the human body, as well as its function in enabling flexion/extension freedom.

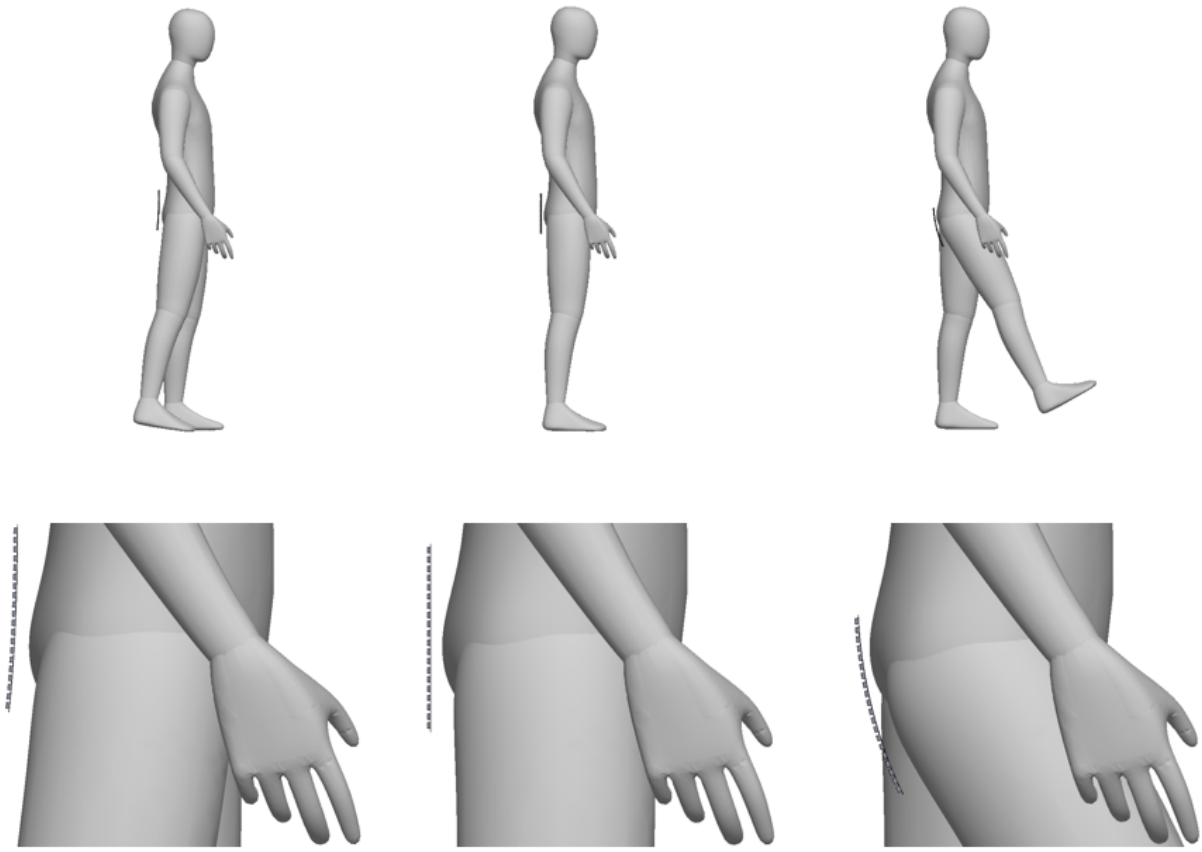

(a) 8° extension. (b) Neutral position. (c) 30° flexion.

Figure 6.23: Artist impression of the leaf flexure design incorporating warping constraints.

7 Discussion

7.1 Interpretation of design performance

The design process in this thesis distinguished between the attachment parts and the mechanism of the orthosis. In this section, the resulting designs for both components are discussed.

7.1.1 Attachment parts

A preliminary attachment parts design was developed in Chapter 4. The aim was to evaluate whether the established orthotic methods and materials are suitable for this application. Additionally, the design margins available for the orthosis mechanism were determined.

The design was developed using a thermoplastic material compatible with a thermoforming process, aligning with common orthotic practice. This design satisfied all **must** statements in Requirements 2a through 3c, confirming suitability of the established orthotic methods and materials for this application. The resulting design margins available for the orthosis mechanism were considered sufficient.

Robustness

The robustness of the attachment parts design is evaluated by assessing the reliability of the obtained results, the available safety margins, and the adaptability of the design.

- The attachment parts design was developed for the hypothetical patient introduced in Section 3.2. This patient was assumed to have complete loss of hip abduction function, whereas in practice, patients often retain some degree of functionality. This thesis thus considered the worst-case scenario in terms of expected adduction load and therefore required adduction stiffness. This conservative approach introduced a safety margin in the design.
- The attachment parts design involved relatively straightforward linear analyses, which provides confidence in the validity of the results.
- For limitations in the COMSOL model (see below), a conservative approach was adopted, using scenarios more demanding than those expected in practice. This introduced an extra safety margin.
- While a thermoplastic material was selected for this design, it can be adjusted to carbon fiber, which is also commonly used in orthotic practice. This may lead to a design that is stronger, stiffer, more compact, and lighter.

Limitations

Although the attachment parts design was developed through a structured approach and yielded promising results, several limitations exist.

- Based on expert advice from Simone Schoon [19], the attachment parts design prioritized pressure minimization among the **should** statements in the requirements. However, this prioritization has not been validated with clinical data, leaving it uncertain whether this was indeed the optimal choice.
- Simplified shapes were assumed for representation of the human body. This may result in deviations in the stiffness behavior of the attachment parts when they are fitted to an actual patient.

- The adduction load distribution from the body to the attachment parts was approximated and may differ from actual physiological load transfer, leading to different deformation of the attachment parts.
- In COMSOL, the adduction load was applied along a line rather than distributed over a surface (see Figure 4.7). This likely results in an overestimation of deformation.
- The fixation points between the attachment parts and the orthosis mechanism were chosen arbitrarily due to the absence of a mechanism design at that stage. These locations may be revised to obtain more accurate stiffness evaluation if deemed necessary.
- The stabilizing effect of the human body pressing outward against the attachment parts was not included in the COMSOL model, likely causing an overestimation of the deformation.
- No technical or clinical testing was conducted to quantitatively verify the results obtained in COMSOL or to validate the overall effectiveness of the design.

7.1.2 Mechanism

For the orthosis mechanism, the goal was to develop an innovative compliant solution by advancing the previously researched design introduced in Section 2.4, or by introducing a new concept. Chapter 5 described the concept phase, where Concepts 4 and 8 were identified as the most promising solutions. Concept 4 represented the concept of the previously researched design, while Concept 8 was a newly developed concept. Preliminary designs were created for both concepts and evaluated quantitatively. Concept 8 showed more potential for flexion stiffness minimization, as well as for enabling a lightweight and compact design. Therefore, Concept 8 was taken forward into the design phase. As a consequence, this thesis did not continue working with the previously researched design.

The selected concept features a leaf flexure located on the posterior side of the patient's body. Chapter 6 presented two mechanism designs based on this concept: one using a conventional leaf flexure, and one using a leaf flexure incorporating warping constraints.

Design performance comparison

The performance of the two mechanism designs is compared in Table 7.1. Both designs satisfy all **must** statements outlined in this table, indicating that both are viable solutions. Differences in performance are assessed through evaluation with respect to the **should** statements.

Among all **should** statements, flexion stiffness minimization was prioritized during the design process. It was hypothesized that incorporation of warping constraints would enable further reduction of the flexion stiffness. The results confirm this hypothesis, as the design using a conventional leaf flexure requires a 7.9 Nm hip flexion moment to achieve a 30° flexion angle, while this is 0.55 Nm in the design using a leaf flexure incorporating warping constraints. This represents a significant improvement of over an order of magnitude.

This reduction in flexion stiffness came at the cost of increased mass and thickness: the mass increased from 0.36 kg to 0.98 kg, and the thickness from 1.0 mm to 4.3 mm. However, relative to the 4.5 cm thickness limit, the difference between the two thicknesses is small. Therefore, the main tradeoff when implementing warping constraints is between flexion stiffness and mass minimization.

In this thesis, the warping constraints were optimized to achieve maximum reduction of flexion stiffness. However, a more moderate implementation is also possible, aiming for partial reduction in flexion stiffness with limited increase in mass. The optimal tradeoff will likely vary between patients, depending on

individual needs and preferences.

Finally, since both designs use the same base leaf flexure geometry, their surface areas are identical. Therefore, this property was not a distinguishing factor in the comparison.

Property	Req	Must	Should	Performance Conventional	Performance Warping Constraints
Adduction stiffness	1a	$\theta_{add} \mid^{M_{add}=57\,\text{Nm}}_{\theta_{flex}\in[-8°,\ 30°]} < 1.0°$		$\theta_{add} \leq 0.31°$	$\theta_{add} \leq 0.12°$
Flexion stiffness	1b	$M_{flex} \mid_{\theta_{flex}=30°} < 43\,\text{Nm}$	Min $M_{flex} \mid_{\theta_{flex}=30°}$	$M_{flex} = 7.9$ Nm	$M_{flex} = 0.55$ Nm
Von Mises stress	1c	$\sigma_{VM,max} \mid^{M_{add}=57\,\text{Nm}}_{\theta_{flex}\in[-8°,\ 30°]} < \sigma_f = 500$ MPa		$\sigma_{VM,max} \leq 487$ MPa	$\sigma_{VM,max} \leq 480$ MPa
Mass	3a	$m_{mech} < 2.5$ kg	Min m_{mech}	$m_{mech} = 0.36$ kg	$m_{mech} = 0.98$ kg
Thickness	3b	$t_{mech} < 4.5$ cm	Min t_{mech}	$t_{mech} = 1.0$ mm	$t_{mech} = 4.3$ mm
Surface area	3c		Min A_{mech}	$A_{mech} = 0.046$ m^2	$A_{mech} = 0.046$ m^2

Table 7.1: Performance comparison of the mechanism design using a conventional leaf flexure, and a leaf flexure incorporating warping constraints. Green circles indicate the best performing design with respect to the **should** statements in the requirements.

Robustness

The robustness of the mechanism designs is evaluated by assessing the reliability of the obtained results, the available safety margins, and the adaptability of the designs.

- The mechanism designs were developed for the hypothetical patient introduced in Section 3.2. This patient was assumed to have complete loss of hip abduction function, whereas in practice, patients often retain some degree of functionality. This thesis thus considered the worst-case scenario in terms of expected adduction load and therefore required adduction stiffness. This conservative approach introduced a safety margin in the designs.

- Section 5.6 introduced a scale model to validate the general working principle of the mechanism. It was also used to qualitatively validate the deformations suggested by COMSOL, thereby increasing confidence in the obtained results.

- Both designs satisfy the minimum required adduction stiffness with significant margin, indicating robust solutions with respect to this requirement. However, it was observed that the dominant deformation mode for adduction is lateral bending through torsion of the leaf flexure. Given that lateral torsional buckling is a known failure mode for leaf flexures, it is important to verify that the designs do not approach this condition. To assess this, the moment-angle relationships for adduction were plotted in the critical position for both designs. These are $\theta_{flex} = 24°$ for the design using a conventional leaf flexure, and $\theta_{flex} = 30°$ for the design using a leaf flexure incorporating warping constraints (see Figures 6.9 and 6.19). The adduction load was extrapolated to twice the expected value, from 57 Nm to 114 Nm, to introduce an extra safety margin. The resulting graphs are shown in Figure 7.1. Both designs remain below a 1.0° adduction angle, meaning that even at twice the expected adduction load, the minimum required adduction stiffness is still met. Additionally, the curves remain smooth and continuous throughout, indicating that no abrupt loss of stiffness occurs, which would be a key indicator of buckling. However, where the curve for the design using a conventional leaf flexure remains almost linear, the curve for the design using a leaf flexure incorporating warping constraints shows a strongly nonlinear trend at adduction moments larger than roughly 60 Nm, indicating that instability is introduced. These results indicate that

mainly the design using a conventional leaf flexure is very robust against lateral torsional buckling, while in the design using a leaf flexure incorporating warping constraints this is a failure mode that must be considered.

- Both designs show a peak von Mises stress that approaches the maximum allowable value, indicating potentially non-robust solutions. However, the measured peak stresses occur near the boundary conditions in the models. While they are not singularities, as mesh refinement resulted in convergence, the proximity to the boundary conditions likely still leads to an overestimation of the realistic peak stress values.

- The flexion stiffness, mass, and thickness of both designs are all far below their respective limits, making them robust against design alterations.

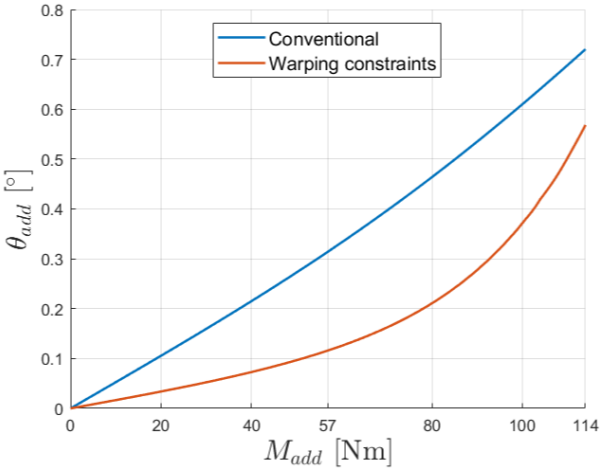

Figure 7.1: Moment-angle relationship for adduction in both designs, computed in the respective critical positions, $\theta_{flex} = 24°$ (conventional) and $\theta_{flex} = 30°$ (with warping constraints).

Notable results

In the full range of motion measurements of adduction stiffness and von Mises stress for both designs (see Figures 6.9 and 6.19), several notable trends can be observed.

Compliant mechanisms typically lose their supporting stiffness with increasing deflection. In this case, adduction stiffness is thus expected to reduce with increasing angles of flexion/extension. Initially, the figures show a trend that follows this expectation. However, beyond a certain flexion angle, the adduction stiffness starts to increase again. This is because as the flexion angle increases, the upper body portion of the leaf flexure length effectively decreases, making it more resistant to adduction. After a certain point, this effect outweighs the stiffness loss due to increased deflection, resulting in the observed increase in adduction stiffness.

The von Mises stress curves initially show an increase in stress with growing angles of flexion/extension, as expected. However, beyond a certain flexion angle, the stress temporarily decreases after which it rises sharply. This pattern results from the deformation behaviour of the leaf flexure and the location where peak stress occurs. At lower flexion angles, the highest curvature, and thus the peak stress, is located at the bottom end of the leaf flexure. As flexion increases, this region straightens out resulting in stress reduction. Meanwhile, curvature at the top end of the leaf flexure grows. Peak stress shifts to this location

and continues to grow with increasing flexion angles.

Limitations

Although the mechanism designs were developed through a structured approach and yielded promising results, several limitations exist.

- Based on expert advice from Simone Schoon [19], the design process prioritized flexion stiffness minimization among the **should** statements in the requirements. However, this prioritization has not been validated with clinical data, leaving it uncertain whether this was indeed the optimal choice.

- The mechanism is fixed to the patient's body through the attachment parts of the orthosis. The COMSOL models use idealized boundary conditions with fully rigid constraints, while in reality the human body is deformable. As a result, the mechanism's adduction stiffness may be lower in practice than suggested by the model.

- The concept includes a linear motion connection between the top end of the leaf flexure and the upper body attachment part of the orthosis. The design or selection of a linear motion connection was excluded in this thesis, while idealized functionality was assumed: frictionless movement in the direction of linear motion, and infinite stiffness in all other directions. In reality, a degree of friction or stiffness is expected in the direction of linear motion, depending on the specific solution, and a degree of compliance is expected in all other directions. As a result, this model likely overestimates flexion compliance and adduction stiffness of the overall mechanism.

- In practice, the leaf flexure may interact with the body. For example, during hip flexion, the leaf flexure may bend around the buttocks, pushing the flexure backward. This interaction could increase flexion stiffness and stress, but may also act as a torsion constraint and increase adduction stiffness. These effects were not incorporated in the COMSOL model.

- No technical or clinical testing was conducted to quantitatively verify the results obtained in COMSOL or to validate the overall effectiveness of the designs.

7.2 Reflection on using a compliant mechanism

Throughout this thesis, several design decisions were made under conditions of limited information. The most fundamental decision was to use a compliant mechanism rather than a traditional mechanism. The results discussed in Section 7.1 confirm that the use of a compliant mechanism in this application is feasible. This section reflects on whether the anticipated benefits of compliant mechanisms highlighted in Section 2.5 – such as compactness, low mass, adaptability to misalignment, and adjustable levels of support – have also been realized.

Compact and low mass

Both variations of the mechanism design – one using a conventional leaf flexure and one using a leaf flexure incorporating warping constraints – satisfy the **must** statements in the mass and size requirements (3a and 3b) with significant margin. Additionally, due to the inherent compliance of the leaf flexure, it is expected to adapt to the curves of the patient's body, thereby further improving space-efficiency. While the possibility that a traditional mechanism could have yielded an even more compact or lightweight design was not explored, the compliant approach clearly led to a favorable outcome.

Adaptability to misalignment

The mechanism theoretically accommodates misalignment for flexion and extension, as its freedom system allows rotation about any axis within a box of parallel lines (see Figure 5.8). This should enable a natural

feeling of flexion/extension freedom for the patient. However, this remains to be confirmed through clinical testing.

Adjustable levels of support
The mechanism allows for adjustable levels of support, as the adduction stiffness can be varied through the implementation of different leaf flexures. This facilitates precise support that serves only as an *addition* to the patient's remaining hip abductor muscle strength, thereby encouraging active muscle engagement. However, this too remains a hypothesis requiring validation in practice.

In summary, the expected benefits of using a compliant mechanism were largely realized, although some still require confirmation through clinical testing. The expected challenges – including complex kinematics, nonlinear analyses, loss of support stiffness at deflection, inherent stiffness in degrees of freedom, and fatigue – were effectively addressed during the design process. Overall, the decision to use a compliant mechanism has proven to be appropriate.

7.3 Comparison with existing designs
In this section, the design developed in this thesis is compared to the state-of-the-art hip orthoses introduced in Section 2.3, as well as the previously researched design introduced in Section 2.4.

7.3.1 State-of-the art hip orthoses
As discussed in Chapter 2, state-of-the-art hip orthoses are not suitable for correcting Trendelenburg gait. They are not designed to constrain movement by force, and therefore lack the load-bearing capacity required to constrain adduction under the adduction moment generated by the body weight. Furthermore, their attachment parts are confection rather than custom-made, resulting in ineffective and uncomfortable constraint transfer to the patient's body. The design developed in this thesis addresses these limitations.

A key aspect in which this design distinguishes itself from state-of-the-art hip orthoses is the use of a compliant mechanism rather than a traditional mechanism. This design decision introduced both benefits and challenges, as discussed in Section 7.2.

A drawback of the improved mechanical performance of this design is its relatively high mass. The orthosis weighs either 2.9 kg or 3.5 kg, depending on whether a conventional leaf flexure or a leaf flexure incorporating warping constraints is used in the mechanism. In comparison, state-of-the-art hip orthoses typically weigh up to 2.3 kg (see Appendix A). Although heavier than the state-of-the-art, these values remain within the limit specified in Requirement 3a, which states that the orthosis must weigh less than 5.0 kg. The attachment parts, weighing 2.5 kg, contribute most to the total mass.

The resulting design is also slightly less compact than state-of-the-art hip orthoses. Again, the attachment parts are the main contributor, as they were designed to minimize pressure by maximizing the contact area (see Figures 2.10 and 4.10). The mechanism, on the other hand, is more compact than those found in state-of-the-art orthoses, even before considering the leaf flexure's potential adaptation to the curves of the human body (see Figures 2.10, 6.13, and 6.23).

7.3.2 Previous research
Section 2.4 introduced a previously researched conceptual design of a compliant hip orthosis specifically aimed at correcting Trendelenburg gait. As this design was purely conceptual and not developed at realistic scale, the comparison focuses on conceptual and methodological differences, including how various limitations have been addressed in this thesis.

The mechanism from this previous research was included in the concept phase of this thesis as Concept 4, and was quantitatively compared with Concept 8, the concept selected for further development. The

primary difference between the concepts is that Concept 4 features leaf flexures on both the anterior and posterior side of the body, whereas Concept 8 includes only one posterior. The quantitative evaluation indicated that Concept 8 offered greater potential for minimizing flexion stiffness, as well as for achieving a lightweight and compact design.

The previous research focused exclusively on maximizing the stiffness ratio between adduction and flexion/extension, without considering the actual required adduction stiffness and flexion/extension compliance. This thesis did consider this, resulting in an actual design with carefully selected dimensions and material. Additionally, this thesis explored incorporation of warping constraints to further reduce flexion stiffness.

Another important limitation addressed in this thesis is evaluation of full range of motion stiffness behaviour. The previous research only considered the neutral position, whereas this thesis ensured sufficient adduction stiffness across the entire range of motion, from 8° extension to 30° flexion. This is particularly important in compliant mechanisms, where support stiffness typically decreases with increasing deflection.

Finally, the previous research did not consider the attachment parts design. In contrast, this thesis developed a design in Chapter 4, demonstrating suitability of the established methods and materials for direct implementation into this orthosis.

On the other hand, the previous research did propose a solution for the linear motion connection between the leaf flexures and the upper body attachment part using wire flexures, whereas this thesis left this component out of scope. However, COMSOL simulations conducted in this thesis indicated that wire flexures are not a feasible solution, as the vertical displacement of the leaf flexure during hip flexion/extension exceeds the linear range that can be accommodated by wires.

7.4 Future research

While promising results were obtained and the proposed design appears to be a viable solution, further research is required to verify its effectiveness and to advance it into a clinically usable product.

7.4.1 Testing

One of the main limitations of this thesis is the absence of a physical test phase. This decision was motivated by the desire to cover the full breadth of the design process, including a preliminary attachment parts design and the exploration of warping constraints in the mechanism. Although technical testing would have been feasible, clinical testing was not, due to the lack of an available patient and limited access to orthotic fabrication resources. In future research, both technical and clinical testing are recommended.

Technical testing

The orthosis attachment parts and mechanism designs developed in this thesis were evaluated using FEM simulations in COMSOL without validating the results experimentally. For the attachment parts, it is recommended to proceed directly to clinical testing, as this aligns with common practice in orthotics. However, as the mechanism developed in this thesis is a compliant solution with complex, nonlinear behaviour, technical testing to validate the COMSOL results is strongly recommended. This requires development of a test setup that replicates the boundary conditions used in COMSOL, as illustrated in Figure 6.5.

Clinical testing

If the results of technical testing align well with the results obtained in COMSOL, the logical next step is to proceed with clinical testing of a prototype. In Chapter 3, the functional needs of the orthosis were translated into quantified requirements. These were aimed at effectively correcting Trendelenburg

gait, facilitating a natural gait pattern, and ensuring patient comfort. Clinical testing should determine whether these goals are actually achieved in practice.

In addition, clinical testing will provide valuable patient feedback. The requirements listed in Section 3.4 include both **must** and **should** statements, representing strict design limits and optimization objectives. The selected limit values and prioritized optimization objectives – flexion stiffness minimization for the mechanism and pressure minimization for the attachment parts – were based on informed estimations and expert advice from Simone Schoon [19]. Patient feedback can confirm whether these choices were appropriate, or whether they should be reconsidered.

Clinical testing will also reveal the impact of the assumptions and simplifications made in the COMSOL models, as outlined in the limitations in Section 7.1. These include the use of simplified geometry for the human body, estimated loading conditions, exclusion of interaction with the patient's body, and idealized boundary conditions. All of these factors are expected to influence the effective adduction and flexion/extension stiffness of the orthosis in practice.

Furthermore, clinical testing can assess whether the orthosis is suitable for a broader patient population. The design developed in this thesis was tailored to the hypothetical patient introduced in Section 3.2, based on population averages. Although the robustness of the design, as discussed in Section 7.1, suggests it may be suitable or adaptable for patients who deviate from these averages, this remains to be validated in practice.

Finally, clinical testing can reveal whether the potential advantages of using a compliant mechanism that still require confirmation, as discussed in Section 7.2, are realized in practice. These include adaptability to the curves of the human body, tolerance to misalignment, and the ability to offer adjustable levels of support.

7.4.2 Linear motion connection

The orthosis mechanism incorporates a linear motion connection between the leaf flexure and the upper body attachment part. While its functionality was assumed and accounted for in the mechanism design, the selection or development of a specific solution was kept out of scope in this thesis.

The current mechanism design leaves sufficient margins for the integration of a linear motion connection. The remaining mass and thickness allowances are 2.1 kg or 1.5 kg, and 4.4 cm or 4.0 cm, depending on the use of a conventional leaf flexure or a leaf flexure incorporating warping constraints.

The previously researched design introduced in Section 2.4 proposed wire flexures. However, as discussed in Section 7.3, this solution is not viable in this context, since wire flexures cannot accommodate the vertical displacement of the leaf flexure during flexion/extension movement.

One potential solution is the use of miniature profile rail guides. These components typically measure up to 75 mm in length, 60 mm in width, and 16 mm in thickness. Their mass, including 20 cm of rail – enough to fit the carriage and facilitate the displacement required during gait – is 0.80 kg. These values fall well within the available design margins. Furthermore they can withstand lateral moments up to 105 Nm, exceeding the 57 Nm adduction moment used in this thesis for the 71 kg hypothetical patient [58].

An alternative highly lightweight and compact solution could involve allowing the leaf flexure to slide in and out of a guiding slot, provided jamming is avoided.

A more advanced direction for future research is the development of a compliant linear motion connection that facilitates large displacements while offering high lateral stiffness to resist the expected adduction load. Although a significant design challenge, such a solution could make a valuable contribution to the

field of compliant mechanisms.

In summary, the linear motion connection is an essential component that requires future research.

7.4.3 Design refinements

In future research, various refinements to the current design can be considered in three categories: adjustments based on patient feedback, design details, and entirely new design directions.

Adjustments based on patient feedback

As discussed in Section 7.4.1, patient feedback plays an essential role in validating the selected limit values in the **must** statements and the prioritized optimization objectives in the **should** statements of the requirements. Based on this feedback, several adjustments may be considered for both the attachment parts and the mechanism of the orthosis.

For the attachment parts, the material may be changed from thermoplastic to carbon fiber to reduce weight. Additionally, their dimensions could be reduced to further decrease mass and size, at the cost of increased pressure on the patient's body.

For the mechanism, patient feedback may be used to decide whether or not, or to what extent, to include warping constraints to minimize flexion stiffness at the cost of increased mass and size. Additionally, the dimensions could be reduced to minimize flexion stiffness, mass, and size, at the cost of reduced adduction stiffness.

In this thesis, the orthosis was designed for full support in Trendelenburg gait correction, and intended to be worn only during walking activities. However, with adjustments as described above, the design could be adapted into an ADL device, suitable for continuous daily wear with minimal downsides and a lower level of support. This is particularly interesting in patients who retain a degree of hip abduction function.

Design details

This thesis focused on the main functional components of the orthosis, without considering detailed elements of the design. These include padding of the attachment parts, connection and ergonomic integration of the various components, and closure systems. Additionally, material selection in this thesis was limited to general material types (thermoplastic was selected for the attachment parts and steel for the mechanism), without choosing specific grades.

Geometrically, rectangular shapes were used for both the leaf flexure and warping constraints in the orthosis mechanism. The warping constraints spread across the entire width of the leaf flexure and were evenly distributed along the leaf flexure's length. Any geometric irregularity could be explored to improve the mechanism's performance.

Manufacturing was only partially addressed. For the attachment parts, a thermoplastic material was selected as this is compatible with the thermoforming process commonly used in orthotic practice. However, manufacturing was not considered for the mechanism design. While the leaf flexure itself is straightforward to produce, the addition of warping constraints presents potential challenges. Producing the leaf flexure including warping constraints as a monolithic part via CNC machining is possible but may introduce internal stresses. Although these stresses do not critically affect stiffness behavior, they could impact fatigue resistance. Alternatively, the warping constraints could be added as separate components through welding, adhesive bonding, clamping, mechanical fastening, or form-closed connections. A benefit of these methods could be to enable manual adjustment of the warping constraints, thereby further enhancing adjustable stiffness characteristics of the mechanism. Alternatively, additive manufacturing may be a feasible solution, provided that a compatible material is selected.

Novel design directions
In addition to refinements of the current design, future work could explore entirely new design ideas. For example, areas of the attachment parts only subjected to tensile load could be replaced with textile material, making the attachment parts more garment-like. In the mechanism, anisotropic materials could be considered to enable directionally dependent stiffness. This could aid in minimizing flexion stiffness while providing sufficient adduction stiffness beyond what is achievable through geometry alone.

Another development direction could be to make the upper body attachment part less restrictive. Since only lateral support is needed to constrain adduction, the attachment part could be redesigned to allow flexion/extension freedom of the spine. A similar principle has been applied in a scoliosis orthosis incorporating a compliant mechanism [40].

Clinical testing may indicate that the fixation of the leg attachment part is insufficiently effective due to the deformability of the upper leg. This could be addressed by integrating a HKAFO (hip-knee-ankle-foot orthosis [59]). This extends the fixation area to include areas more rigid than the upper leg, which is relatively soft and deformable. Additionally, these regions contain anatomical protrusions such as the knee and foot, which provide natural anchor points and enhance overall stability.

7.5 Broader implications
In addition to the direct outcomes of this thesis, the work carries broader implications for the fields of orthotics and compliant mechanisms.

7.5.1 For the field of orthotics
This thesis demonstrates that the use of a compliant mechanism is feasible, even in applications that require high support stiffness at large deflections. As discussed in Section 2.5, this is one of the main challenges associated with compliant mechanisms. Successful implementation in such a demanding application suggests that compliant mechanisms could also be feasibly implemented in other orthoses. These orthoses could then also benefit from the potential advantages of compliant mechanisms outlined in Section 2.5.

Additionally, compliant mechanisms may be particularly useful in joints that do not rotate about a fixed axis. For instance, the rotation axis of the knee translates during motion, and spine movement is accommodated through combined rotation between vertebrae. The inherent adaptability to misalignment of compliant mechanisms makes them highly suitable for these applications.

Furthermore, compliant mechanisms can address spatial challenges in orthotic design. Traditional mechanisms use revolute joints to facilitate movement freedom, which must be placed lateral to the anatomical joint to align with its rotation axis. In areas with limited space, such as between the fingers, this configuration can be impractical. Compliant mechanisms can be positioned differently around the joint, thereby introducing a potential solution.

Finally, the ability to adjust support levels in compliant mechanisms opens opportunities in rehabilitation programs. By gradually reducing the support stiffness according to the principle of progressive overload, patients can be encouraged to build muscle strength during recovery while receiving adequate support.

7.5.2 For the field of compliant mechanisms
Current research on compliant mechanisms has primarily focused on precision engineering applications. Although the potential benefits of compliant mechanisms in orthoses have been recognized, research on design implementation remains limited. By demonstrating the feasibility of using a compliant mechanism in an orthosis, this thesis opens doors for further exploration in this direction. This could also extend to related fields involving biomechanics, such as exosuits and wearable robotics.

Additionally, while previous research introduced warping constraints as a space-efficient solution for selectively improving torsion stiffness in leaf flexures [48], this was only indicated by a single study, and implementation into an actual design was not yet investigated. In this thesis, warping constraints were explored to further reduce flexion stiffness while maintaining sufficient adduction stiffness. The flexion stiffness was reduced by over an order of magnitude, confirming the potential of warping constraints as suggested in previous research. The general implication of this result is that warping constraints can significantly improve the ratio between lateral and bending stiffness in leaf flexures at large deflections. This may be used in other compliant systems to maintain support stiffness at large deflections, which is a common challenge in compliant mechanisms, as discussed in Section 2.5. The main drawback of warping constraints identified in this thesis is increased mass: their implementation led to approximately a threefold increase. Thus, incorporating warping constraints introduces a design tradeoff between stiffness behaviour and mass, which must be carefully considered in other applications. Whereas this thesis prioritized stiffness behavior, this tradeoff is not binary. Rather, it exists on a continuum in which intermediate solutions can be explored to balance both objectives.

8 Conclusion

The objective of this thesis was to develop a hip orthosis that uses a compliant mechanism to correct Trendelenburg gait. The design process distinguished between the attachment parts and the mechanism of the orthosis.

For the attachment parts, the goal was to evaluate whether the established orthotic methods and materials are suitable for this application. A preliminary attachment parts design confirmed their suitability and was used to determine the design margins available for the orthosis mechanism.

For the orthosis mechanism, the goal was to develop an innovative compliant solution by either advancing the previously researched design or introducing a novel concept. The mechanism concept phase demonstrated that a new concept was more promising, offering greater potential for flexion stiffness minimization, as well as a lightweight and compact design. This concept was therefore selected for further development in the design phase.

During the mechanism design phase, two design variants were developed: one using a conventional leaf flexure, and one using a leaf flexure incorporating warping constraints. It was expected that incorporation of warping constraints would enable further reduction of the flexion stiffness, which was confirmed by the results. The hip flexion moment required to achieve a 30° flexion angle was 7.9 Nm in the design using a conventional leaf flexure, and 0.55 Nm in the design using a leaf flexure incorporating warping constraints. The main tradeoff for this improvement was increased mass, from 0.36 kg to 0.98 kg. Both designs provided sufficient adduction stiffness to constrain adduction under the adduction moment applied by the body weight, and are therefore effective in correcting Trendelenburg gait.

The design results demonstrate that the use of a compliant mechanism is feasible in this application. Furthermore, the potential benefits of a compliant mechanism – compactness, low mass, adaptability to misalignment, and adjustable levels of support – were largely realized. These results confirm that the choice to use a compliant mechanism was appropriate.

The design developed in this thesis distinguishes itself from state-of-the-art hip orthoses due to its effectiveness in correcting Trendelenburg gait, and its comfortable and effective force transfer to the patient body enabled by custom-made attachment parts. Also, the use of a compliant mechanism is a novelty in orthotic design. Compared to the previously researched design, this concept offers improved performance, as established in the concept phase, and was developed and evaluated at a realistic scale rather than purely at a conceptual level.

Although the results obtained in this thesis are promising, future research remains necessary to verify the design's effectiveness and to advance it into a clinically usable product. Technical testing is needed to validate the FEM-obtained stiffness results of the orthosis mechanism, and clinical testing is needed to verify whether the design effectively corrects Trendelenburg gait in practice.

The findings of this thesis have meaningful broader implications for both the fields of orthotic design and compliant mechanisms. In orthotics, the successful use of a compliant mechanism in this application suggests feasibility in other orthoses, potentially enabling them to achieve the same benefits. In the field of compliant mechanisms, this work highlights opportunities to expand into biomechanical applications. Moreover, the successful integration of warping constraints to reduce flexion stiffness while maintaining

adduction stiffness in this orthosis indicates their potential for broader implementation in compliant mechanisms to improve the ratio between lateral and bending stiffness in leaf flexures at large deflections.

In summary, this thesis presented a promising orthosis design using a compliant mechanism to correct Trendelenburg gait. The work contributes to the fields of orthotic design and compliant mechanisms, and provides a solid foundation for future research.

Bibliography

[1] P. Vugts, J. Rommers, B. T. Sterke, and J. Herder, "Conceptual design of a compliant hip orthosis for trendelenburg gait," in *International Design Engineering Technical Conferences and Computers and Information in Engineering Conference*, vol. 85444. American Society of Mechanical Engineers, 2021, p. V08AT08A004.

[2] PHED 301 Students, *Advanced Anatomy*, 2nd ed. Pressbooks, 2018.

[3] P. J. Mansfield and D. A. Neumann, *Essentials of kinesiology for the physical therapist assistant*, 3rd ed. Elsevier Health Sciences, 2018.

[4] M. Schuenke, E. Schulte, and U. Schumacher, *Thieme atlas of anatomy: General anatomy and musculoskeletal system*, 3rd ed. Thieme, 2020.

[5] C. A. Fukuchi, R. K. Fukuchi, and M. Duarte, "A public dataset of overground and treadmill walking kinematics and kinetics in healthy individuals," *PeerJ*, vol. 6, 2018.

[6] M. Y. Choi, D. H. Kong, J. S. Kim, K. S. Chung, J. H. Lee, S. B. Kim, and J. K. Ha, "Rehabilitation program after medial open wedge high tibial osteotomy," *Arthroscopy and orthopedic sports medicine*, vol. 6, no. 1, pp. 1–8, 2019.

[7] V. N. Gandbhir, J. C. Lam, and A. Rayi, "Trendelenburg gait," in *StatPearls [Internet]*. StatPearls Publishing, 2022.

[8] S. Gogu and V. N. Gandbhir, "Trendelenburg sign," 2020.

[9] G. Elumalai, A. K. Jha, P. Kanagarajan, and S. Sanyal, "Soccer syndrome–3: Common sacral malalignments and its manual diagnostic techniques," *American Journal of Sports Science*, vol. 4, no. 2, pp. 25–37, 2016.

[10] J. A. Herring, *Tachdjian's Pediatric Orthopaedics: From the Texas Scottish Rite Hospital for Children*, 6th ed. Elsevier, 2021.

[11] Physiopedia contributors, "Trendelenburg sign," 2023. [Online]. Available: https://www.physio-pedia.com/index.php?title=Trendelenburg_Sign&oldid=341396

[12] R. C. Evans, *Illustrated orthopedic physical assessment*, 3rd ed. Elsevier Health Sciences, 2008.

[13] A. Van Tongel and G. Fabry, "Epiphysiodesis of the greater trochanter in legg-calvé-perthes disease: the importance of timing," *Acta orthopaedica belgica*, vol. 72, no. 3, p. 309, 2006.

[14] D. Knudson, "The biomechanics of stretching," *Journal of Exercise Science and Physiotherapy*, vol. 2, pp. 3–12, 2006.

[15] S. Odak and J. Ivory, "Management of abductor mechanism deficiency following total hip replacement," *The Bone & Joint Journal*, vol. 95, no. 3, pp. 343–347, 2013.

[16] A. Loureiro, P. M. Mills, and R. S. Barrett, "Muscle weakness in hip osteoarthritis: a systematic review," *Arthritis care & research*, vol. 65, no. 3, pp. 340–352, 2013.

[17] M. H. Arokoski, M. Haara, H. J. Helminen, and J. P. Arokoski, "Physical function in men with and without hip osteoarthritis," *Archives of physical medicine and rehabilitation*, vol. 85, no. 4, pp. 574–581, 2004.

[18] K. Lung and F. Lui, "Anatomy, abdomen and pelvis, superior gluteal nerve," 2018.

[19] S. Schoon, Personal conversation with expert from Orthopedie Techniek Heiloo B.V., April 2021.

[20] N. A. Garrett, M. Brasure, K. H. Schmitz, M. M. Schultz, and M. R. Huber, "Physical inactivity: Direct cost to a health plan," *American Journal of Preventive Medicine*, vol. 27, no. 4, pp. 304–309, 2004. [Online]. Available: https://www.sciencedirect.com/science/article/pii/S0749379704001916

[21] World Health Organization, "Physical activity," Available at https://www.who.int/news-room/fact-sheets/detail/physical-activity.

[22] M. Rietveld, "A user-centered design of a hip-brace to reduce trendelenburg gait," 2021.

[23] Orthomerica Products, Inc., "Newport 3 Hip orthosis," Available at https://www.orthomerica.com/products/newport/newport-3/.

[24] Becker Orthopedic, "Care and Use Instructions: Lerman Hip Abduction Rotation Orthosis 2000," Brochure. [Online]. Available: https://beckerwebsite.blob.core.windows.net/instructions//145_Patient%20Instructions.pdf

[25] E. Verbrugge, Personal conversation with expert from Rijndam Revalidatie, February 2022.

[26] I. Lageschaar, Personal conversation with expert from Wouda Orthopedie, May 2022.

[27] A. C. Lall, G. R. Schwarzman, M. R. Battaglia, S. L. Chen, D. R. Maldonado, and B. G. Domb, "Greater trochanteric pain syndrome: an intraoperative endoscopic classification system with pearls to surgical techniques and rehabilitation protocols," *Arthroscopy techniques*, vol. 8, no. 8, pp. e889–e903, 2019.

[28] Y. Ishii, H. Noguchi, M. Takeda, J. Sato, and Y. Domae, "Efficacy of an abduction brace in preventing initial dislocation in the early postoperative period after primary total hip arthroplasty," 2012.

[29] S. K. Storer and D. L. Skaggs, "Developmental dysplasia of the hip," *American Family Physician*, vol. 74, no. 8, pp. 1310–1316, 2006.

[30] K. Wong, M. Sivan, and G. Matthews, "Flexion reminder device to discourage recurrent posterior dislocation of a total hip replacement: a case report," *Journal of Medical Case Reports*, vol. 2, no. 1, pp. 1–4, 2008.

[31] T. Sato, T. Yamaji, H. Inose, Y. Sekino, S. Uchida, S. Usuda, K. Takagishi, K. Shirakura, and H. Watanabe, "Effect of a modified s-form hip brace, wish type, for patients with painful osteoarthritis of the hip: a role in daily walking as a hip muscle exercise," *Rheumatology International*, vol. 28, no. 5, pp. 419–428, 2008.

[32] A. Nérot and M. Nicholls, "Clinical study on the unloading effect of hip bracing on gait in patients

with hip osteoarthritis," *Prosthetics and Orthotics International*, vol. 41, no. 2, pp. 127–133, 2017.

[33] Össur, "Unloader Hip," Available at https://www.ossur.com/en-us/bracing-and-supports/hip/unloader-hip.

[34] Y. Kusumoto, T. Matsuda, K. Fujii, K. Miyamoto, K. Takaki, and O. Nitta, "Effects of an underwear-type hip abduction orthosis on sitting balance and sit-to-stand activities in children with spastic cerebral palsy," *Journal of Physical Therapy Science*, vol. 30, no. 10, pp. 1301–1304, 2018.

[35] Ottobock, "Cosa Active hip abduction orthosis," Available at https://www.ottobock.africa/en/your-individual-fitting/orthoses/products-from-a-to-z/cosa-active/.

[36] N. L. of Medicine, "Scissor gait," Available at https://www.ncbi.nlm.nih.gov/medgen/68547#:~:text=Definition,in%20a%20scissors%2Dlike%20movement.

[37] L. L. Howell, *Compliant Mechanisms*, 1st ed. wiley, 2001.

[38] R. A. Bos, D. H. Plettenburg, and J. L. Herder, "Exploratory design of a compliant mechanism for a dynamic hand orthosis: Lessons learned," in *2017 International Conference on Rehabilitation Robotics (ICORR)*. IEEE, 2017, pp. 603–608.

[39] T. Cedillo, R. Flores-Luna, and E. Ramirez-Diaz, "Fem dynamic analysis of a compliant mechanism," in *Proceedings of the 14th IFToMM World Congress*, 2015, pp. 41–45.

[40] J. Ring and C. Kim, "A passive brace to improve activities of daily living utilizing compliant parallel mechanisms," in *International Design Engineering Technical Conferences and Computers and Information in Engineering Conference*, vol. 50152. American Society of Mechanical Engineers, 2016, p. V05AT07A015.

[41] S. Jun, X. Zhou, D. K. Ramsey, and V. N. Krovi, "Smart knee brace design with parallel coupled compliant plate mechanism and pennate elastic band spring," *Journal of Mechanisms and Robotics*, vol. 7, no. 4, p. 041024, 2015.

[42] J. Liu, Y. Cheng, S. Zhang, Z. Lu, and G. Gao, "Design and analysis of a rigid-flexible parallel mechanism for a neck brace," *Mathematical Problems in Engineering*, vol. 2019, pp. 1–20, 2019.

[43] R. Mallat, M. Khalil, G. Venture, V. Bonnet, and S. Mohammed, "Human-exoskeleton joint misalignment: A systematic review," in *2019 fifth international conference on advances in biomedical engineering (ICABME)*. IEEE, 2019, pp. 1–4.

[44] I. Rijken, Personal conversation with physiotherapist and falling prevention expert from Reva Centre, May 2023.

[45] L. L. Howell, S. P. Magleby, B. M. Olsen, and J. Wiley, *Handbook of compliant mechanisms*. Wiley Online Library, 2013.

[46] D. Wiersma, S. Boer, R. G. Aarts, and D. M. Brouwer, "Design and performance optimization of large stroke spatial flexures," *Journal of computational and nonlinear dynamics*, vol. 9, no. 1, p. 011016, 2014.

[47] M. Naves, D. M. Brouwer, and R. G. Aarts, "Large-stroke flexure hinges," *Mikroniek*, vol. 57, no. 3,

pp. 5–9, 2017.

[48] M. Nijenhuis, M. Naves, and D. Brouwer, "High torsion stiffness leafspring flexure element using distributed warping constraints," in *22nd International Conference & Exhibition, EUSPEN 2022*. EUSPEN, 2022, pp. 119–122.

[49] TU Delft, "Dined anthropometric database," Apr 2020. [Online]. Available: https://dined.io.tudelft.nl/en

[50] J.-F. Kahn, F. Favriou, J.-C. J. MONOD, and HUGUES, "Influence of posture and training on the endurance time of a low-level isometric contraction," *Ergonomics*, vol. 40, no. 11, pp. 1231–1239, 1997.

[51] T. Yoshizawa, K. Higashi, and T. Katou, "Measuring hip flexor and extensor strengths across various postures using a fixed belt," *Journal of physical therapy science*, vol. 29, no. 4, pp. 572–575, 2017.

[52] Ansys GRANTA EduPack software, ANSYS, Inc., Cambridge, UK, 2024. [Online]. Available: www.ansys.com/materials

[53] R. C. Hibbeler, *Mechanics of materials*, 9th ed. Pearson, 2013.

[54] G. Radaelli and J. L. Herder, "Isogeometric shape optimization for compliant mechanisms with prescribed load paths," in *International design engineering technical conferences and computers and information in engineering conference*, vol. 46360. American Society of Mechanical Engineers, 2014, p. V05AT08A046.

[55] COMSOL Multiphysics *et al.*, "Structural mechanics module–user's guide," *COMSOL® Software Documentation*, 2013.

[56] S. P. Timoshenko and J. N. Goodier, *Theory of elasticity*. McGraw-hill New York, 1982, vol. 3.

[57] H. Sönnerlind, "What is geometric nonlinearity?" *COMSOL Blog*, 2015.

[58] Ewellix, "Miniature profile rail guides – lls catalogue," 2023. [Online]. Available: https://medialibrary.ewellix.com/asset/18486

[59] P. Amiri, M. J. Sadigh, A. Esrafilian, and M. T. Karimi, "An analytical approach to investigate arm free standing of a paraplegic subject while using a new hkafo orthosis," in *2012 IEEE International Conference on Cyber Technology in Automation, Control, and Intelligent Systems (CYBER)*. IEEE, 2012, pp. 303–308.

[60] Orthomerica Products, Inc., Personal conversation, March 2022.

[61] Materials lab 3mE Delft University of technology, Hardness test, June 2022.

[62] Orthomerica Products, Inc., "California Hip Orthosis," Available at https://beagleorthopaedic.com/california-hip-system-orthomerica.

[63] Basko Healthcare, "Productcatalogus," Available at https://docplayer.nl/12061621-Productcatalogus-basko-com.html, 2015.

[64] Thuasne, "Hiploc Evo," Available at https://se.thuasne.com/sv/alla-produkterortopedi/hoft/

hiploc-evo.

[65] Vitego, “Hip joint orthosis Thuasne HipLoc Evo,” Available at https://www.vitego-shop.de/bandage-thigh-hip-thuasne-hip-joint-orthosis-hiploc-evo.

[66] Medical Expo by Virtual Expo Group, “X-Act ROM Hip Brace,” Available at https://www.medicalexpo.com/prod/donjoy/product-96003-598399.html.

[67] DJO Global, “Donjoy X-Act ROM Hip,” Brochure. [Online]. Available: https://tsbbracing.ca/wp-content/uploads/2020/07/Donjoy-X-Act-ROM-Hip.pdf

[68] Optec, “TLC Hip Abduction Brace,” Available at https://optecusa.com/product/prefab-tlc-hip-abduction-brace/.

[69] Bauerfeind, “Softec Coxa,” Available at https://www.bauerfeind-group.com/en/products/supports-and-orthoses/knee-hip-thigh/details/product/softec-coxa.

[70] ——, “Softec Coxa,” Brochure. [Online]. Available: https://www.bauerfeind.nl/fileadmin/user_upload/bauerfeind-international.com/_downloads/_instructions/_orthoses/GA_SofTec_Coxa.pdf

[71] Vitego, “Hip orthosis Bauerfeind SofTec Coxa,” Available at https://www.vitego-shop.de/bandage-hip-bauerfeind-softec-coxa.

[72] Össur, “Rebound Hip,” Available at https://www.ossur.com/en-us/bracing-and-supports/hip/rebound-hip.

[73] ——, “Rebound Hip,” Brochure. [Online]. Available: https://assets.ossur.com/library/30991/Rebound%20Hip%20%E4%BD%BF%E7%94%A8%E8%AF%B4%E6%98%8E.pdf

[74] Medi, “Hip One,” Available at https://www.medi.de/en/products/medi-hip-one/.

[75] Teufel, “DynaCox Evolution,” Available at https://www.teufel-international.com/products/orthotics/hip-orthosis-dynacox-evolution/?lang=en.

[76] ——, “DynaCox Evolution User Manual,” Available at https://www.teufel-international.com/wp-content/uploads/downloads/Produktdaten_ProductData/Orthetik/2050_Huefte_Hip/DynaCoxEvolution/DynaCoxEvo_UserManual_9039508901_Rev202207_DE_EN.pdf.

[77] Becker Orthopedic, “Lerman Hip Abduction Rotation Orthosis 2000,” Available at https://www.beckerorthopedic.com/Product/PrefabricatedOrthoses/Hip/145#documents.

[78] Basko Healthcare, “Lerman Hip Abduction Rotation Orthosis 2000,” Available at https://basko.com/nl-nl/Producten/Orthesen-en-Bandages/Heup/Details/Lerman-Hip-Abduction-Rotation-Orthosis-HARO-2000.

A State-of-the-art hip orthoses

A.1 Introduction

This appendix shows the currently available hip orthoses that allow for an adduction constraint while providing flexion/extension freedom, indicating that they can potentially be used to correct Trendelenburg gait. For each orthosis the prescription indications, influence on hip movement, production materials, and mass are shown.
The prescription indications are literal citations from the manufacturer's websites. Not every manufacturer is open about material use for their orthoses, meaning that in some cases there is no, or only partial information available regarding the materials.

A.2 Newport Hip Orthosis by Orthomerica

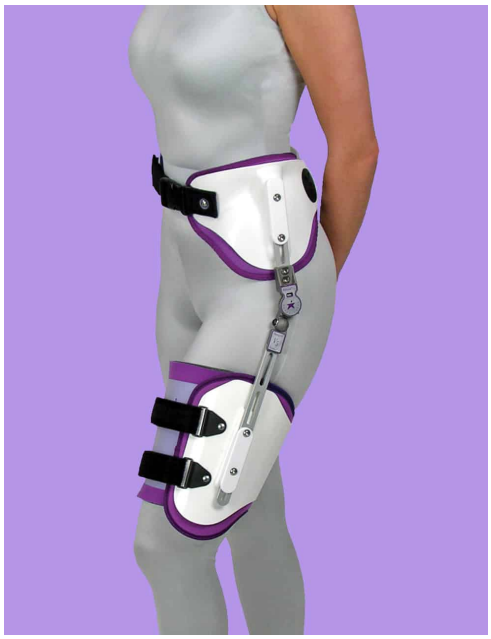

Figure A.1: Newport Hip Orthosis by Orthomerica. [23]

Indications [23]

- Post-operative hip revision patients.
- Primary arthroplasty patients at risk to dislocate.
- Patients needing stability after dislocation.
- Inoperable patients requiring hip stabilization.
- Patients who can benefit from a hip orthosis to reinforce hip precautions.

Hip movement influence [23]

- Flexion/extension: Fully allowed between limits.
- Abduction/adduction: Fixed at a set angle.
- Internal/external rotation: Fully restricted.

Materials

- Shells: Polypropylene. [60]
- Joint/bar mechanisms: Bars are aluminum, joint is steel. [61]
- Pads/attachment: No information.

Mass

- 1.5 kg, measured using a bathroom scale.

A.3 S-form hip brace, WISH type by Gunma University

Figure A.2: S-form hip brace, WISH type by Gunma University. [31]

Indications
- Painful hip osteoarthritis. [31]

Hip movement influence [31]
- Flexion/extension: Fully allowed.
- Abduction/adduction: Abduction fully allowed, adduction fully restricted.
- Internal/external rotation: Fully restricted.

Materials [31]
- Shells: Polypropylene.
- Joint/bar mechanisms: No information.
- Pads/attachment: No information.

Mass
- 0.9 kg [31].

A.4 California Hip Orthosis by Orthomerica

Figure A.3: California Hip Orthosis by Orthomerica. [62]

Indications [62]
- Post-operative hip revision patients.
- CVA, spinal cord injury or head trauma patients.
- Patients non-compliant with rigid plastic hip orthoses.
- Patients whose cognitive function impairs their ability to follow hip precautions.
- Patients who are at risk for dislocation.

Hip movement influence [63]
- Flexion/extension: Fully allowed between limits.
- Abduction/adduction: Fixed at a set angle.
- Internal/external rotation: Fully restricted.

Materials
- Shells: No information.
- Joint/bar mechanisms: No information.
- Pads/attachment: No information.

Mass
- No information.

A.5 Hiploc Evo by Thuasne

Indications [64]
- Luxation endangered hip joints.
- After endoprosthetic care.

Hip movement influence [64]
- Flexion/extension: Fully allowed between limits.
- Abduction/adduction: Fully restricted.
- Internal/external rotation: Fully restricted.

Materials [64]
- Shells: Polyethylene.
- Joint/bar mechanisms: Aluminum.
- Pads/attachment: Acrylonitrile butadiene styrene (ABS) for the pads and polyamide for the attachment.

Mass
- 2.0 kg [65].

Figure A.4: Hiploc Evo by Thuasne. [64]

A.6 DonJoy X-Act ROM Hip Brace by DJO Global

Indications [67]
- Minimally invasive hip procedures.
- Labral repair, with or without gluteus medius repair.
- Post-op proximal hamstring repair.
- Effective ROM control following primary or hip revision surgery.

Hip movement influence [67]
- Flexion/extension: Fully allowed between limits.
- Abduction/adduction: Fixed at set angle.
- Internal/external rotation: Fully restricted.

Materials
- Shells: No information.
- Joint/bar mechanisms: No information.
- Pads/attachment: No information.

Mass
- No information.

Figure A.5: DonJoy X-Act ROM Hip Brace by DJO Global. [66]

A.7 TLC Abduction Brace by Optec

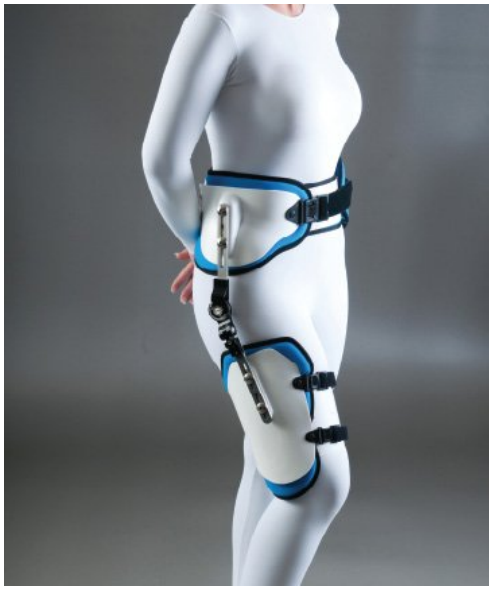

Figure A.6: TLC Abduction Brace by Optec. [68]

Indications [68]
- Arthoplasty.
- Hip Dislocation or Potential High Risk Dislocation.
- Hip Displasia (Anterior or Posterior).
- Hip Management/ Immobilization.
- Hip Revisions.
- Hip Surgery.
- Post-Operative.
- Pre-Operative.
- Stabilize, Align and Reinforce Hip.

Hip movement influence [68]
- Flexion/extension: Fully allowed between limits.
- Abduction/adduction: Fully allowed between limits.
- Internal/external rotation: Fully restricted.

Materials
- Shells: No information.
- Joint/bar mechanisms: No information.
- Pads/attachment: No information.

Mass
- No information.

A.8 SofTec Coxa by Bauerfeind

Figure A.7: SofTec Coxa by Bauerfeind. [69]

Indications [69]
- Prevention of dislocation.
- Total hip-replacement surgery.
- Total hip-revision surgery.
- Femoral-head resection (Girdlestone arthroplasty).
- Hip spacer for two-stage revision procedures.

Hip movement influence [69]
- Flexion/extension: Fully allowed between limits.
- Abduction/adduction: Fully allowed between limits.
- Internal/external rotation: Fully restricted.

Materials [70]
- Shells: Polyethylene and polypropylene.
- Joint/bar mechanisms: Steel.
- Pads/attachment: Polyester, viscose, polyurethane, elastodiene, ethylene vinyl acetate, elastane and cotton.

Mass
- 2.30 kg [71].

A.9 Rebound Hip by Össur

Figure A.8: Rebound Hip by Össur. [72]

Indications [72]
- Postoperative after total hip arthroplasty (revision).
- Postoperative hip arthroscopy.
- Post-op following FAI arthroscopic surgery.
- Post-op following Gluteus medius repair surgery.
- Post-op following hamstring repair surgery.
- Inoperable hip abnormalities.
- Preventively when there is risk of hip dislocation.
- Conventional treatment after dislocation/reduction.

Hip movement influence [72]
- Flexion/extension: Fully allowed between limits.
- Abduction/adduction: Fully allowed between limits.
- Internal/external rotation: Fully restricted.

Materials [73]
- Shells: Polyethylene.
- Joint/bar mechanisms: Aluminum and steel.
- Pads/attachment: Synthetic polymers, polyester and polyurethane.

Mass
- No information.

A.10 Hip One by Medi

Figure A.9: Hip One by Medi. [74]

Indications [74]
- (Traumatic) dislocation of the hip joint.
- Postoperative conditions (e.g., following hip arthroplasty).
- Hip prosthesis displacement.

Hip movement influence [74]
- Flexion/extension: Fully allowed between limits.
- Abduction/adduction: Fixed at set angle.
- Internal/external rotation: Fully restricted.

Materials
- Shells: No information.
- Joint/bar mechanisms: No information.
- Pads/attachment: No information.

Mass
- No information.

A.11 Dynacox Evolution by Teufel

Figure A.10: Dynacox Evolution by Teufel. [75]

Indications [75]
- After repositioning of a luxated hip joint.
- Instability after total hip replacement (THR).
- Muscular imbalance.
- After revision surgery.

Hip movement influence [76]
- Flexion/extension: Fully allowed between limits.
- Abduction/adduction: Fully restricted.
- Internal/external rotation: Fully restricted.

Materials [76]
- Shells: Polyethylene.
- Joint/bar mechanisms: Steel.
- Pads/attachment: Polyester, Coolmax, and Spandex.

Mass
- No information.

A.12 Lerman Hip Abduction Rotation Orthosis 2000 by Becker Orthopedic

Figure A.11: Lerman Hip Abduction Rotation Orthosis 2000 by Becker Orthopedic. [77]

Indications [78]
- Hip Osteoarthritis.
- Coxitis.
- Hip dysplasia.
- Hip luxation.
- Total hip replacement.

Hip movement influence [77]
- Flexion/extension: Fully allowed between limits.
- Abduction/adduction: Fixed at set angle.
- Internal/external rotation: Fully restricted.

Materials
- Shells: No information.
- Joint/bar mechanisms: No information.
- Pads/attachment: No information.

Mass
- No information.

A.13 Unloader Hip by Össur

Figure A.12: Unloader Hip by Össur. [33]

Indications [33]
- Hip osteoarthritis (OA).
- Femoroacetabular impingement (FAI).
- Labrum tears.
- Other conditions that may benefit from repositioning of the hip and/or compression around the greater trochanters.

Hip movement influence [33] [32]
- Flexion/extension: Fully allowed.
- Abduction/adduction: Fully allowed. However, abduction can be supported up to 9.3%.
- Internal/external rotation: Fully allowed. However, the leg is being pulled into an externally rotated position.

Materials [33]
- Lycra (polyurethane) shorts. No information for the rest of the orthosis.

Mass
- No information.

A.14 Cosa Active by Ottobock

Figure A.13: Cosa active by Ottobock. [35]

Indications [35]
- Diplegia, spastic.
- Hip dysplasia.
- Hip joint subluxation, congenital.
- Hypotonicity.
- Tetraplegia, spastic.

Hip movement influence [35]
- Flexion/extension: Fully allowed.
- Abduction/adduction: Large adduction associated with scissor gait prevented. Legs cannot cross each other.
- Internal/external rotation: Fully allowed.

Materials
- No information.

Mass
- No information.

B Finite Element Method (FEM) models

B.1 Introduction

This appendix provides an overview of the Finite Element Method (FEM) models developed throughout this thesis. The models are presented in sufficient detail to ensure clarity and reproducibility of the research findings.

The FEM models presented in this appendix encompass the essential aspects: geometry, material properties, boundary conditions, meshing, and study settings.

Any parameter, configuration, or setting that is not specifically mentioned in this appendix is assumed to be set to its default value. This ensures that the focus remains on the critical and customized aspects of the models, thereby maintaining conciseness and avoiding unnecessary repetition.

B.2 COMSOL model for approximating the load distribution shape between the patient's body and the attachment parts of the orthosis

1 Global Definitions

GLOBAL SETTINGS

Unit system	SI

2 Component 1

2.1 DEFINITIONS

2.1.1 Nonlocal Couplings

Average 1

Coupling type	Average
Operator name	aveop1

SELECTION

Geometric entity level	Point
Selection	Geometry geom1: Dimension 0: Point 11

2.1.2 Pairs

Identity Boundary Pair 1

Pair type	Identity pair
Pair name	p1

SOURCE SELECTION

Geometric entity level	Boundary
Selection	Geometry geom1: Dimension 1: Boundaries 4–8

DESTINATION SELECTION

Geometric entity level	Boundary
Selection	Geometry geom1: Dimension 1: Boundary 14

Identity Boundary Pair 2

Pair type	Identity pair
Pair name	p2

SOURCE SELECTION

Geometric entity level	Boundary
Selection	Geometry geom1: Dimension 1: Boundaries 4–8

DESTINATION SELECTION

Geometric entity level	Boundary
Selection	Geometry geom1: Dimension 1: Boundary 9

2.2 GEOMETRY 1

UNITS

Length unit	m
Angular unit	deg

2.2.1 UB (r1)

POSITION

Description	Value
Position	{-0.075, 0}

SIZE

Description	Value
Width	0.4
Height	0.45

2.2.2 Hip joint UB (pt1)

POINT

Description	Value
Point coordinate	{0, 0}

2.2.3 Center of gravity (pt3)

POINT

Description	Value
Point coordinate	{0.075, 0.1}

2.2.4 Leg (r2)

POSITION

Description	Value
Position	{-0.075, -0.4}

SIZE

Description	Value
Width	0.2
Height	0.4

2.2.5 Hip joint leg (pt2)

POINT

Description	Value
Point coordinate	{0, 0}

2.2.6 Attachment parts

2.2.6.1 Rectangle to add (r3)

POSITION

Description	Value
Position	{-0.1, -0.35}

SIZE

Description	Value
Width	0.025
Height	0.7

2.2.6.2 Rectangle to subtract (r4)

POSITION

Description	Value
Position	{-0.0875, -0.1}

SIZE

Description	Value
Width	0.0125
Height	0.2

2.2.7 Difference (dif1)

SETTINGS

Description	Value
Objects to add	r3
Objects to subtract	r4

2.2.8 Form Assembly (fin)

SETTINGS

Description	Value
Action	Form an assembly
Create pairs	Off

2.3 MATERIALS

2.3.1 Steel: Human Body

SELECTION

Geometric entity level	Domain
Selection	Geometry geom1: Dimension 2: Domain 2, 3

MATERIAL PARAMETERS

Name	Value	Unit	Property group
Density	7800	kg/m³	Basic
Young's modulus	2.1E11	Pa	Young's modulus and Poisson's ratio
Poisson's ratio	0.28	1	Young's modulus and Poisson's ratio

Linear Elastic Material

SETTINGS

Description	Value
Material symmetry	Isotropic
Specify	Young's modulus and Poisson's ratio
Young's modulus	From material
Poisson's ratio	From material
Density	From material
Use mixed formulation	None

2.3.2 Rigid Material Model: Attachment parts (splint)

SELECTION

Geometric entity level	Domain
Selection	Geometry geom1: Dimension 2: Domain 1

2.4 SOLID MECHANICS

2.4.1 Prescribed Displacement: Hip joint UB and hip joint leg coupling

SELECTION

Geometric entity level	Point
Selection	Geometry geom1: Dimension 0: Point 16

Prescribed Displacement

SETTINGS

Description	Value	Unit
Prescribed in x direction	On	1
Prescribed in y direction	On	1
Prescribed in z direction	Off	1
Displacement constraint, x-component	aveop1(u)	m
Displacement constraint, y-component	aveop1(v)	m
Displacement constraint, z-component	0	m

2.4.2 Fixed Constraint: Leg on ground

SELECTION

Geometric entity level	Boundary
Selection	Geometry geom1: Dimension 1: Boundary 10

2.4.3 Point Load: Gravity adduction force

SELECTION

Geometric entity level	Point
Selection	Geometry geom1: Dimension 0: Point 17

Force

SETTINGS

Description	Value	Unit
Load type	Total force	
Point load	User defined	
Point load	{0, -1, 0}	N

2.5 MESH 1

2.5.1 Settings

Sequence type	Physics-controlled mesh
Element size	Extremely fine

2.5.2 Size (size)

SETTINGS

Description	Value
Maximum element size	0.0085
Minimum element size	1.7E-5
Curvature factor	0.2
Predefined size	Extremely fine

2.5.3 Free Triangular 1 (ftri1)

SELECTION

Geometric entity level	Domain
Selection	Remaining

3 Study 1

3.1 STATIONARY

STUDY SETTINGS

Description	Value
Include geometric nonlinearity	Off

PHYSICS AND VARIABLES SELECTION

Physics interface	Solve for	Equation form
Solid Mechanics (solid)	On	Automatic (Stationary)

MESH SELECTION

Component	Mesh
Component 1	Mesh 1

B.3 COMSOL model for stiffness analysis of the orthosis attachment parts

1 Global Definitions

GLOBAL SETTINGS

Unit system	SI

2 Component 1

2.1 GEOMETRY 1

2.1.1 LiveLink for SOLIDWORKS 1 (cad1)

SETTINGS

Description	Value
Length unit	From COMSOL
Synchronize with	Specified document
Document	C:\Users\Stijn\Documents\Werktuigbouwkunde\Master\Scriptie\Comsol\Connection parts\Final\Att parts assembly.SLDASM

2.2 MATERIALS

2.2.1 ABS 40% Carbon Fiber

SELECTION

Geometric entity level	Domain
Selection	Geometry geom1: Dimension 3: All domains

MATERIAL PARAMETERS

Name	Value	Unit	Property group
Density	1250	kg/m^3	Basic
Young's modulus	2.5E10	Pa	Young's modulus and Poisson's ratio
Poisson's ratio	0.33	1	Young's modulus and Poisson's ratio

Linear Elastic Material

SETTINGS

Description	Value
Material symmetry	Isotropic
Specify	Young's modulus and Poisson's ratio
Young's modulus	From material
Poisson's ratio	From material
Density	From material
Use mixed formulation	None

2.3 SOLID MECHANICS

2.3.1 Edge Load: UB portion

SELECTION

Geometric entity level	Edge
Selection	Geometry geom1: Dimension 1: Edges 34, 45

Force

SETTINGS

Description	Value	Unit
Load type	Force per unit length	
Load	User defined	
Load	{0, 5500*(-1.8 + 8*z), 0}	N/m

2.3.2 Edge Load: Leg portion

SELECTION

Geometric entity level	Edge
Selection	Geometry geom1: Dimension 1: Edges 29, 42

Force

SETTINGS

Description	Value	Unit
Load type	Force per unit length	
Load	User defined	
Load	{0, -5500*(1.8 + 8*z), 0}	N/m

2.3.3 Fixed Constraint

SELECTION

Geometric entity level	Boundary
Selection	Geometry geom1: Dimension 2: Boundaries 6–7

2.4 MESH 1

2.4.1 Settings

SETTINGS

Description	Value
Sequence type	Physics-controlled mesh

2.4.2 Size (size)

SETTINGS

Description	Value
Predefined size	Normal
Maximum element size	0.07
Minimum element size	0.0126
Curvature factor	0.6
Resolution of narrow regions	0.5
Maximum element growth rate	1.5

2.4.3 Free Tetrahedral 1 (ftet1)

SELECTION

Geometric entity level	Domain
Selection	Remaining

3 Study 1

3.1 STATIONARY

STUDY SETTINGS

Description	Value
Include geometric nonlinearity	On

PHYSICS AND VARIABLES SELECTION

Physics interface	Solve for	Equation form
Solid Mechanics (solid)	On	Automatic (Stationary)

MESH SELECTION

Component	Mesh
Component 1	Mesh 1

B.4 SolidWorks model for the preliminary design of Concept 4

B.4.1 Geometry

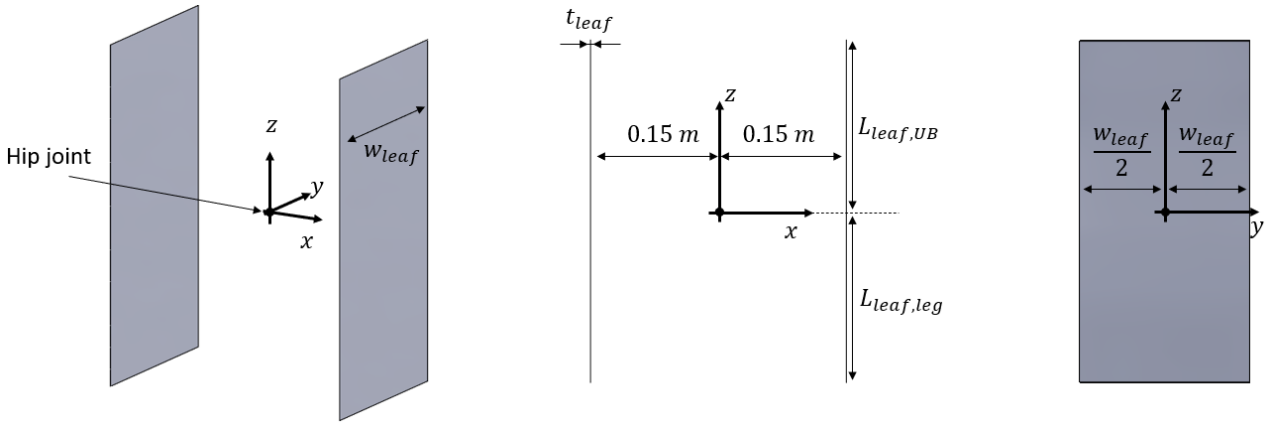

Figure B.1: Geometry of the SolidWorks model for the preliminary design of Concept 4. Showcased with arbitrarily selected values for the dimensional parameters.

B.4.2 Material

Model Type: Linear Elastic Isotropic

Units: SI - N/m^2 (Pa)

Name: Steel

Property	Value	Units
Elastic Modulus	2.1e+11	N/m^2
Poisson's Ratio	0.28	N/A
Mass Density	7800	kg/m^3

Figure B.2: Material applied to the leaf flexures.

B.4.3 Boundary conditions

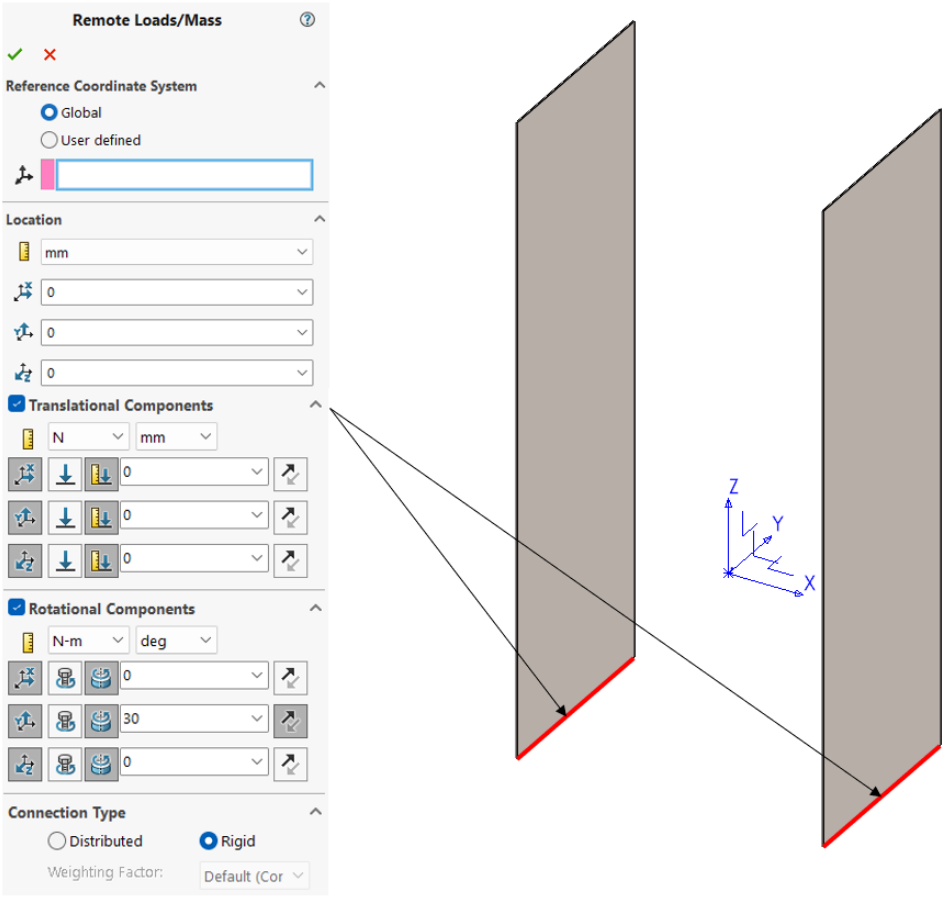

Figure B.3: Boundary condition applied to the bottom end of the leaf flexures.

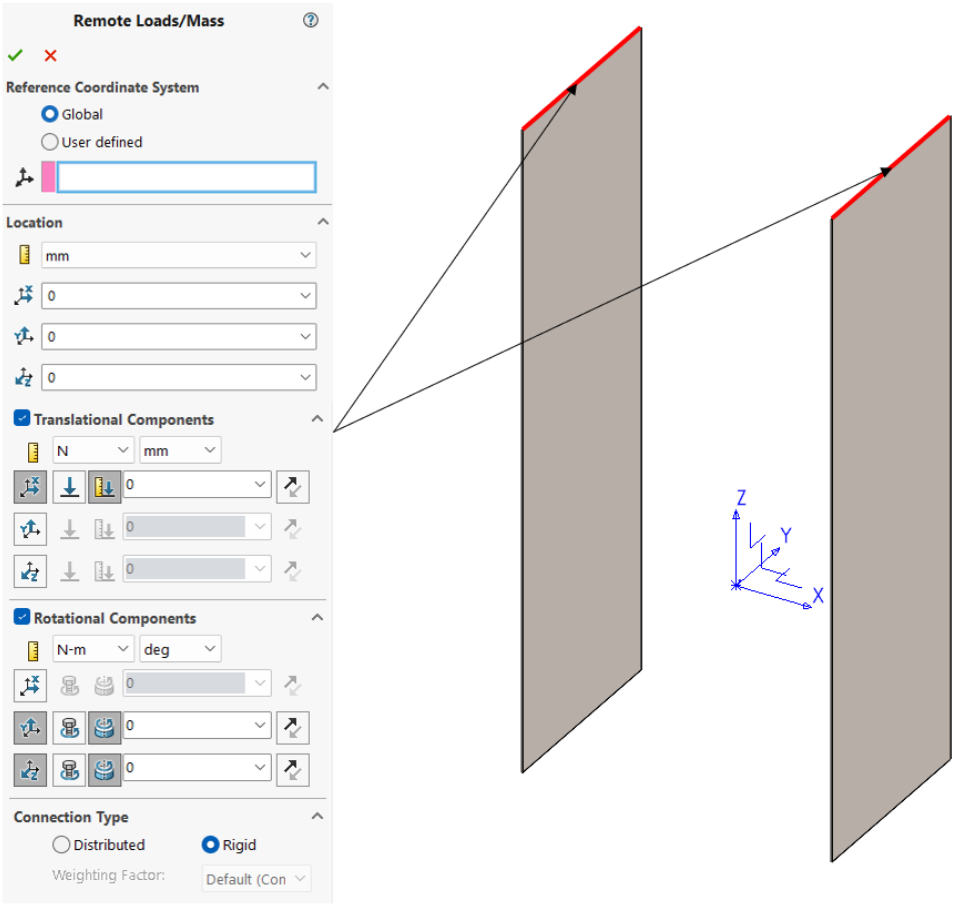

Figure B.4: Boundary condition applied to the top end of the leaf flexures.

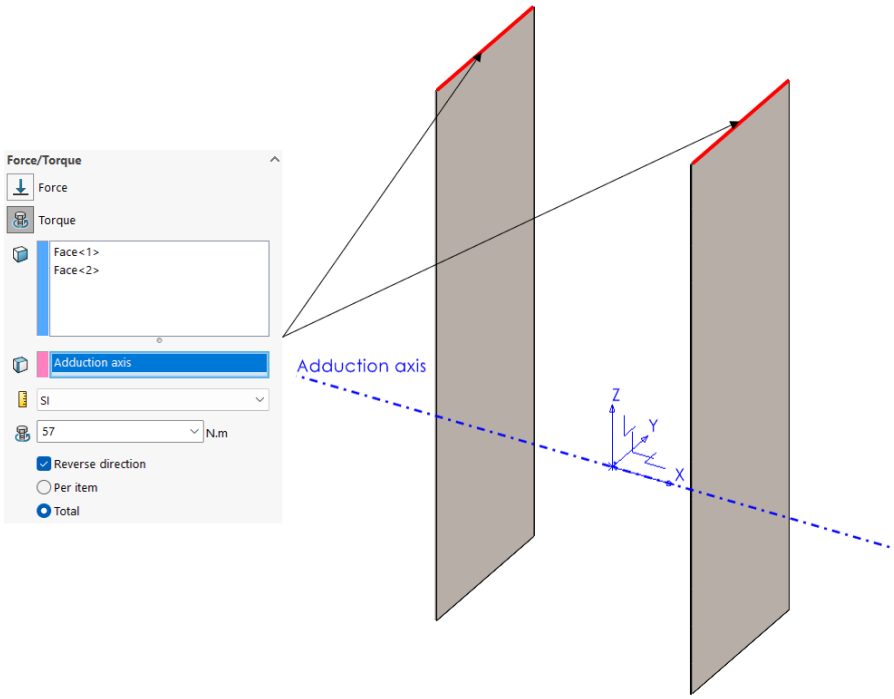

Figure B.5: Adduction moment applied to the top end of the leaf flexures.

B.4.4 Mesh

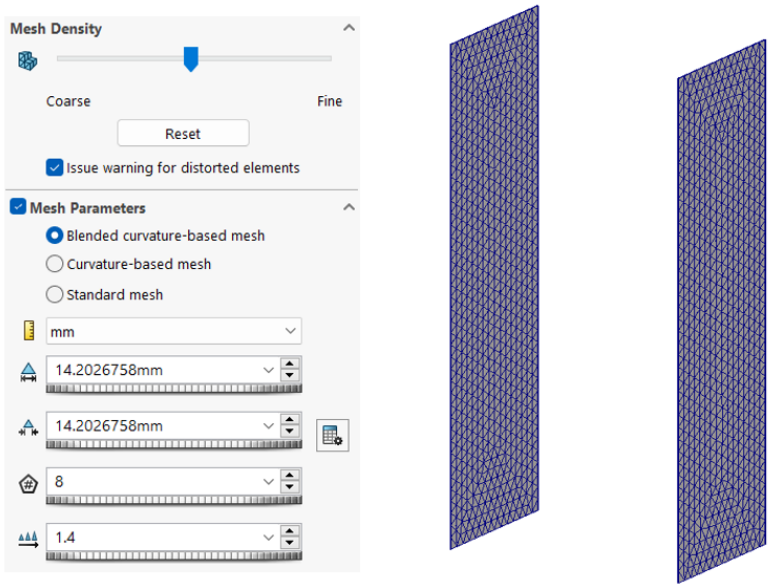

Figure B.6: Specifications of the standard mesh automatically generated by SolidWorks. The mesh is made out of tetrahedral solid elements.

B.4.5 Study settings

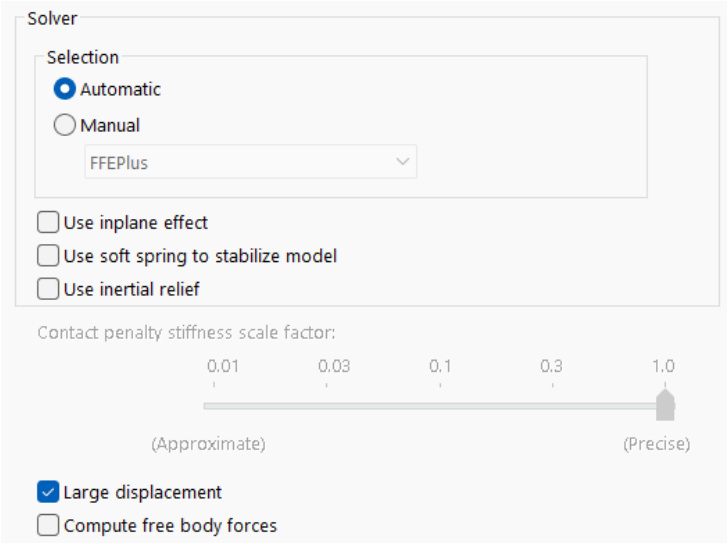

Figure B.7: Settings of the static study conducted.

B.5 SolidWorks model for the preliminary design of Concept 8

B.5.1 Geometry

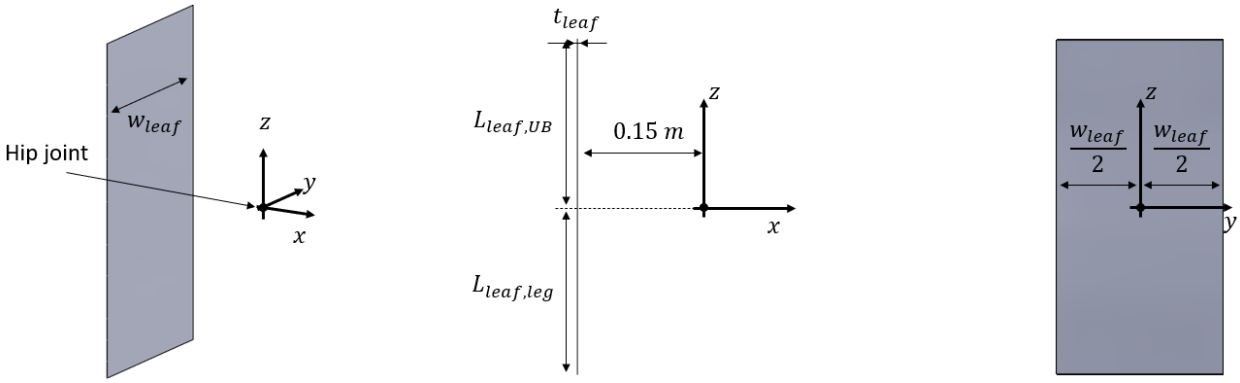

Figure B.8: Geometry of the SolidWorks FEM model for the preliminary design of Concept 8. Showcased with arbitrarily selected values for the dimensional parameters.

B.5.2 Material

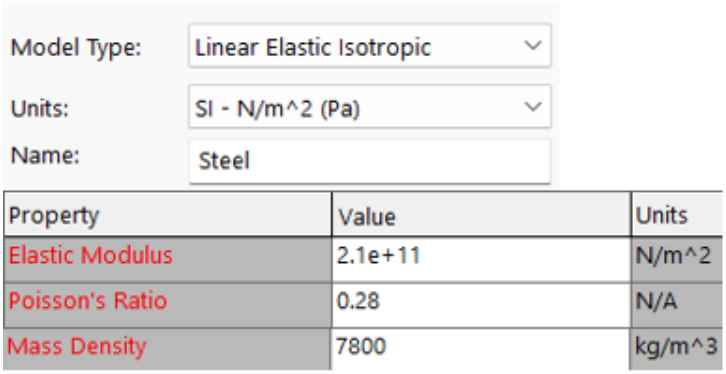

Figure B.9: Material applied to the leaf flexure.

B.5.3 Boundary conditions

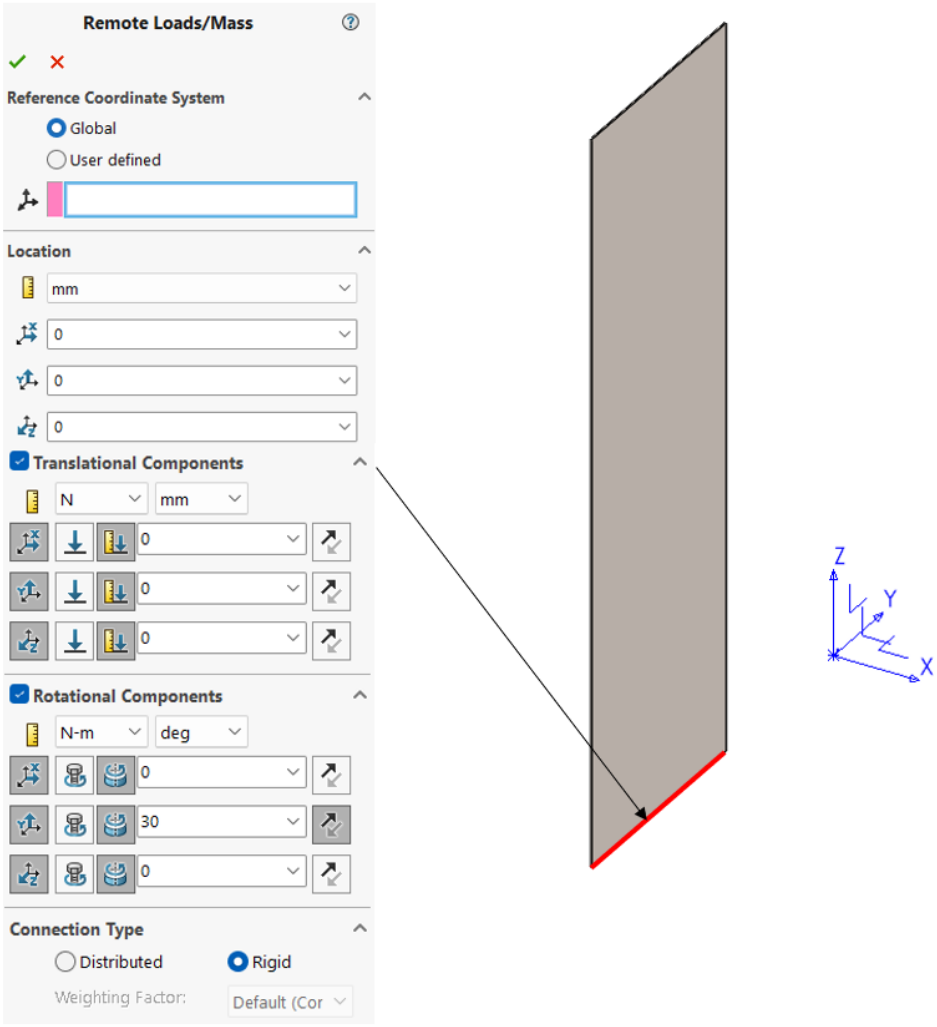

Figure B.10: Boundary condition applied to the bottom end of the leaf flexure.

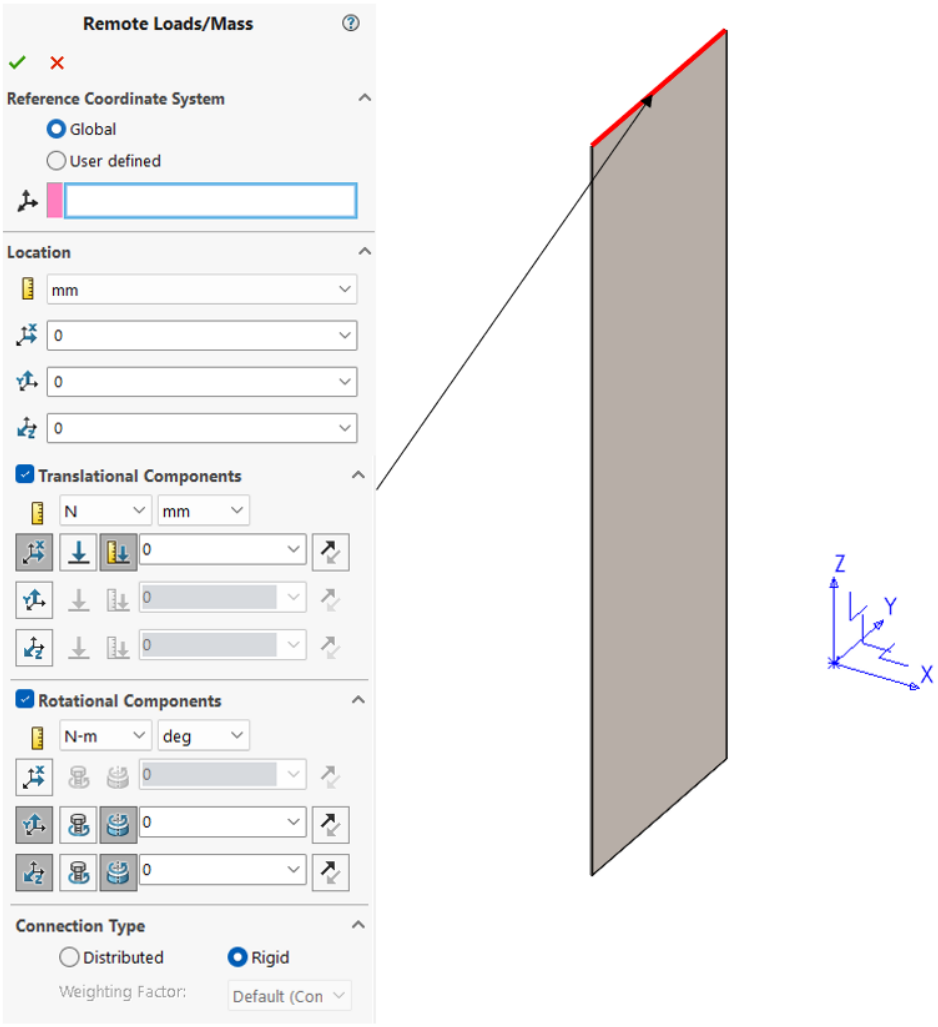

Figure B.11: Boundary condition applied to the top end of the leaf flexure.

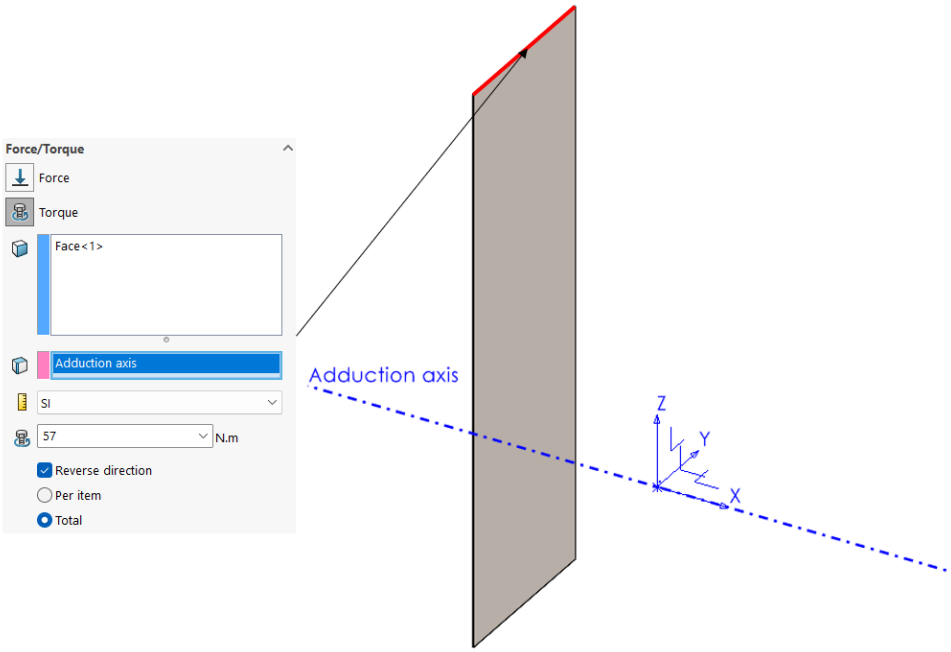

Figure B.12: Adduction moment applied to the top end of the leaf flexure.

B.5.4 Mesh

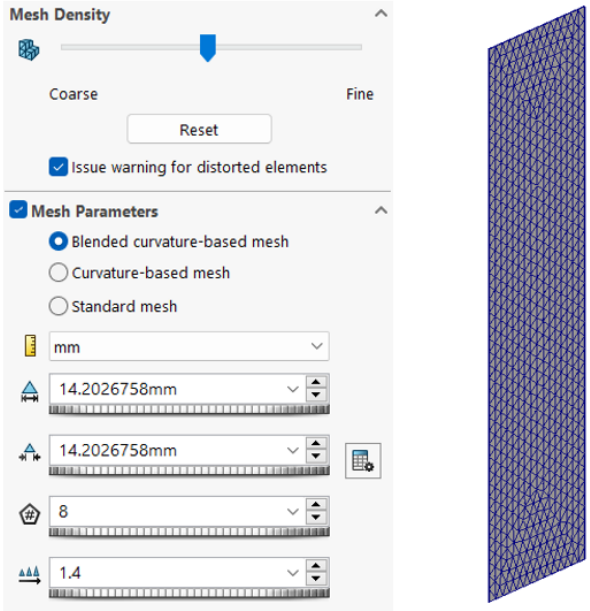

Figure B.13: Specifications of the standard mesh automatically generated by SolidWorks. The mesh is made out of tetrahedral solid elements.

B.5.5 Study settings

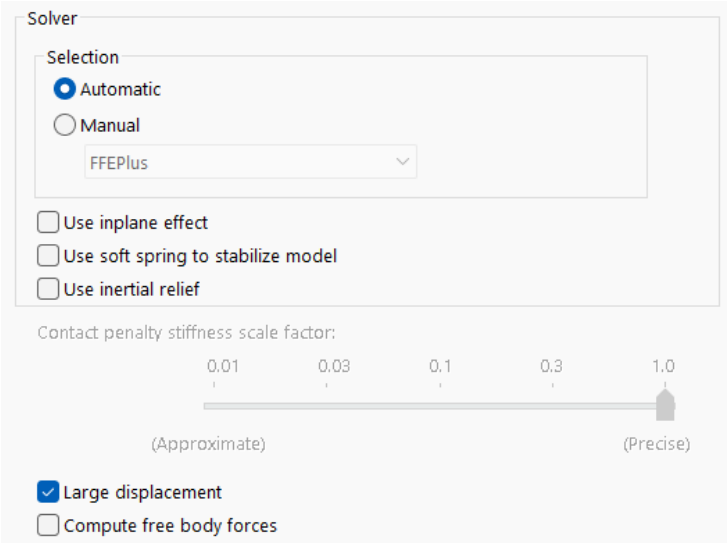

Figure B.14: Settings of the static study conducted.

B.6 Beam Code model for FEM software selection

Operating the MATLAB code provided below requires the following files, which are available upon request:

- AssembleMatricesBeams
- DefineCrossSection
- mesh2tri
- plotBeams
- PlotBeamsCrossSections
- solveNONLINstaticCOR

```
clear all
close all
clc

par.nTimestep    = 50;
par.step="off"
par.nIter        = 100;
par.conv         = 1e-6;
par.plots        = 'off';
par.getKend      = 0;

%% Model

% Generation of coordinates and connectivities

L_leaf_leg = 0.20;
L_leaf_UB = 0.20;
```

```
L_leaf = L_leaf_leg + L_leaf_UB; %[m]
n_leaf = 40; %[nodes]

d_hip = 0.15; %[m]
n_hip_flexure = 15; %[nodes]

L_legbone = 0.20; %[m]
n_legbone = 20; %[nodes]

%Leaf flexure                                          %Offset between leaf flexure and leg bone                    %Leg bone
x = [linspace(-d_hip, -d_hip, n_leaf)                  linspace(-d_hip, 0, n_hip_flexure)                    linspace(0, 0, n_legbone)]';
x([n_leaf+1 n_leaf+n_hip_flexure])=[];


y = [linspace(0, 0, n_leaf)                            linspace(0, 0, n_hip_flexure)                         linspace(0, 0, n_legbone)]';
y([n_leaf+1 n_leaf+n_hip_flexure])=[];

z = [linspace(L_leaf_UB, -L_leaf_leg, n_leaf)          linspace(-L_leaf_leg, -L_leaf_leg, n_hip_flexure)     linspace(-L_leaf_leg, 0, n_legbone)]';
z([n_leaf+1 n_leaf+n_hip_flexure])=[];


nbeam = numel(x);

m.X = [x,y,z,zeros(3,nbeam)'];

m.elementNodes= [1:nbeam-1; 2:nbeam]'     ;
m.numberNodes       = size(m.X,1);
m.numberElements    = size(m.elementNodes,1);
m.eqn               = 6*m.numberNodes;
m.x                 = reshape(m.X',m.eqn,1) ;

%Leaf flexure material
m.E         = 2.1e11 * ones(1,m.numberElements); %Young's modulus
m.G         = 8.2e10 * ones(1,m.numberElements); %Shear modulus

%Offset and leg bone material ("rigid")
m.E(n_leaf:m.numberElements) = 2.1e11*1000000; %Young's modulus offset and leg
m.G(n_leaf:m.numberElements) = 8.2e10*1000000; %Shear modulus offset and leg

%Width and thickness
t = 1.3/1000; %[m]
```

```
w = 0.20; %[m]

H = t;
W = w;

m = DefineCrossSection(m,'rectangle',H,W);

%%Use this for a single orientation point
CSO = [100 0 0]';   % cross section orientation. Is the point towards
    which e03 points. Used to be fixed [0.00001 0.000001 1]'
m.GuideCurve = repmat(CSO,1,m.numberElements);
m.guidecurve = reshape(m.GuideCurve,3*m.numberElements,1) ;

%% core

for e = 1:m.numberElements
%modified rotRo1 met richting e03 naar bepaald punt (niet de snelste
    versie)
x21=(m.X(m.elementNodes(e,2),1:3)'-m.X(m.elementNodes(e,1),1:3)');
e01     = (x21)/norm(x21);
e03star = cross(e01, m.guidecurve(3*(m.elementNodes(e,1)-1)+[1:3]) -  m.
    X(m.elementNodes(e,1),1:3)');
e03     = e03star/norm(e03star);
e02     = cross(e03,e01);
Ro      = [e01 e02 e03];

m.tr1(:,:,m.elementNodes(e,1))        = eye(3)*Ro;
m.tr2(:,:,m.elementNodes(e,1))        = eye(3)*Ro;
end

m.tr1(:,:,m.numberElements)        = eye(3)*Ro;
m.tr2(:,:,m.numberElements)        = eye(3)*Ro;

m.Rg1               = repmat(eye(3),1,1,m.numberElements);
m.Rg2               = repmat(eye(3),1,1,m.numberElements);

m.D                 = zeros(6,m.numberNodes)';
m.d                 = zeros(m.eqn,1);

def='def';
grid on

%% BOUNDARY CONDITIONS on begin- and endpoint
pointconstraints=zeros(6,m.numberNodes); %Creates a 6 by N array with
    zeros
pointconstraints([1 5 6], 1) = 1; %Top end leaf flexure
pointconstraints([1 2 3 4 5 6], nbeam) = 1; %Hip joint

Fe  = zeros(m.eqn,1); %Applied load (gradually)
```

```
PreFe  = zeros(m.eqn,1); %Applied load (instantly)
Fe(4) = -57; %[Nm] Applied adduction moment

dofs.bc = find(pointconstraints)';
dofs.dp = zeros(sum(pointconstraints,'all'),1);
activeconstraints = [8];
dofs.dp(activeconstraints) = -30/180*pi; %Prescribed flexion angle

dofs.all    = (1:m.eqn)';
%dofs.bc     = bc(~isnan([dofs.dp]));
%dofs.dp     = dofs.dp(~isnan([dofs.dp]));
dofs.R      = sparse(1:length(dofs.bc),[dofs.bc],1+0*dofs.bc,length(dofs
    .bc),m.eqn);

def='def';
[history, m] = solveNONLINstaticCOR(m,dofs,par,Fe,PreFe);
plotBeams(m)
PlotBeamsCrossSections(m,par,def)
view(0, 0) %x-z-plane
% view(90, 0) %y-z-plane
grid off
axis off

%Flexion reaction moment measurement (to be measured at Fe(4) = 0; [Nm])
RM_flex = history(50).RF(8)

%Adduction angle
theta_add_rad = 0; % Initialize the total sum

for n = 1:50
    theta_add_rad = theta_add_rad - history(n).m.D(1,4);
end
theta_add_deg = theta_add_rad/pi*180
```

B.7 COMSOL model for FEM software selection

1 Global Definitions

1.1 PARAMETERS

PARAMETERS 1

Name	Expression	Value	Description
L_leaf_leg	0.20	0.2	m
L_leaf_ub	0.20	0.2	m
w_leaf	0.20	0.2	m
t_leaf	1.3/1000	0.0013	m
d_hip	0.15	0.15	m
theta_flex	30/180*pi	0.5236	rad
M_add	57	57	Nm

2 Component 1

2.1 GEOMETRY 1

2.1.1 Block 1 (blk1)

POSITION

Description	Value
Position	{-t_leaf - d_hip, -w_leaf/2, -L_leaf_leg}

AXIS

Description	Value
Axis type	z - axis

SIZE AND SHAPE

Description	Value
Width	t_leaf
Depth	w_leaf
Height	L_leaf_ub + L_leaf_leg

2.2 MATERIALS

2.2.1 Steel

SELECTION

Geometric entity level	Domain
Selection	Geometry geom1: Dimension 3: All domains

MATERIAL PARAMETERS

Name	Value	Unit	Property group
Density	7800	kg/m³	Basic
Young's modulus	2.1E11	Pa	Young's modulus and Poisson's ratio
Poisson's ratio	0.28	1	Young's modulus and Poisson's ratio

Linear Elastic Material

SETTINGS

Description	Value
Material symmetry	Isotropic
Specify	Young's modulus and Poisson's ratio
Young's modulus	From material
Poisson's ratio	From material
Density	From material
Use mixed formulation	None

2.3 SOLID MECHANICS

2.3.1 Rigid Connector: Upper Body

SELECTION

Geometric entity level	Boundary
Selection	Geometry geom1: Dimension 2: Boundary 4

Connection Type

SETTINGS

Description	Value
Connection type	Rigid

Center of Rotation

SETTINGS

Description	Value
Center of rotation	Automatic
Offset	Off

Prescribed Displacement at Center of Rotation

SETTINGS

Description	Value	Unit
Prescribed in x direction	On	
Prescribed in y direction	Off	
Prescribed in z direction	Off	
Displacement constraint, x-component	0	m
Displacement constraint, y-component	0	m
Displacement constraint, z-component	0	m

Prescribed Rotation

SETTINGS

Description	Value
By	Constrained rotation
Constrain rotation around x-axis	Off
Constrain rotation around y-axis	On
Constrain rotation around z-axis	On

Applied Moment 1

SETTINGS

Description	Value	Unit
Direction	Space-fixed direction	
Applied moment, x-component	-M_add	N·m
Applied moment, y-component	0	N·m
Applied moment, z-component	0	N·m

2.3.2 Rigid Connector: leg

SELECTION

Geometric entity level	Boundary
Selection	Geometry geom1: Dimension 2: Boundary 3

Connection Type

SETTINGS

Description	Value
Connection type	Rigid

Center of Rotation

SETTINGS

Description	Value	Unit
Center of rotation	User defined	
Global coordinates of center of rotation, x-component	0	m
Global coordinates of center of rotation, y-component	0	m
Global coordinates of center of rotation, z-component	0	m
Offset	Off	

Prescribed Displacement at Center of Rotation

SETTINGS

Description	Value	Unit
Prescribed in x direction	On	
Prescribed in y direction	On	
Prescribed in z direction	On	
Displacement constraint, x-component	0	m
Displacement constraint, y-component	0	m
Displacement constraint, z-component	0	m

Prescribed Rotation

SETTINGS

Description	Value	Unit
By	Prescribed rotation	
Axis of rotation, x-component	0	
Axis of rotation, y-component	-1	
Axis of rotation, z-component	0	
Angle of rotation	theta_flex	rad

Reaction Force Settings

SETTINGS

Description	Value
Evaluate reaction forces	On
Apply reaction only on rigid body variables	Off

2.4 MESH 1

2.4.1 Size (size)

SETTINGS

Description	Value
Sequence type	Physics-controlled mesh
Element size	Normal

SETTINGS

Description	Value
Maximum element size	0.04
Minimum element size	0.0072
Curvature factor	0.6
Resolution of narrow regions	0.5
Maximum element growth rate	1.5
Predefined size	Normal

2.4.2 Free Tetrahedral 1 (ftet1)

SELECTION

Geometric entity level	Domain
Selection	Remaining

3 Study 1

3.1 STATIONARY

STUDY SETTINGS

Description	Value
Include geometric nonlinearity	On

PHYSICS AND VARIABLES SELECTION

Physics interface	Solve for	Equation form
Solid Mechanics (solid)	On	Automatic (Stationary)

MESH SELECTION

Component	Mesh
Component 1	Mesh 1

3.2 SOLVER CONFIGURATIONS

3.2.1 Solution 1

Stationary Solver 1 (s1)

GENERAL

Description	Value
Defined by study step	Stationary

Fully Coupled 1 (fc1)

METHOD AND TERMINATION

Description	Value
Nonlinear method	Constant (Newton)

B.8 COMSOL model for the mechanism design using a conventional leaf flexure

1 Global Definitions

GLOBAL SETTINGS

Unit system	SI

1.1 PARAMETERS

PARAMETERS 1

Name	Expression	Value	Description
L_leaf_leg	0.20	0.2	m
L_leaf_ub	0.20	0.2	m
w_leaf	0.20	0.2	m
t_leaf	1.3/1000	0.0013	m
d_hip	0.15	0.15	m
theta_flex	0	0	rad
M_add	0	0	Nm

The numerical values for the dimensional parameters shown here are placeholders that will be adjusted during the final design process.

The numerical values for these two input parameters depend on the specific analysis to be conducted. They can be defined under the study settings using the auxiliary sweep option.

2 Component 1

2.1 DEFINITIONS

2.1.1 Nonlocal Couplings

Average 1

Coupling type	Average
Operator name	aveop1

SELECTION

Geometric entity level	Edge
Selection	Geometry geom1: Dimension 1: Edges 7, 11, 17

2.2 GEOMETRY 1

2.2.1 Work Plane 1 (wp1)

PLANE DEFINITION

Description	Value
Plane	yz - plane
Offset type	Distance
x-coordinate	-d_hip-t_leaf

UNITE OBJECTS

Description	Value
Unite objects	On

Plane Geometry (sequence2D)

Rectangle: Leaf Flexure (r1)

POSITION

Description	Value
Base	Corner
Position	{-w_leaf/2, -L_leaf_leg}

SIZE

Description	Value
Width	w_leaf
Height	L_leaf_ub + L_leaf_leg

Rectangle: Mesh refinement face 1 (r2)

POSITION

Description	Value
Base	Corner
Position	{-w_leaf/2, L_leaf_ub - w_leaf/16}

SIZE

Description	Value
Width	w_leaf/8
Height	w_leaf/16

Rectangle: Mesh refinement face 2 (r3)

POSITION

Description	Value
Base	Corner
Position	{w_leaf/2 - w_leaf/8, L_leaf_ub - w_leaf/16}

SIZE

Description	Value
Width	w_leaf/8
Height	w_leaf/16

Rectangle: Mesh refinement face 3 (r4)

POSITION

Description	Value
Base	Corner
Position	{w_leaf/2 - w_leaf/8, -L_leaf_leg}

SIZE

Description	Value
Width	w_leaf/8
Height	w_leaf/16

Rectangle: Mesh refinement face 4 (r5)

POSITION

Description	Value
Base	Corner
Position	{-w_leaf/2, -L_leaf_leg}

SIZE

Description	Value
Width	w_leaf/8
Height	w_leaf/16

2.3 MATERIALS

2.3.1 Steel

SELECTION

Geometric entity level	Boundary
Selection	Geometry geom1: Dimension 2: All boundaries

MATERIAL PARAMETERS

Name	Value	Unit	Property group
Density	7800	kg/m³	Basic
Young's modulus	2.1E11	Pa	Young's modulus and Poisson's ratio
Poisson's ratio	0.28	1	Young's modulus and Poisson's ratio

Linear Elastic Material

SETTINGS

Description	Value
Material symmetry	Isotropic
Specify	Young's modulus and Poisson's ratio
Young's modulus	From material
Poisson's ratio	From material
Density	From material

2.4 SHELL

SELECTION

Geometric entity level	Boundary
Selection	Geometry geom1: Dimension 2: All boundaries

2.4.1 Thickness and Offset 1

SETTINGS

Description	Value	Unit
Initial thickness	t_leaf	m
Position	Bottom surface on boundary	

2.4.2 Rigid Connector Leg

SELECTION

Geometric entity level	Edge
Selection	Geometry geom1: Dimension 1: Edges 2, 9, 13

Center of Rotation

SETTINGS

Description	Value	Unit
Center of rotation	User defined	
Global coordinates of center of rotation, x-component	0	m
Global coordinates of center of rotation, y-component	0	m
Global coordinates of center of rotation, z-component	0	m
Offset	Off	

Prescribed Displacement at Center of Rotation

SETTINGS

Description	Value	Unit
Prescribed in x direction	On	
Prescribed in y direction	On	
Prescribed in z direction	On	
Displacement constraint, x-component	0	m
Displacement constraint, y-component	0	m
Displacement constraint, z-component	0	m

Prescribed Rotation

SETTINGS

Description	Value	Unit
By	Prescribed rotation	
Axis of rotation, x-component	0	
Axis of rotation, y-component	-1	
Axis of rotation, z-component	0	
Angle of rotation	theta_flex	rad

Reaction Force Settings

SETTINGS

Description	Value
Evaluate reaction forces	On
Apply reaction only on rigid body variables	Off

2.4.3 Rigid Connector UB

SELECTION

Geometric entity level	Edge
Selection	Geometry geom1: Dimension 1: Edges 7, 11, 17

Center of Rotation

SETTINGS

Description	Value
Center of rotation	Automatic
Offset	Off

Prescribed Displacement at Center of Rotation

SETTINGS

Description	Value	Unit
Prescribed in x direction	On	
Prescribed in y direction	Off	
Prescribed in z direction	Off	
Displacement constraint, x-component	0	m
Displacement constraint, y-component	0	m
Displacement constraint, z-component	0	m

Prescribed Rotation

SETTINGS

Description	Value	Unit
By	Prescribed rotation	
Axis of rotation, x-component	-1	
Axis of rotation, y-component	0	
Axis of rotation, z-component	0	
Angle of rotation	atan(aveop1(v)/(L_leaf_ub + aveop1(w)))	rad

Applied Adduction Moment

SETTINGS

Description	Value	Unit
Direction	Space-fixed direction	
Applied moment, x-component	-M_add	N·m
Applied moment, y-component	0	N·m
Applied moment, z-component	0	N·m

2.5 CUSTOM MESH

2.5.1 Global element size (size)

SETTINGS

Description	Value
Maximum element size	w_leaf/16
Minimum element size	1E-12
Curvature factor	0.6
Resolution of narrow regions	0.5
Maximum element growth rate	1.5
Custom element size	Custom

This value can be adjusted to control mesh size of the main leaf flexure face.

2.5.2 Free Quad: Mesh refinement faces (fq2)

SELECTION

Geometric entity level	Boundary
Selection	Geometry geom1: Dimension 2: Boundaries 1, 3–5

Local element size (size1)

SETTINGS

Description	Value
Maximum element size	w_leaf/64
Minimum element size	0.0108
Minimum element size	Off
Curvature factor	0.6
Curvature factor	Off
Resolution of narrow regions	0.5
Resolution of narrow regions	Off
Maximum element growth rate	1.5
Maximum element growth rate	Off
Custom element size	Custom

This value can be adjusted to control mesh size of the mesh refinement faces.

2.5.3 Free Quad: Main leaf flexure face (fq1)

SELECTION

Geometric entity level	Boundary
Selection	Geometry geom1: Dimension 2: Boundary 2

3 Study 1

The study incorporated in this appendix showcases *an example* of a study that may be conducted. In this case, three study steps are defined:

- First, a 30 degree flexion angle is prescribed to the bottom end of the leaf flexure.
- Subsequently, a 57 Nm adduction moment applied to the top end of the leaf flexure is added to this deformed configuration.
- Lastly, under the 57 Nm adduction moment, the bottom end of the leaf flexure is moved from 30 degree flexion to 8 degree extension.

3.1 PRESCRIBED THETA_FLEX=30 DEGREE

STUDY SETTINGS

Description	Value
Include geometric nonlinearity	On

PHYSICS AND VARIABLES SELECTION

Physics interface	Solve for	Equation form
Shell (shell)	On	Automatic (Stationary)

MESH SELECTION

Component	Mesh
Component 1	Custom mesh

3.1.1 Study extensions

STUDY EXTENSIONS

Description	Value
Auxiliary sweep	On
Sweep type	Specified combinations

Values for the input parameters and the number of steps over which they are applied can be adjusted here.

PARAMETERS

Parameter name	Parameter value list
theta_flex (rad)	range(0,0.05817764173314431,0.5235987755982988)

3.2 APPLIED M_ADD=57 NM AT PRESCRIBED THETA_FLEX=30 DEGREE

STUDY SETTINGS

Description	Value
Include geometric nonlinearity	On

PHYSICS AND VARIABLES SELECTION

Physics interface	Solve for	Equation form
Shell (shell)	On	Automatic (Stationary)

MESH SELECTION

Component	Mesh
Component 1	Custom mesh

3.2.1 Study extensions

STUDY EXTENSIONS

Description	Value
Auxiliary sweep	On
Sweep type	Specified combinations

Values for the input parameters and the number of steps over which they are applied can be adjusted here.

PARAMETERS

Parameter name	Parameter value list
theta_flex (rad)	0.5235987755982988*1^range(1,10)
M_add (Nm)	range(0,6.333333333333333,57)

3.3 APPLIED M_ADD=57 NM OVER RANGE THETA_FLEX=30 DEGREE TO -8 DEGREE

STUDY SETTINGS

Description	Value
Include geometric nonlinearity	On

PHYSICS AND VARIABLES SELECTION

Physics interface	Solve for	Equation form
Shell (shell)	On	Automatic (Stationary)

MESH SELECTION

Component	Mesh
Component 1	Custom mesh

3.3.1 Study extensions

STUDY EXTENSIONS

Description	Value
Auxiliary sweep	On
Sweep type	Specified combinations

Values for the input parameters and the number of steps over which they are applied can be adjusted here.

PARAMETERS

Parameter name	Parameter value list
M_add (Nm)	57*1^range(1,50)
theta_flex (rad)	range(0.5235987755982988,-0.013535206444037657,-0.13962634015954636)

3.4 SOLVER CONFIGURATIONS

3.4.1 Solution 1

Stationary Solver 1 (s1)

GENERAL

Description	Value
Defined by study step	Prescribed theta_flex=30 degree

METHOD AND TERMINATION

Description	Value
Nonlinear method	Constant (Newton)
Maximum number of iterations	25

Can be changed to "Automatic (Newton)" to improve but slow down convergence.

Can be increased to improve but slow down convergence.

Stationary Solver 2 (s2)

GENERAL

Description	Value
Defined by study step	Applied M_add=57 Nm at prescribed theta_flex=30 degree

METHOD AND TERMINATION

Description	Value
Nonlinear method	Constant (Newton)
Maximum number of iterations	25

Can be changed to "Automatic (Newton)" to improve but slow down convergence.

Can be increased to improve but slow down convergence.

Stationary Solver 3 (s3)

GENERAL

Description	Value
Defined by study step	Applied M_add=57 Nm over range theta_flex=30 degree to -8 degree

METHOD AND TERMINATION

Description	Value
Nonlinear method	Constant (Newton)
Maximum number of iterations	25

Can be changed to "Automatic (Newton)" to improve but slow down convergence.

Can be increased to improve but slow down convergence.

4 Measurements

4.1 DERIVED VALUES

4.1.1 Global Evaluation: theta_add

EXPRESSIONS

Expression	Unit
-shell.thx_srig2	deg

4.1.2 Global Evaluation: M_flex

EXPRESSIONS

Expression	Unit
-shell.srig1.RMy	N*m

4.1.3 Surface Maximum: Max Mises

SELECTION

Geometric entity level	Boundary
Selection	Geometry geom1: Dimension 2: All boundaries

EXPRESSIONS

Expression	Unit
shell.mises_max*((Y+w_leaf/2)^2+(Z+L_leaf_leg)^2>(1/1000)^2)*((Y+w_leaf/2)^2+(Z-L_leaf_ub)^2>(1/1000)^2)*((Y-w_leaf/2)^2+(Z+L_leaf_leg)^2>(1/1000)^2)*((Y-w_leaf/2)^2+(Z-L_leaf_ub)^2>(1/1000)^2)	N/m^2

CONFIGURATION

Point type	Lagrange points
Lagrange order	5

B.9 COMSOL model for the mechanism design using a leaf flexure incorporating warping constraints

1 Global Definitions

GLOBAL SETTINGS

Unit system	SI

1.1 PARAMETERS

PARAMETERS 1

Name	Expression	Value	Description
L_leaf_leg	0.06	0.06	m
L_leaf_ub	0.17	0.17	m
w_leaf	0.2	0.2	m
t_leaf	1.0/1000	0.001	m
t_wc	5.0/1000	0.005	m
d_wc	5.0/1000	0.005	m
n_wc	10	10	
d_hip	0.15	0.15	m
theta_flex	0	0	rad
M_add	0	0	Nm

The numerical values for the dimensional parameters shown here are placeholders that will be adjusted during the final design process.

The numerical values for these two input parameters depend on the specific analysis to be conducted. They can be defined under the study settings using the auxiliary sweep option.

2 Component 1

2.1 DEFINITIONS

2.1.1 Nonlocal Couplings

Average 1

Coupling type	Average
Operator name	aveop1

SELECTION

Geometric entity level	Edge
Selection	Geometry geom1: Dimension 1: Edge 123

2.2 GEOMETRY 1

2.2.1 Work Plane 1 (wp1)

PLANE DEFINITION

Description	Value
Plane	yz - plane

Description	Value
Offset type	Distance
x-coordinate	-d_hip-t_leaf

UNITE OBJECTS

Description	Value
Unite objects	On

Plane Geometry (sequence2D)

Rectangle: Leaf Flexure (r1)

POSITION

Description	Value
Base	Corner
Position	{-w_leaf/2, -L_leaf_leg}

SIZE

Description	Value
Width	w_leaf
Height	L_leaf_ub + L_leaf_leg

2.2.2 Block 1: Warping Constraint (blk2)

POSITION

Description	Value
Base	Corner
Position	{-d_hip - t_leaf - d_wc, -w_leaf/2, -L_leaf_leg + (L_leaf_ub + L_leaf_leg - n_wc*t_wc)/(n_wc + 1)}

SIZE AND SHAPE

Description	Value
Width	d_wc
Depth	w_leaf
Height	t_wc

2.2.3 Array 1: Warping Constraints (arr2)

SETTINGS

Description	Value
Array type	Linear
Size	n_wc
Displacement	{0, 0, t_wc + (L_leaf_ub + L_leaf_leg - n_wc*t_wc)/(n_wc + 1)}

2.2.4 Explicit Selection 1 (sel1)

EXPLICIT PROPS

Description	Value
Geometric entity level	Boundary
Selection	Geometry geom1: Dimension 2: Boundaries 51–71
Group by continuous tangent	On

2.3 MATERIALS

2.3.1 Steel

SELECTION LEAF FLEXURE

Geometric entity level	Boundary
Selection	Explicit Selection 1

SELECTION WARPING CONSTRAINTS

Geometric entity level	Domain
Selection	Geometry geom1: Dimension 3: All domains

MATERIAL PARAMETERS

Name	Value	Unit	Property group
Density	7800	kg/m³	Basic
Young's modulus	2.1E11	Pa	Young's modulus and Poisson's ratio
Poisson's ratio	0.28	1	Young's modulus and Poisson's ratio

Linear Elastic Material

SETTINGS

Description	Value
Material symmetry	Isotropic
Specify	Young's modulus and Poisson's ratio
Young's modulus	From material
Poisson's ratio	From material
Density	From material

2.4 SHELL

SELECTION

Geometric entity level	Boundary
Selection	Explicit Selection 1

2.4.1 Thickness and Offset 1

SETTINGS

Description	Value	Unit
Initial thickness	t_leaf	m
Position	Bottom surface on boundary	

2.4.2 Rigid Connector leg

Center of Rotation

SETTINGS

Description	Value	Unit
Center of rotation	User defined	
Global coordinates of center of rotation, x-component	0	m
Global coordinates of center of rotation, y-component	0	m
Global coordinates of center of rotation, z-component	0	m
Offset	Off	

Prescribed Displacement at Center of Rotation

SETTINGS

Description	Value	Unit
Prescribed in x direction	On	
Prescribed in y direction	On	
Prescribed in z direction	On	
Displacement constraint, x-component	0	m
Displacement constraint, y-component	0	m
Displacement constraint, z-component	0	m

Prescribed Rotation

SETTINGS

Description	Value	Unit
By	Prescribed rotation	
Axis of rotation, x-component	0	
Axis of rotation, y-component	-1	
Axis of rotation, z-component	0	
Angle of rotation	theta_flex	rad

Reaction Force Settings

SETTINGS

Description	Value
Evaluate reaction forces	On
Apply reaction only on rigid body variables	Off

2.4.3 Rigid Connector UB

SELECTION

Geometric entity level	Edge
Selection	Geometry geom1: Dimension 1: Edge 123

Center of Rotation

SETTINGS

Description	Value
Center of rotation	Automatic
Offset	Off

Prescribed Displacement at Center of Rotation

SETTINGS

Description	Value	Unit
Prescribed in x direction	On	
Prescribed in y direction	Off	
Prescribed in z direction	Off	
Displacement constraint, x-component	0	m
Displacement constraint, y-component	0	m
Displacement constraint, z-component	0	m

Prescribed Rotation

SETTINGS

Description	Value	Unit
By	Prescribed rotation	
Axis of rotation, x-component	-1	
Axis of rotation, y-component	0	
Axis of rotation, z-component	0	
Angle of rotation	atan(aveop1(v)/(L_leaf_ub + aveop1(w)))	rad

Applied Adduction Moment

SETTINGS

Description	Value	Unit
Direction	Space-fixed direction	
Applied moment, x-component	-M_add	N·m
Applied moment, y-component	0	N·m
Applied moment, z-component	0	N·m

2.5 SOLID MECHANICS

SELECTION

Geometric entity level	Domain
Selection	Geometry geom1: Dimension 3: All domains

2.6 MULTIPHYSICS

2.6.1 Solid-Thin Structure Connection 1

Connection Settings

SETTINGS

Description	Value
Connection type	Shared boundaries
Selection	Geometry geom1: Dimension 2: Boundaries 52, 54, 56, 58, 60, 62, 64, 66, 68, 70

Coupled Interfaces

SETTINGS

Description	Value
Solid mechanics	Solid Mechanics (solid)
Thin structure	Shell (shell)

2.7 CUSTOM MESH

2.7.1 Global element size (size)

SETTINGS

Description	Value
Maximum element size	w_leaf/4
Minimum element size	1E-12
Curvature factor	0.6
Resolution of narrow regions	0.001
Maximum element growth rate	1.5
Custom element size	Custom

This value can be adjusted to control the element size of the sections of the leaf flexure between the warping constraints.

2.7.2 Mapped 1: Side of Warping Constraints (map1)

SELECTION

Geometric entity level	Boundary
Selection	Geometry geom1: Dimension 2: Boundary 2

Distribution Depth Warping Constraints (dis1)

SELECTION

Geometric entity level	Edge
Selection	Geometry geom1: Dimension 1: Edge 5

SETTINGS

Description	Value
Number of elements	2

This value can be adjusted to control the number of elements through the depth of the warping constraints.

Distribution Thickness Warping Constraints (dis2)

SELECTION

Geometric entity level	Edge
Selection	Geometry geom1: Dimension 1: Edge 1

SETTINGS

Description	Value
Number of elements	2

This value can be adjusted to control the number of elements through the thickness of the warping constraints.

2.7.3 Swept 1: Through width Warping Constraint (swe1)

SELECTION

Geometric entity level	Domain
Selection	Geometry geom1: Dimension 3: Domain 1

Distribution width (dis1)

SELECTION

Geometric entity level	Domain
Selection	Geometry geom1: Dimension 3: Domain 1

SETTINGS

Description	Value
Number of elements	4

This value can be adjusted to control the number of elements through the width of the warping constraints and leaf flexure.

2.7.4 Copy Domain to all Warping constraints 1 (cpd1)

SETTINGS

Source Domains	Geometry geom1: Dimension 3: Domain 1
Destination Domains	Remaining

2.7.5 Mapped 2 (map2)

SELECTION

Geometric entity level	Boundary
Selection	Remaining

3 Study 1

The study incorporated in this appendix showcases *an example* of a study that may be conducted. In this case, three study steps are defined:

- First, a 30 degree flexion angle is prescribed to the bottom end of the leaf flexure.
- Subsequently, a 57 Nm adduction moment applied to the top end of the leaf flexure is added to this deformed configuration.
- Lastly, under the 57 Nm adduction moment, the bottom end of the leaf flexure is moved from 30 degree flexion to 8 degree extension.

3.1 PRESCRIBED THETA_FLEX=30 DEGREE

STUDY SETTINGS

Description	Value
Include geometric nonlinearity	On

PHYSICS AND VARIABLES SELECTION

Physics interface	Solve for	Equation form
Shell (shell)	On	Automatic (Stationary)

MESH SELECTION

Component	Mesh
Component 1	Custom mesh

3.1.1 Study extensions

STUDY EXTENSIONS

Description	Value
Auxiliary sweep	On
Sweep type	Specified combinations

Values for the input parameters and the number of steps over which they are applied can be adjusted here.

PARAMETERS

Parameter name	Parameter value list
theta_flex (rad)	range(0,0.05817764173314431,0.5235987755982988)

3.2 APPLIED M_ADD=57 NM AT PRESCRIBED THETA_FLEX=30 DEGREE

STUDY SETTINGS

Description	Value
Include geometric nonlinearity	On

PHYSICS AND VARIABLES SELECTION

Physics interface	Solve for	Equation form
Shell (shell)	On	Automatic (Stationary)

MESH SELECTION

Component	Mesh
Component 1	Custom mesh

3.2.1 Study extensions

STUDY EXTENSIONS

Description	Value
Auxiliary sweep	On
Sweep type	Specified combinations

Values for the input parameters and the number of steps over which they are applied can be adjusted here.

PARAMETERS

Parameter name	Parameter value list
theta_flex (rad)	0.5235987755982988*1^range(1,10)
M_add (Nm)	range(0,6.333333333333333,57)

3.3 APPLIED M_ADD=57 NM OVER RANGE THETA_FLEX=30 DEGREE TO -8 DEGREE

STUDY SETTINGS

Description	Value
Include geometric nonlinearity	On

PHYSICS AND VARIABLES SELECTION

Physics interface	Solve for	Equation form
Shell (shell)	On	Automatic (Stationary)

MESH SELECTION

Component	Mesh
Component 1	Custom mesh

3.3.1 Study extensions

STUDY EXTENSIONS

Description	Value
Auxiliary sweep	On
Sweep type	Specified combinations

Values for the input parameters and the number of steps over which they are applied can be adjusted here.

PARAMETERS

Parameter name	Parameter value list
M_add (Nm)	57*1^range(1,50)
theta_flex (rad)	range(0.5235987755982988,-0.013535206444037657,-0.13962634015954636)

3.4 SOLVER CONFIGURATIONS

3.4.1 Solution 1

Stationary Solver 1 (s1)

GENERAL

Description	Value
Defined by study step	Prescribed theta_flex=30 degree

METHOD AND TERMINATION

Description	Value
Nonlinear method	Constant (Newton)
Maximum number of iterations	25

Can be changed to "Automatic (Newton)" to improve but slow down convergence.

Can be increased to improve but slow down convergence.

Stationary Solver 2 (s2)

GENERAL

Description	Value
Defined by study step	Applied M_add=57 Nm at prescribed theta_flex=30 degree

METHOD AND TERMINATION

Description	Value
Nonlinear method	Constant (Newton)
Maximum number of iterations	25

Can be changed to "Automatic (Newton)" to improve but slow down convergence.

Can be increased to improve but slow down convergence.

Stationary Solver 3 (s3)

GENERAL

Description	Value
Defined by study step	Applied M_add=57 Nm over range theta_flex=30 degree to -8 degree

METHOD AND TERMINATION

Description	Value
Nonlinear method	Constant (Newton)
Maximum number of iterations	25

Can be changed to "Automatic (Newton)" to improve but slow down convergence.

Can be increased to improve but slow down convergence.

4 Measurements

4.1 DERIVED VALUES

4.1.1 Global Evaluation: theta_add

EXPRESSIONS

Expression	Unit
-shell.thx_srig2	deg

4.1.2 Global Evaluation: M_flex

EXPRESSIONS

Expression	Unit
-shell.srig1.RMy	N*m

4.1.3 Surface Maximum: Max Mises

SELECTION

Geometric entity level	Boundary
Selection	Explicit Selection 1

EXPRESSIONS

Expression	Unit
shell.mises_max*((Y+w_leaf/2)^2+(Z+L_leaf_leg)^2>(1/1000)^2)*((Y+w_leaf/2)^2+(Z-L_leaf_ub)^2>(1/1000)^2)*((Y-w_leaf/2)^2+(Z+L_leaf_leg)^2>(1/1000)^2)*((Y-w_leaf/2)^2+(Z-L_leaf_ub)^2>(1/1000)^2)	N/m^2

CONFIGURATION

Point type	Lagrange points
Lagrange order	5